Cardiac consequences of metabolic derangements: role of mitochondrial oxidative stress and autophagy

Ph.D. thesis

Gábor Koncsos, M.Sc.

Semmelweis University
Doctoral School of Pharmaceutical Sciences

Supervisor: Zoltán Giricz, Pharm.D., Ph.D.

Official reviewers: Gergő Szanda, M.D., Ph.D.
István Lekli, Pharm.D., Ph.D.

Head of the Final Examination Committee:
Éva Szökő, Pharm.D., Ph.D., D.Sc.

Members of the Final Examination Committee:
Zsuzsanna Miklós, M.D., Ph.D.
Árpád Márki, M.Sc., Ph.D.

Budapest
2018

1 Table of contents

1 Table of contents 1
2 List of Abbreviations 5
3 Introduction 9
3.1 Metabolic diseases in cardiovascular system 9
3.1.1 Hyperlipidemia 9
3.1.2 Diabetes and prediabetes 11
3.2 Molecular pathology of metabolc diseases in the heart 13
3.2.1 Cardiac mTOR activity 14
3.2.2 Cardiac autophagy 15
3.2.3 Cardiac cell death pathways 17
3.3 Cardiac mitochondria in metabolic diseases 19
3.3.1 Mitochondrial oxidative stress 19
3.3.2 Mitochondrial dynamics and quality control 20
3.3.3 Morphological and functional properties of mitochondrial subpopulations in the heart 23
3.3.4 Mitochondrial isolation with nagarse - methodological obstacles in cardiac mitochondrial studies 24
4 Aims 25
5 Materials and methods 26
5.1 Animal models and experimental designs 26
5.2 Assesment of sensory neuropathy 29
5.3 Evaluation of body fat content 29
5.4 Cardiac function by echocardiography 29
5.5 Hemodynamic measurements, left ventricular pressure-volume analysis 30
5.6 Adipokine array from rat plasma 31

5.7 Biochemical measurements 31
5.8 Histology 32
5.9 Nitrotyrosine immunostainig of left ventricular samples 32
5.10 Quantitative RT-PCR 33
5.11 Measurement of pancreatic insulin 33
5.12 Electron microscopy 33
5.13 Mitochondrial enzyme activity measurements 34
5.14 Preparation of isolated mitochondria 35
5.15 Measurement of mitochondrial respiration 37
5.16 Measurement of mitochondrial membrane potential 37
5.17 Detection of H2O2 formation in mitochondria 38
5.18 Measurement of Ca2+ - uptake in mitochondria 38
5.19 Western blot of left ventricle lysates and isolated mitochondria fractions 38
5.20 Statistical analysis 41
6 Results 42
6.1 Effect of high-cholesterol diet in Wistar rats 42
6.1.1 Elevated serum cholesterol level in hypercholesterolemic rats 42
6.1.2 Hypercholesterolemia downregulates autophagy 42
6.1.3 Hypercholesterolemia activates mTOR in the heart 44
6.1.4 Apoptosis but not necroptosis is elevated in hypercholesterolemia 45
6.2 Effect of high-fat diet and streptozotin treatment in Long-Evans rats 46
6.2.1 Moderately increased adiposity in prediabetic animals 46
6.2.2 Impaired glucose tolerance, insulin resistance, and sensory neuropathy evidence disturbed carbohydrate metabolism in prediabetes 48
6.2.3 Diastolic dysfunction and hypertrophy in prediabetes with no sign of fibrosis 50

6.2.4 Elevated reactive oxygen species formation in cardiac subsarcolemmal mitochondria in prediabetic rats 53
6.2.5 Alterations in cardiac mitofusin-2 expression and mitophagy in prediabetes 60
6.2.6 Expression of cardiac Bcl-2 decreases in prediabetes 64
6.2.7 No changes in cardiac HSPs in prediabetes 64
6.3 Detection and quantification of proteins in cardiac mitochondrial subpopulations 65
6.3.1 Differential amounts of proteins in mouse and rat cardiac SSM and IFM 65
6.3.2 Nagarse treatment influences protein signals in SSM and IFM from mouse hearts 70
6.3.3 Nagarse treatment has no effect on respiration of mitochondrial subfractions 72
7 Discussion 73
7.1 Hypercholesterolemia modulates cardiac mTOR and autophagy 73
7.1.1 Hypercholesterolemia increases mTOR activity and attenuates autophagy in rat heart 73
7.1.2 Hypercholesterolemia increases apoptosis, but not necroptosis in rat heart.. 74
7.2 Prediabetes induced diastolic dysfunction by mild mitochondrial oxidative stress and impaired mitophagy 76
7.2.1 Prediabetes induces mild diastolic dysfunction and hypertrophy without fibrosis 76
7.2.2 Prediabetes induces mild elevation of oxidative stress in cardiac subsarcolemmal mitochondria 77
7.2.3 No changes in cardiac Ca2+ homeostasis in prediabetes 79
7.2.4 Apoptosis is not modulated by prediabetes in cardiomyocytes 80
7.2.5 Early sign of altered mitochondrial fusion and mitophagy in prediabetes 81
7.3 Detection of mitochondrial proteins is influenced by mitochondrial isolation with nagarse 83

7.4 Limitations 87
8 Conclusions 88
8.1 Hypercholesterolemia activates cardiac mTOR and apoptosis but downregulates autophagy 88
8.2 Prediabetes induces mild diastolic dysfunction and hypertrophy by elevated mitochondrial oxidative stress 88
8.3 Nagarse treatment of cardiac subsarcolemmal and interfibrillar mitochondria accounts for inaccurate quantification of proteins 89
9 Summary 90
10 Összefoglalás 91
11 References 92
12 List of own publications 120
12.1 Own publications involved in the current thesis 120
12.2 Own publications not involved in the current thesis 121
13 Acknowledgements 123

2 List of Abbreviations

4E-BP1	-	eIF-4E binding protein 1
ACC	-	acetyl-CoA carboxylase
AMP/ADP/ATP	-	adenosine mono-/di-/triphosphate
AMPKα	-	AMP-activated protein kinase α
ANP	-	atrial natriuretic peptide
Atg	-	autophagy-related protein
ATP5A	-	ATP synthase subunit alpha
BAT	-	interscapular brown adipose tissue
Bax	-	Bcl-2-associated X protein
BCA	-	bicinchoninic acid
Bcl-2	-	B-cell lymphoma 2 protein
BID	-	BH3-interacting domain death agonist protein
BNIP3	-	Bcl-2/adenovirus E1B 19 kDa protein-interacting protein 3
BNP	-	brain natriuretic peptide
BSA	-	bovine serum albumin
CAD	-	coronary artery disease
CaMKIIδ	-	Ca^{2+}/calmodulin-dependent protein kinase II;
CAT	-	carboxyatractyloside
CHOL	-	hypercholesterolemic group
Class-III PI3K	-	class-III phosphatidylinositol-3-kinase
CO	-	cardiac output
COL1/3	-	collagen type I and III
CON	-	control group
COX4	-	cytochrome c oxidase subunit 4 isoform 1
CP	-	common protocol (of mitochondrial isolation from mouse/rat heart)
CRP	-	C-reactive protein
CT	-	computed tomography
CVD	-	cardiovascular disease
Cx43	-	connexin 43
DJ-1 (PARK7)	-	protein deglycase DJ-1 (Parkinson disease protein 7)

dP/dtmax	-	maximal slope of LV systolic pressure increment
dP/dtmin	-	maximal slope of LV diastolic pressure decrement; τ= time constant of LV pressure decay
DLP1	-	dynamin-like protein 1
EDPVR	-	end-diastolic pressure-volume relationship
EF	-	ejection fraction
ELISA	-	enzyme-linked immunosorbent assay
ESPVR	-	end-systolic pressure-volume relationship
FIS1	-	mitochondrial fission 1 protein
FS%	-	fractional shortening %
GAPDH	-	glyceraldehyde 3-phosphate dehydrogenase
GOT	-	glutamate oxaloacetate transaminase
GPT	-	glutamate pyruvate transaminase
GSK3β	-	glycogen synthase kinase-3 beta
HDL	-	high density lipoprotein
HE	-	hematoxylin-eosin
HR	-	heart rate
HSP	-	heat shock protein
I/R	-	ischemia/reperfusion as
IDL	-	intermediate density lipoprotein
IFM	-	interfibrillar mitochondria
IFM+N	-	interfibrillar mitochondria treated with nagarse
IFM+N+I	-	interfibrillar mitochondria treated with nagarse and protease inhibitor
IGF-1	-	insulin-like growth factor-1
IPC	-	ischemic preconditioning
ITT	-	insulin tolerance test
LC3	-	microtubule-associated protein light chain 3
LDL	-	low density lipoprotein
LV mass	-	left ventricular mass
LVAWTs	-	left ventricular anterior wall thickness, diastolic
LVAWTs	-	left ventricular anterior wall thickness, systolic

LVEDP	-	left ventricular end-diastolic pressure
LVEDV	-	left ventricular end-diastolic volume
LVESP	-	left ventricular end-systolic pressure
LVESV	-	left ventricular end-systolic volume
LVPWTd	-	left ventricular posterior wall thickness, diastolic
LVPWTs	-	left ventricular posterior wall thickness, systolic
MA	-	Masson's trichrome
MAP	-	mean arterial pressure
MFN1/2	-	mitofusin 1 and 2
MLKL	-	mixed lineage kinase domain-like protein
MOPS	-	3-[N-Morpholino]-propanesulfonic acid
mPTP	-	mitochondrial permeability transition pore
mTOR	-	mechanistic target of rapamycin
NBR1	-	neighbor of BRCA1 gene 1
$NO^{\bullet}$	-	nitric oxide
NORM	-	normocholesterolemic group
NRF1/2	-	nuclear respiratory factor 1 and 2
OGTT	-	oral glucose tolerance test
OLETF	-	Otsuka Long-Evans Tokushima fatty (rat)
OPA1	-	optic atrophy 1
PARP	-	poly (ADP-ribose) polymerase
PGC-1α	-	peroxisome proliferator-activated receptor gamma coactivator
PLB	-	phospholamban
PMSF	-	phenylmethylsulfonyl fluoride
PNM	-	perinuclear mitochondria
PRED	-	prediabetic group
PRSW	-	preload recruitable stroke work
PVDF	-	polyvinylidene fluoride
RAB7	-	ras-related protein Rab-7a
Raptor	-	regulatory-associated protein of mTOR
Rictor	-	rapamycin-insensitive companion of mTOR
RIP1/3	-	receptor-interacting serine/threonine-protein kinase 1 and 3

RIPA - radioimmunoprecipitation assay

ROS - reactive oxygen species

Rubicon - run domain Beclin-1-interacting and cysteine-rich domain containing protein

RV - right ventricle

S6 - ribosomal S6 protein

S6K1 - S6 Kinase 1

SERCA2A - sarco/endoplasmic reticulum Ca^{2+}ATPase II

SOD - superoxide dismutase

SQSTM1/p62 - sequestosome 1

SSM - subsarcolemmal mitochondria

SSM+N - subsarcolemmal mitochondria treated with nagarse

STZ - streptozotocin

SV - stroke volume

SW - stroke work

T1DM - Type 1 diabetes mellitus

T2DM - Type 2 diabetes mellitus

TBS-T - tris-buffered saline-Tween 20

TFAM - mitochondrial transcription factor A

TFBM - dimethyladenosine transferase 1, mitochondrial

TG - triglyceride

TIMP-1 - TIMP metallopeptidase inhibitor 1

Tm - oxidized tropomyosin

TNFα - tumor necrosis factor alpha

TPR - total peripheral resistance

ULK1 - unc-51-like kinase 1

VDAC - voltage-dependent anion-selective channel protein

VLDL - very low density lipoprotein

Work; dP/dtmax-EDV - the slope of the dP/dtmax-end-diastolic volume relationship

α-MHC - alpha-myosin heavy chain

β-MHC - beta-alpha-myosin heavy chain

3 Introduction

3.1 Metabolic diseases in cardiovascular system

There is an overall agreement in the scientific and clinical community that metabolic disorders including obesity, hyperlipidemia or diabetes can increase the incidence of cardiovascular diseases (CVDs) such as myocardial infarction or cardiomyopathies[1] and they attenuate or inhibit the intrinsic adaptation mechanism of the heart to ischemic insult[2]. Furthermore, it was shown previously that these comorbidities also reduce or inhibit the effect of cardioprotective therapeutical interventions such as ischemic pre-[3] or postconditioning[4]. Therefore, it is important to study the effect of metabolic diseases on the cardiovascular system to identify novel targets for future cardioprotective therapies.

3.1.1 Hyperlipidemia

Hyperlipidemia is a family of metabolic disorders, which can be defined by elevated cholesterol (hypercholesterolemia) and/or triglyceride (hypertriglyceridemia) levels in the blood. These lipids (or fats) are not soluble in the plasma, therefore, they are transported by lipoproteins in the circulation system. Based on the content, density and size of lipoproteins, they can be divided into different subpopulations including chylomicrons, very low-density lipoprotein (VLDL), intermediate-density lipoprotein (IDL), low-density lipoprotein (LDL) and high-density lipoprotein (HDL), which have essential role in the transport of lipids among different organs[5]. LDL transports fats from the liver to the other tissues, while cholesterol is returned by HDL to the liver. Serum total cholesterol, LDL, HDL and triglyceride are the most common diagnostic markers of lipid homeostasis (Table 1). In hypercholesterolemia, decreased levels of HDL cholesterol and increased levels of LDL cholesterol are responsible for atherogenic conditions. Although both plasma triglyceride and cholesterol levels are increased in most forms of hyperlipidemias, the studying of changes in plasma cholesterol levels without altered plasma triglyceride level may also be important. Therefore, in this thesis, the focus is on the role of hypercholesterolemia without elevation of plasma triglyceride level.

The cause of hypercholesterolemia can be genetic (e.g. familial hypercholesterolemia via defect of LDL-receptor), unhealthy lifestyle, or both. Polygenic hypercholesterolemia

may also occur in healthy, but genetically susceptible individuals, however, its polygenic background is still not fully understood. Moreover, this phenotype may be aggravated by various factors including smoking, hypertension, atherogen diet (elevated cholesterol and saturated fat intake), obesity and diabetes[6].

In the early 1950s, the Framingham heart study demonstrated for the first time that besides age, sex, and smoking, hypercholesterolemia is a major risk factor for developing coronary artery disease (CAD) due to altered LDL and HDL cholesterol levels[7]. Hypercholesterolemia have significant cardiac consequences, since they are among the major risk factors of CAD via atherosclerosis and sudden coronary death due to myocardial infarction[8-10]. The role of atherosclerosis is well studied in these pathologies; however, myocardial effects of hypercholesterolemia are less understood. Hypercholesterolemia was previously shown to worsen cardiac systolic and diastolic function in cholesterol-fed rabbits[11]. Furthermore, we have previously shown that cholesterol feeding leads to mild contractile dysfunction and cardiac oxidative stress[12]. These data suggest that cardiac metabolism may be affected by hypercholesterolemia well before or even without the development of atherosclerosis.

Ischemic conditioning (*i.e.*, ischemic pre-, per- and postconditioning) of the heart performed by applying short cycles of ischemia/reperfusion (I/R) protects the myocardium against I/R injury[2, 13]. However, cardioprotective effects of ischemic conditioning are attenuated in the presence of cardiovascular risk factors such as aging[14, 15], diabetes[16, 17] and hypercholesterolemia as well[18-20]. Similarly, our previous studies demonstrated that cardioprotection by various forms of ischemic conditioning is impaired in cholesterol-fed rats[4, 21-23].

Although cardioprotective signaling pathways are well established, it is still unclear which processes are responsible for the loss of cardioprotection in hypercholesterolemia.

Table 1. American Heart Association guidelines for cholesterol and triglycerides levels in adults.
LDL, low-density lipoprotein; HDL, high-density lipoprotein; TG, triglyceride. Table was adapted from Phoebe et. al, 2010[24].

	Total (mmol/L)	LDL (mmol/L)	HDL (mmol/L)	TG (mmol/L)
Optimal/Near optimal	< 5.2	2.6 - 3.3	1.0 - 1.6	< 1.7
Borderline high	5.2 - 6.2	3.3 - 4.1	-	1.7 - 2.2
High	-	4.1 - 4.9	-	2.2 - 5.6
Very high	> 6.2	> 4.9	< 1.0	> 5.6

3.1.2 Diabetes and prediabetes

Diabetes is characterized by elevated fasting (≥7.0 mmol/L) or non-fasting (≥11.1 mmol/L) blood glucose levels termed hyperglycemia, which leads to defects in insulin secretion, insulin action, or both[25]. Chronic hyperglycemia could lead to long-term damage and failure of different organs and tissues, such as the eyes, kidneys, nerves, blood vessels and the heart[26]. Diabetes can be divided into 2 main groups: type 1 and type 2 diabetes.

Type 1 diabetes mellitus (T1DM) is defined as a deficiency of insulin production due to the autoimmune destruction of pancreatic beta cells. T1DM can lead to absolute insulin deficiency and it can cause polyuria, thirst and weight loss with a propensity of ketosis. Most commonly, T1DM occurs in young individuals and accounts for approximately 5–10% of all cases of diabetes[1, 26]. Based on the significant pathological and therapeutic differences between type 1 and 2 diabetes, T1DM will not be further investigated in this thesis.

Type 2 diabetes mellitus (T2DM) is a common civilization disease, which is defined by an inadequate compensatory insulin secretory response to increased blood glucose level, and a combination of resistance to insulin action[27]. In the early stage of T2DM, cells become resistant to insulin. Insulin resistance can develop due to a deficiency of insulin receptors, a result of which is an elevated blood glucose level. Because of hyperglycemia, pancreatic beta cells produce more insulin to equilibrate the state of insulin resistance. Finally, this process leads to chronic production of insulin, which is responsible for the insufficient or exhausted beta cell activity[26]. T2DM is more frequent

(approximately 90-95% of all cases) than T1DM and it has growing prevalence worldwide. In most cases, T2DM is associated with obesity and sedentary lifestyle[27, 28]. It is well established that T2DM is an independent risk factor of CVDs such as heart failure and myocardial infarction as well as vascular complications, which contribute to their increased morbidity and mortality[1, 29, 30]. In the multiethnic Northern Manhattan Study cohort, presence of T2DM increased the risk of LV hypertrophy with approximately 1.5 fold[31]. Epidemiological studies have demonstrated that the incidence of both microvascular and macrovascular complications are directly associated with the degree of hyperglycemia[32, 33], and that glucose control in patients with T2DM reduced macrovascular complications[34, 35].

Since incidence of T2DM is growing in developing and developed societies, more people are influenced by its non-ischemic cardiac complications, for example, diabetic cardiomyopathy often develops. One of the most severe cardiovascular consequences of diabetes, diabetic cardiomyopathy is defined by diabetes-associated changes in the structure and function of the myocardium, which is not directly attributable to other confounding factors such as CAD or hypertension[36]. Pathological processes of diabetic cardiomyopathy include the presence of myocardial damage, reactive hypertrophy, and intermediary fibrosis, structural and functional changes of the small coronary vessels, disturbance of the management of the metabolic cardiovascular load. T2DM also leads to myocardial lipotoxicity that may contribute to cell death and thus to cardiac dysfunction[37]. These alterations make the diabetic heart susceptible to ischemia and less able to recover from an ischemic attack[37].

Before the development of overt T2DM, a period of prediabetic state (*i.e.*, impaired glucose and insulin tolerance, insulin and leptin resistance, oscillations of normo- and hyperglycemic states, hypertriglyceridemia, hypertension, mild to moderate obesity) occurs[25, 38], which may also promote cardiovascular complications[39-41]. Although various organizations have attempted to define prediabetes, to date no consensus has been reached. The World Health Organization has defined prediabetes as a state of intermediate hyperglycemia based on two specific parameters: impaired fasting glucose, which is defined by fasting plasma glucose of 6.1-6.9 mmol/L and impaired glucose tolerance, which is defined by plasma glucose of 7.8-11.0 mmol/L after a 2 h oral glucose tolerance test (OGTT)[42]. The American Diabetes Association has the same cut-off value for OGTT

(7.8-11.0 mmol/L), but this organization defined a lower cut-off value for fasting plasma glucose (5.5-6.9 mmol/L), and as an additional parameter, hemoglobin A1c (HbA1c) is taken into account, with a range of 5.7% to 6.4%[26]. However, the range of these glucose parameters are lower than in diabetes (see above).

In 2011, the Centers for Disease Control estimated that 79 million Americans had prediabetes, which were 35% of people over the age of 20. Moreover, based on data from the National Health and Nutrition Examination Survey, worldwide prevalence of prediabetes may currently approach 840 million[43]. Although it was previously shown that people with prediabetes in general have approximately 20% risk of CVDs[44, 45], other studies showed conflicting results[46, 47]. Based on these investigations, incidence of prediabetes shows a growing tendency, which could also increase the risk of cardiovascular complications similarly to as seen in T2DM.

Although cardiac pathophysiological alterations are relatively well characterized in fully developed diabetes (*i.e.,* diabetic cardiomyopathy), information about prediabetes is quite limited. Moreover, development of diabetes leads to systemic sensory neuropathy that has been shown to result in diastolic dysfunction in the rat heart[48, 49]. Although it was previously demonstrated that prediabetes promote sensory neuropathy in C57BL/6J mice[50], it is still unclear, whether prediabetic sensory neuropathy occurs in other species such as rats. Since more people are influenced by prediabetes, the examination of its molecular background is also important. In Wistar rats, high caloric diet resulted in obesity-induced prediabetes, which impaired mitochondrial function and reduced basal contractile function and tolerance to acute oxygen deprivation[51]. Furthermore, it has been reported that prediabetes induced mild diastolic dysfunction in Otsuka Long-Evans Tokushima fatty (OLETF) rats, which is a genetic model for spontaneous long-term hyperglycemia[52], however, cardiac consequences of prediabetes and their molecular mechanism is unknown in non-genetic prediabetic settings.

3.2 Molecular pathology of metabolic diseases in the heart

A disturbed metabolic status due to diabetes or hyperlipidemia may result in altered signaling pathways in cardiac cells. In diabetes-induced hyperglycemia, different molecular mechanisms may change such as insulin signaling via PI-3K pathway[53, 54], formation of advanced glycation end products, activation of protein kinase C, increased

glucose flux through the hexosamine pathway[54], activation of the 12/15-lipoxygenase pathway[55] which finally lead to superoxide production[54]. Additionally, diabetes could lead to impaired Ca^{2+} handling due to glucose-dependent modifications of Ca^{2+}/calmodulin-dependent protein kinase II (CAMKIIδ), which leads to diabetic cardiomyopathy via contractile dysfunction. Furthermore, metabolic diseases could be associated with other altered cellular and molecular mechanisms such as autophagy/mitophagy or necroptosis, which are still not well-characterized in metabolic cardiac dysfunctions.

Therefore, this thesis focuses on the molecular aspects of cardiac function in metabolic diseases including hypercholesterolemia and diabetes/prediabetes.

3.2.1 Cardiac mTOR activity

The mechanistic target of rapamycin (mTOR) is a serine/threonine protein kinase, which plays a central role in cellular growth and metabolism. It exists in two complexes: mTORC1 with regulatory-associated protein of mTOR (Raptor) and mTORC2 with rapamycin-insensitive companion of mTOR (Rictor). It is well-established that mTORC1 can be activated by various upstream regulators such as amino acids, growth factors as well as elevated glucose and oxygen levels[56, 57]. This complex is highly connected with insulin-like growth factor-1 (IGF-1) and Akt/PKB signaling. Regulation of mTORC1 by the IGF-1/Akt pathway occurs through phosphorylation of the TSC1/2 (hamartin-tuberin) complex, which leads to its inhibition and subsequent activation of mTORC1[58, 59]. Furthermore, it was also demonstrated that rapamycin can inhibit mTORC1, but not mTORC2, however, prolonged treatment with rapamycin could inhibit mTORC2 activity[60]. Although it has been shown that mTORC2 activity has important role in ischemic preconditioning (IPC)-induced cardioprotection via ribosomal S6 signaling[61], it is even unclear which signals can modulate the activity of mTORC2. The main substrates of mTORC1 activity are S6 Kinase 1 (S6K1) and eIF-4E binding protein 1 (4E-BP1)[60]. S6K1 is a positive regulator of translation, initiation and elongation when it is phosphorylated by mTORC1 via its ability to phosphorylate multiple substrates including ribosomal S6 protein or 4E-BP1[60].

Previous studies demonstrated that chronically activated cardiac mTOR suppresses insulin receptor substrate 1 (an important protein of insulin signaling) in diabetes[62] and

cardiac autophagy in obesity[63]. However, the role of cardiac mTOR is still unclear in hypercholesterolemia and prediabetes.

3.2.2 Cardiac autophagy

Autophagy is a ubiquitous cellular housekeeping process[64-66], which is involved in protein quality control and cardiac cytoprotection[67-69].

It has 3 different types: macro-, micro and chaperone-mediated autophagy. Moreover, macroautophagy has further cargo-selective subtypes such as macrophagy (removal of protein macromolecules), mitophagy (removal of damaged or senescent mitochondria) or glycophagy (removal of glycogen macromolecules)[70]. In macroautophagy (hereafter referred to as autophagy) the cytoplasmic contents are sequestered within double membrane vacuoles called autophagosomes and subsequently delivered to the lysosome for degradation. In the beginning of autophagosomal formation, a pre-autophagosomal structure is formed intracellularly, which is also called isolation membrane or phagophore. The activity of class III phosphatidylinositol 3-kinase (PI3K), Vps34, Beclin-1 and autophagy-related (Atg) proteins (e.g. Atg12-Atg5-Atg16L) play an essential role in the early stages of the autophagosome formation. During sequestration and elongation processes, sequestome 1 or ubiquitin-binding protein p62 (SQSTM1/p62), which is the key autophagy adaptor is activated by lipidation and mediates protein cargo into forming phagophore. Then, SQSTM1/p62 complexes with the Atg homologue microtubule-associated protein light chain 3 (LC3) protein, which is converted from cytosolic LC3-I to LC3-II by Atg7 and Atg3, and targeted to the elongating autophagosome membrane. Detection of both SQSTM1/p62 and LC3-I/II are used experimentally to investigate cardiac autophagy in cells and tissues. Then, isolation membranes fuse and engulf damaged organelles and protein aggregates and formed autophagosome. In degradation step, autophagosomes fuse with lysosomes, which contains permeases and acid hydrolases and forming autophagolysosomes. Finally, this structure leads the degradation of intra-autophagosomal content due to acid hydrolases and permeases of lysosome[70-72] (Figure 1). Autophagy occurs constitutively at low levels under normal conditions in most cells, including cardiomyocytes. Defective autophagy results in the accumulation of protein aggregates and abnormal organelles which are toxic to the cell and lead to cell death[73]. However, it is known that autophagy is elevated under

nutrient and oxidative stress in I/R injury[74]. Number of known cardioprotective treatments have been shown to trigger autophagy including statins[75], lipopolysaccharide[76], resrevatrol[69] and sevoflurane[77]. Our research group previously have shown that IPC induces autophagy under normal conditions in adult rat hearts and that autophagy is necessary for cardioprotection by IPC[78]. Similarly, Rohailla *et al.* showed that remote IPC increased autophagy and decreased the expression of proteins related to mTOR in mice[79]. It is well established that activity of mTOR pathway modulates autophagy[80]. Starvation induces autophagy via inhibition of mTORC1 and it is suppressed in energy rich conditions, which is adaptive and accurately regulated. Nutrients and growth factors have a stimulating effect on mTORC1, which inhibits unc-51-like kinase 1 (ULK1), thereby suppressing autophagy[81] (Figure 1). During energy depletion, adenosine monophosphate (AMP) accumulates in the cell, which stimulates autophagy through AMP-activated protein kinase (AMPK) activation[82, 83]. Previous data suggests that mTOR signaling might be elevated while autophagy is diminished in the hearts of hyperlipidemic Yucatan pigs[84], and we have shown that in mice diet-induced obesity results in disturbed cardiac autophagy which is accompanied by increased myocardial injury after I/R[85].

Cardiac autophagy could be activated by various signals such as protein kinase C[86], reactive oxygen species (ROS)[72, 87], nitric oxide ($NO^{\bullet}$)[88] and it was shown that suppressed cardiac autophagy plays an important role in type 2 diabetes and in its complications[89], however, its effect on prediabetes and hypercholesterolemia has not been well-studied yet.

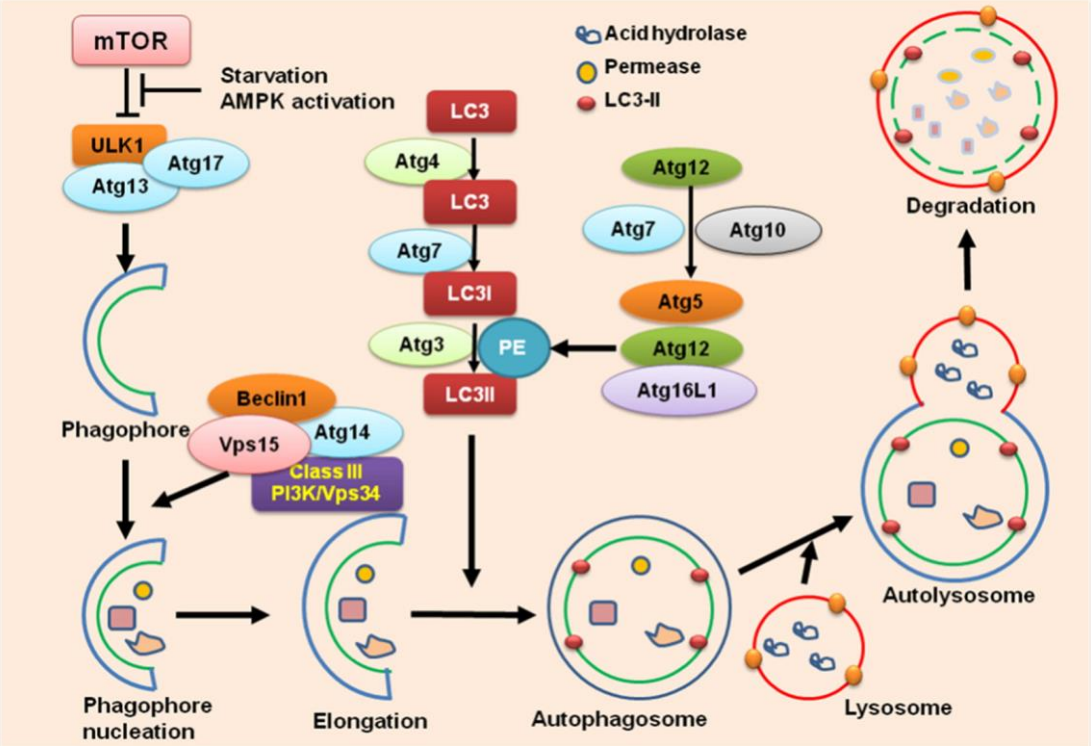

Figure 1. Schematic representation of autophagic process.
Starvation or AMPK activation inhibits mTOR and induces isolation membrane (termed phagophore) formation via ULK1 and Beclin-1 complexes. During the nucleation and elongation steps of autophagy, senescent and/or dysfunctional intracellular materials are engulfed into phagophore, which grows to autophagosome. Formation of Atg5/Atg12/Atg16L1 complex, and then LC3-I/LC3-II transformation have a pivotal role in the development of autophagosome. Finally, autophagosome fuses with lysosome to generate autolysosome, where its contents are degraded by lysosomal enzymes such as acid hydrolases and permeases. AMPK, AMP-activated protein kinase; ULK1, unc-51-like kinase 1; mTOR, mechanistic target of rapamycin; Atg, autophagy-related protein; Class-III PI3K, class-III phosphatidylinositol-3-kinase; LC3, microtubule-associated protein light chain 3; PE, phosphatidylethanolamine. Figure was adopted from Mei et al. 2015[71].

3.2.3 Cardiac cell death pathways

Insufficient autophagy can promote programmed cell death, for example apoptosis[72, 90], which results in cardiac damage[91]. Apoptosis is an evolutionary conserved and highly regulated process of programmed cell death, which plays a key role in the maintenance of the balance between cell proliferation and cell death under physiological conditions via activation of caspases[91, 92].

Furthermore, apoptosis changes in different pathologies such as cancer[93], neurodegenerative diseases for instance Alzheimer's disease[92] or I/R injury of the heart[94].

Necrosis is another type of cell death, which is characterized by loss of plasma membrane integrity, and reduced adenosine triphosphate (ATP) levels in cells[95]. Apoptosis and necrosis can be divided into two main pathways: the extrinsic pathway involves cell surface death receptors while the intrinsic pathway utilizes the mitochondria and endoplasmic reticulum, which is regulated by Bcl-2 family[95].

Besides apoptosis and necrosis, necroptosis (programmed necrosis) is another type of programmed cell death process, which occurs upon stimulation of death receptors in the absence of caspase-8 activation[96, 97]. Disturbances in cellular energetics, excessive reactive oxygen species production or metabolic changes have been shown to elicit necroptosis and apoptosis (Figure 2)[97-100]. It has been shown that apoptosis is upregulated in the hearts of hamsters on hypercholesterolemic diet[98]. Furthermore, it was also demonstrated that tumor necrosis factor alpha (TNFα)-induced oxidative stress increased necroptosis in parallel with autophagy[101] and that suppression of autophagy flux contributes to RIP1-RIP3 interaction and necroptosis of cardiomyocytes[102]. However, there is no information about hyperlipidemia-induced necroptosis and its connection with apoptotic and autophagic processes in the heart. Therefore, we hypothesized that hypercholesterolemia may also increase activation of pro-death pathways such as apoptosis and necroptosis in the rat heart.

In fully developed diabetes, increased level of cardiac apoptosis has been found[103]. It was also demonstrated that apoptosis and necrosis was increased in ischemic and non-ischemic human diabetic myocardium[104].

It has been shown that activated apoptosis has an important role in diabetes[105, 106], which could be connected to an impaired mitochondrial function[107] and autophagy[105, 108]. Moreover, apoptosis can lead to an imbalance in the calcium homeostasis, which could mediate contractile dysfunction in diabetic cardiomyopathy[109], however, the role of cardiac apoptosis and necroptosis in hypercholesterolemia and prediabetes is still unclear.

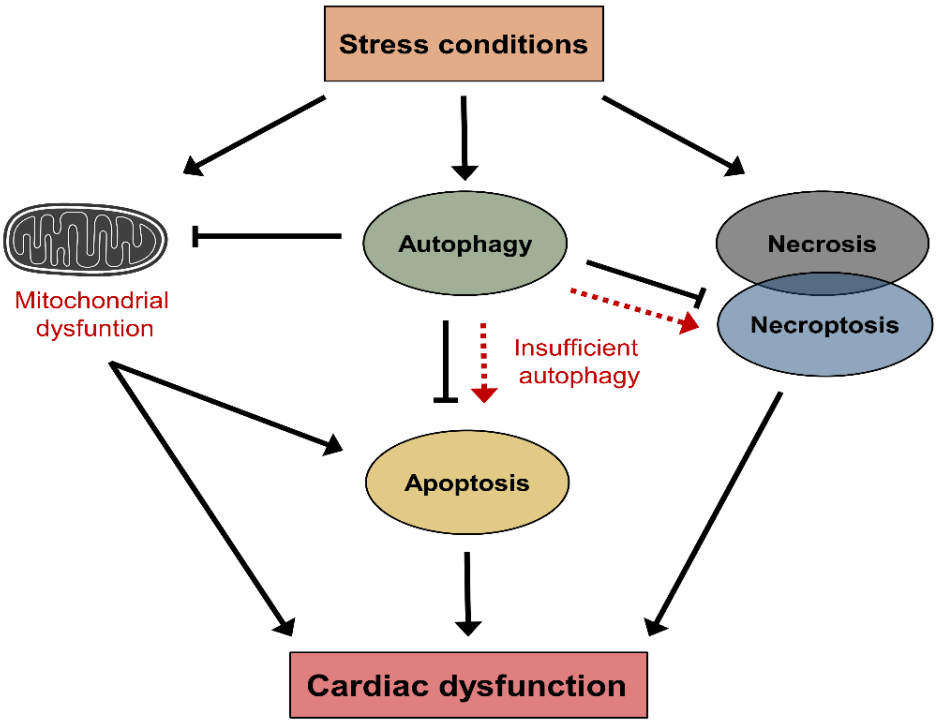

Figure 2. Schematic representation of stress-induced cell responses.
Stress conditions such as ischemia or nutrition stress can lead to cellular damage through the induction of mitochondrial dysfunction and activation of cell death pathways (i.e., necrosis). During stress conditions, autophagy can also be activated which prevents further cellular damages by the elimination of damaged organelles. However, insufficient autophagy may lead to cell death through the induction of cardiac apoptosis or necroptosis, which could be associated with cardiac dysfunction.

3.3 Cardiac mitochondria in metabolic diseases

3.3.1 Mitochondrial oxidative stress

It is well-established that mitochondria are "cellular engines", which are responsible for normal energy status and homeostasis of the heart. However, stress stimuli such as I/R-induced oxidative stress and Ca^{2+} signal open mitochondrial permeability transition pore (mPTP) and activates the intrinsic pathway of cell death[95]. Therefore, oxidative metabolism of mitochondria has an important role in both physiological and pathophysiological processes[110, 111].

In the myocardium, the number and size of the mitochondria are very high due to the high demand of ATP. The ATP is formed by oxidative phosphorylation. During the oxidative phosphorylation, ROS or reactive nitrogen species (RNS) are also formed,

which are toxic byproducts of mitochondria. The most common forms of free radicals are identified in the human heart including superoxide anion ($O_2^{\bullet -}$), the hydroxyl radical ($OH^{\bullet}$), hydrogen peroxide (H_2O_2), singlet oxygen, peroxynitrite ($ONOO^-$) and $NO^{\bullet}$[112]. Mitochondria is a major source of ROS in I/R[113]. In cellular stress, ROS can be formed by mitochondrial electron transport damage and uncoupling, nicotinamide adenine dinucleotide phosphate (NADPH) oxidase, uncoupled nitric oxide synthase (NOS), xanthine oxidase, cytochrome P450 monooxygenase, and cyclooxygenase, while activities of endogenous free radical scavenging enzymes such as superoxide dismutase (SOD), glutathione peroxidase GPx and catalase (CAT) are lower in the mitochondria[114]. The highly reactive radicals damage mitochondrial and cellular DNA, proteins, lipids, which could lead to mitochondrial dysfunction.

Reactive oxygen and nitrogen species production are increased in metabolic derangements such as obesity[115], hyperglycemia, hyperlipidemia, hyperinsulinemia, and insulin resistance which characterize type 2 diabetes[112]. Thus, mitochondria have pivotal role in these metabolic disorders including obesity and type 2 diabetes[110, 116-119], however, their status and effect is less understood in prediabetes.

3.3.2 Mitochondrial dynamics and quality control

Mitochondria are highly dynamic and interconnected organelles, their morphology and size change continuously. To adapt to changes in the intracellular environment due to stress conditions (*i.e.,* ischemic insult)[120], mitochondria are constantly undergo fusion and fission, which is termed mitochondrial dynamics[121]. Mitochondrial turnover, including mitochondrial dynamics, biogenesis, and mitophagy has essential role in mitochondrial quality control, shape, connectivity, cellular redox state and cell death (Figure 3)[121].

Mitochondrial biogenesis results in increased individual mitochondrial mass and copy number of mitochondria. The process is influenced by various factors such as caloric restriction, low temperature, oxidative stress and cell division[116, 122]. Peroxisome proliferator-activated receptor gamma coactivator 1-alpha (PGC-1α) is the master regulator of mitochondrial biogenesis, which activates various transcription factors, including nuclear respiratory factor 1 and 2 (NRF1-2), mitochondrial transcription factor A (TFAM) and dimethyladenosine transferase 1 (TFBM)[122, 123]. It was demonstrated that

mitochondrial biogenesis was impaired in diabetes[124] and obesity[125] due to decreased expression of PGC-1α. Furthermore, testicular level of PGC-1α was also decreased, while NRF1 and NRF2 was not altered in prediabetic rats[126].

Fusion results in interconnected mitochondrial network and leads to the elongation of mitochondria. This process needs mitochondrial fusion proteins including mitofusin 1 (MFN1) and 2 (MFN2) which are localized in the outer mitochondrial membrane and optic atrophy 1 protein (OPA1), which is localized in the inner mitochondrial membrane[120]. It was shown previously that lack of MFN1 and MFN2 resulted in a rapid lethal cardiac failure in MFN1/MFN2 double knockout mice, suggesting that the mitochondrial fusion events have essential role in cardiac homeostasis[127].

During fission mitochondria become smaller and more fragmented. Fission has an important role in increased number of mitochondria, translocation of mitochondria to daughter cells during mitosis as well as if damaged mitochondria needs to be removed by mitophagy[128]. As the first step of fission, dynamin-related protein 1 (DRP1) is recruited from cytosol to the outer mitochondrial membrane. Then, DRP1 translocation leads to formation of smaller, fragmented daughter mitochondria and the sequestration of damaged parts[129]. Furthermore, mitochondrial fission 1 protein (FIS1) has also important role in fission, which anchors to the outer mitochondrial membrane as a receptor for DRP1[130].

It was evidenced that stress conditions like ischemia[131], depolarization[132] or highly elevated production of ROS[133] can trigger mitochondrial fission, due to depolarization of mitochondrial membrane. Since the healthy daughter mitochondria with normal membrane potential can merge by mitochondrial fusion, the survival of interconnected mitochondrial network is ensured[120].

Impaired daughter mitochondria can be eliminated by mitophagy after mitochondrial fission. Mitophagy is a specific form of autophagy, which eliminates damaged or senescent mitochondria from the cell[134]. It was evidenced that MFN2 has important role to recruit Parkin to the outer mitochondrial membrane and induce Parkin-, LC3-, and SQSTM1/p62-mediated mitophagy[135]. Since mitochondrial function is heavily influenced by mitochondrial dynamics including mitochondrial biogenesis, fusion, fission, and autophagy-mitophagy (Figure 3), and since these processes have been linked to the development of diabetic cardiomyopathy[105, 106, 108, 136], we hypothesized that altered

mitochondrial dynamics might be involved in the mechanism of deteriorated cardiac functions in prediabetes.

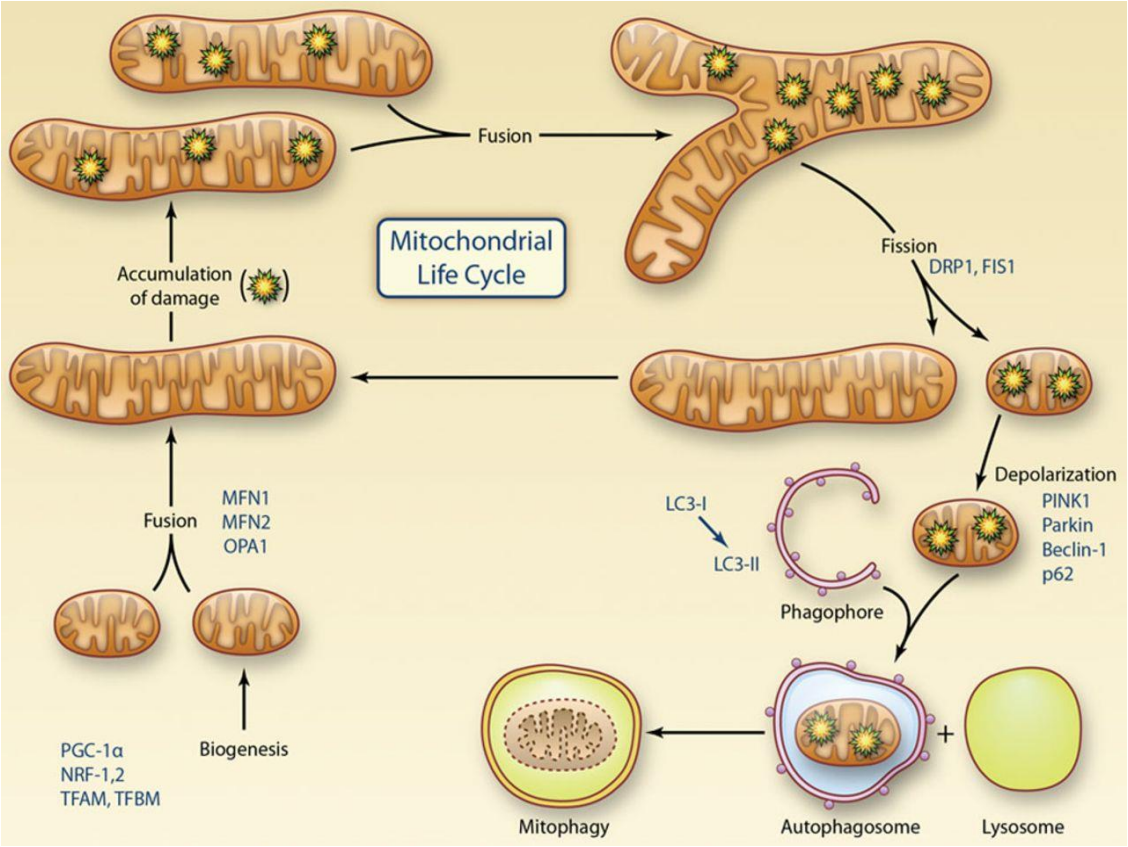

Figure 3. Representation of the mitochondrial life cycle including the role of mitochondrial dynamics and mitophagy in quality control.
Mitochondrial biogenesis is regulated by PGC-1α, which activates transcriptional factors including NRF-1 and 2, TFAM and TFBM. Mitochondria undergo cycles of fusion (mediated by MFN1, MFN2, and OPA1) to form elongated mitochondrial networks and fission (mediated by DRP1 and FIS1) to form smaller individual organelles. After the fission, isolated and damaged components are eliminated by mitophagy. In the activation of mitophagy, PINK1, Parkin, Beclin-1, SQSTM1/p62 and LC3 play an important role to remove damaged mitochondria from the cell. PGC-1α, peroxisome proliferator-activated receptor gamma coactivator 1-alpha; NRF1-2, nuclear respiratory factor 1 and 2; TFAM, mitochondrial transcription factor A; TFBM, dimethyladenosine transferase 1; MFN 1-2, mitofusin 1 and 2; OPA1, optic atrophy 1 protein; DRP1, dynamin-related protein 1; FIS1, mitochondrial fission 1 protein; SQSTM1/p62, sequestosome 1. Figure was adapted from Kluge et al. 2013[137].

3.3.3 Morphological and functional properties of mitochondrial subpopulations in the heart

There are three distinct fractions of cardiac and skeletal muscle mitochondria according to their subcellular localization. Subsarcolemmal mitochondria (SSM), which are located near the sarcolemma, interfibrillar mitochondria (IFM), which are situated among myofibrils, and perinuclear mitochondria (PNM), which are clustered around the nucleus (Figure 4)[138]. It was previously shown that these fractions are different in morphology: SSM have lamelliform cristae while most of IFM show tubular cristae[139]. Additionally, it has been described in transmission electron microscopic studies that IFM and PNM have similar size and distribution in cardiomyocytes[140, 141]. Furthermore, SSM and IFM are different in respiratory rates and mitochondrial enzyme activities[142, 143]. In contrast, functional or proteomics data on PNM have not been published to date. SSM and IFM differ in function under pathophysiological conditions. For example, aging decreases the rate of oxidative phosphorylation only in IFM[144], and functional differences between SSM and IFM have been shown with high-fat diet[145] and diabetes[146].

Although functional properties of SSM and IFM are well-described, differences in their protein constitution are less studied. Previously, we showed that connexin 43 (Cx43) is located predominantly in SSM[147], and mitofilin level is higher in IFM[148]. Furthermore, the rate of mitochondrial protein synthesis is different in SSM and IFM[148, 149]. Despite these reports, the biology behind the proteomic differences is largely unknown, and a specific protein marker that allows the identification of mitochondrial subfractions has not been identified yet.

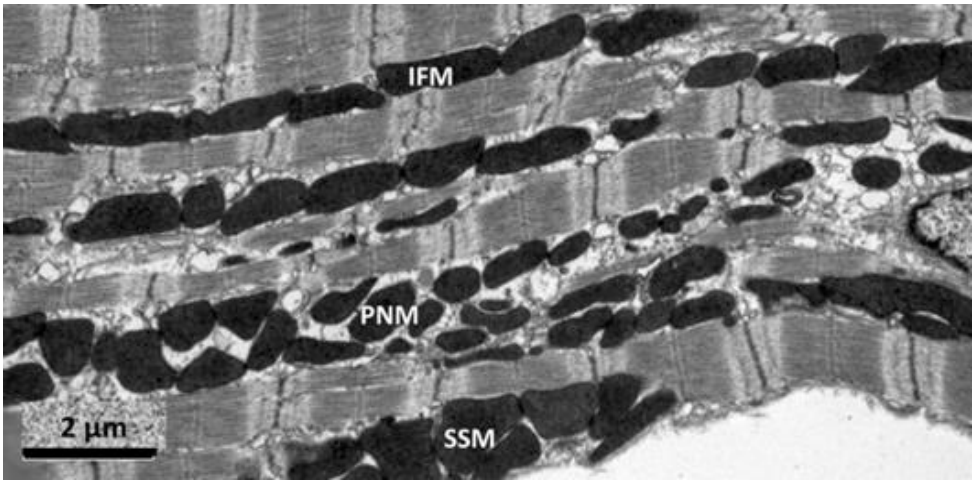

Figure 4. Representative electron micrograph of mitochondrial subfractions from murine heart. *SSM, subsarcolemmal mitochondria; IFM, interfibrillar mitochondria, PNM, perinuclear mitochondria. Figure was adapted from Ong et al. 2013*[150].

3.3.4 Mitochondrial isolation with nagarse - methodological obstacles in cardiac mitochondrial studies

Differentiation between IFM and SSM in biochemical assays depends on the use of different isolation methods. Palmer and colleagues demonstrated first that SSM could be isolated via homogenization by a Polytron method, while IFM could be extracted from cardiac tissue only with additional protease treatment. For the release of IFM from the myofibrils, trypsin[145, 146], proteinase K[151, 152], or most commonly nagarse[144, 147, 153, 154] treatments are used. Nagarse is a bacterial serine-type endopeptidase (EC: 3.4.21.62), which is a member of the subtilisin family[155, 156] with practically no substrate specificity. Other than enzymatic digestion, a method with mechanical disruption has also been described for the isolation of SSM, however, it is rarely referenced[157, 158].

Although the use of proteases is necessary for the isolation of IFM by the most widely accepted method, enzymatic digestion with bacterial proteases might influence the mitochondrial protein content and/or mitochondrial function. It was recently shown that nagarse treatment significantly influenced mitochondrial respiration and enzyme activity of SSM isolated from mouse skeletal muscle[156], however, the effect of nagarse on cardiac mitochondrial proteins has not been studied in detail. Thus, one of the goals of this thesis was to examine, whether the nagarse-based method for the isolation of IFM affects the detection of mitochondrial proteins in cardiac mitochondrial subfractions.

4 Aims

The role of hypercholesterolemia and prediabetes including their molecular aspects in cardiovascular system is still not well-investigated. Furthermore, we hypothesized that nagarse treatment may influence the quantification of specific mitochondrial proteins in our animal models. Therefore, our aims were the follows:

- To investigate the status of autophagy and mTOR and examine apoptosis and necroptosis pathways in a hypercholesterolemic rat model.
- To characterize functional, morphological and molecular features of a diet-induced prediabetes model in rats.
- To investigate the effect of prediabetes on the cardiovascular system.
- To examine whether the nagarse-based method for the isolation of IFM affect the detection of mitochondrial proteins in cardiac mitochondrial subfractions.

5 Materials and methods

These studies conform to the Guide for the Care and Use of Laboratory Animals published by the US National Institutes of Health (NIH publication No. 85–23, revised 1996) and was approved by the animal ethics committee of the Semmelweis University, Budapest, Hungary (registration numbers: XIV-I-001/450-6/2012) or animal welfare office of the Justus-Liebig University, Giessen, Germany. Chemicals were purchased from Sigma, St. Louis, MO, USA unless otherwise noted.

5.1 Animal models and experimental designs

5.1.1 Animal model of hypercholesterolemia

To investigate the effect of hypercholesterolemia, six-weeks-old male Wistar rats (Crl:WI Strain Code: 003; Charles River Laboratories) were fed with control chow (NORM; n=9) or chow enriched with 2% cholesterol and 0.25% cholic acid (CHOL; n=9) for 12 weeks (Figure 5). Animals were allowed to food and water *ad libitum* and chow was changed daily. After the feeding period, body weight of animals were measured and they were anesthetized with diethyl ether and given 500 U/kg heparin i.v. Blood sample (500 μL) was taken from tail vein for further experiments. Hearts were excised and perfused with Krebs-Henseleit buffer according to Langendorff at 37 °C for 10 min as previously described[159]. Hearts were taken and snap-frozen for further biochemical assays.

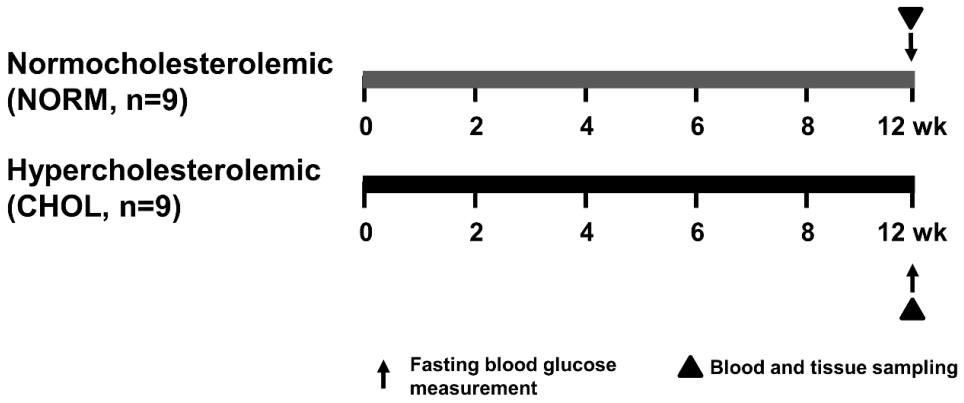

Figure 5. Experimental protocol for assessing the effect of hypercholesterolemia in vivo. *Fasting blood glucose, TG and cholesterol were measured at week 12. Tissue sampling was performed after terminal procedures. NORM, normocholesterolemic; CHOL, hypercholesterolemic.*

5.1.2 Animal model of prediabetes

To characterize a prediabetic animal model, male Long-Evans rats of 5-7 weeks of age were purchased from Charles River Laboratories. Animals were housed in a room maintained at 12 h light-dark cycles and constant temperature of 21 °C. Animals were allowed to food and water *ad libitum*. After one week of acclimatization rats were divided into two groups: control (CON; n=20) and prediabetic group (PRED; n=20) (Figure 6). The control group was fed control chow, while the prediabetic group was fed a chow supplemented with 40% lard as a high-fat diet. Body weights were measured weekly. Blood was taken and fasting blood glucose levels were measured from the saphenous vein every second week with a blood glucose monitoring system (Accu-Check, Roche). To facilitate the development of prediabetes and, animals on high-fat diet received 20 mg/kg streptozotocin (STZ, Santa Cruz Biotechnology) intraperitoneally (i.p.) at the fourth week of the diet according to Mansor *et al.*[160], while the control group was treated with same volume of ice-cold citrate buffer as vehicle. At the 20th week oral glucose tolerance test (OGTT) was performed in overnight fasted rats with per os administration of 1.5 g/kg glucose and measurements of plasma glucose levels at 15, 30, 60 and 120 minutes. Insulin tolerance test (ITT) was also performed at week 20 in overnight fasted rats. Insulin (0.5 IU/kg, Humulin R, Ely Lilly) was injected i.p. and plasma glucose levels were checked at 15, 30, 45, 60, 90 and 120 minutes. At week 21 of the diet, animals were anesthetized

with pentobarbital (60 mg/kg, i.p., Euthasol, Produlab Pharma). Echocardiography and cardiac catheterization were performed, then hearts were excised, shortly perfused with oxygenated Krebs-Henseleit buffer in Langendorff mode as described earlier and heart weights were measured. Epididymal and interscapular brown fat tissue, which are the markers of adiposity[161, 162], were isolated and their weights were measured. Blood and tissue samples were collected and stored at -80 °C.

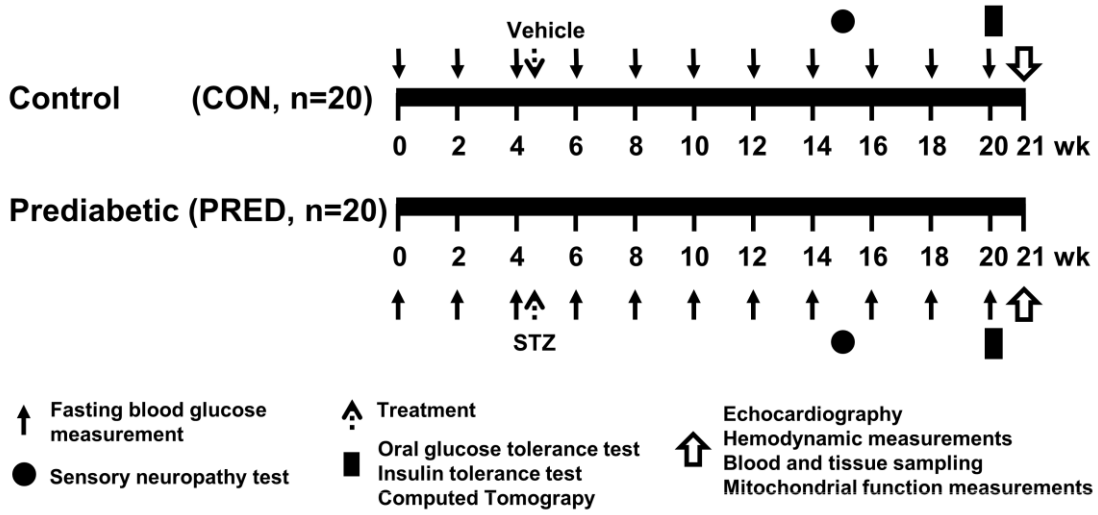

Figure 6. Experimental protocol for assessing the effect of prediabetes in vivo.
Long-Evans rats were fed with either CON diet for 21 weeks, or with high-fat diet and treated with 20 mg/kg STZ at week 4 to induce prediabetes (PRED). Body weights were measured weekly and blood samples were taken from the saphenic vein every second week. Sensory neuropathy was measured at week 15. OGTT, ITT and CT were performed at week 20. Echocardiography, hemodynamic analysis and parameters of mitochondrial function were measured at week 21 of diet. Tissue sampling was performed after terminal procedures. CON, control; PRED, prediabetic; STZ, streptozotocin; OGTT, oral glucose tolerance test; ITT, insulin tolerance test; CT, computer tomography.

5.1.3 Animal model to investigate the effect of nagarse on mitochondrial subfractions

To investigate the effect of nagarse on cardiac mitochondrial subfractions, 10-12 weeks old male C57Bl6J mice (25-30 g, Janvier, Le Genest-Saint-Isles, France) and 8-10 weeks old male Wistar Han rats (300-350 g, Janvier) were used. Animals were kept in dark/light cycles of 12 h each and had free access to standard chow and drinking water. Mice were anaesthetized with 5% isoflurane and sacrificed by cervical dislocation. Rats were anaesthetized with 4% isoflurane, subsequently hearts were removed, and cardiac tissue was collected.

5.2 Assessment of sensory neuropathy

To test if sensory neuropathy develops in prediabetes, plantar Von Frey test was performed on Long-Evans rats. At week 15 of the diet, rats were placed in a plastic cage having a wire mesh bottom to allow full access to the paws. After 5-10 min acclimation time, mechanical hind paw withdrawal thresholds were measured by a dynamic plantar aesthesiometer (UGO-Basile) as previously described[163].

5.3 Evaluation of body fat content

At week 20 of the diet, computer tomography (CT) measurements were performed on NanoSPECT/CT PLUS (Mediso) on Long-Evans rats. The semicircular CT scanning was acquired with 55 kV tube voltage, 500 ms of exposure time, 1:4 binning and 360 projections in 18 minutes 7s. During the acquisitions, rats were placed in prone position in a dedicated rat bed, and were anesthetized with 2% isoflurane in oxygen. Temperature of the animals was kept at 37.2±0.3 °C during imaging. In the reconstruction, 0.24 mm in-plane resolution and slice thickness were set and Butterworth filter was applied (volume size: 76.8*76.8*190 mm). Images were further analyzed with VivoQuant (inviCRO LLC) dedicated image analysis software products by placing appropriate Volume-of-Interests (VOI) on the whole body fat of animals. The aim of segmentation was to separate the fat from other tissues. The connected threshold method helped to choose the adequate attenuated pixels for fat tissue analysis, then the isolated points were detected by erode 4 voxel and dilate 4 voxel steps. After the measurements animals recovered from anesthesia.

5.4 Cardiac function by echocardiography

Before euthanasia, to measure cardiac function on Long-Evans rats, echocardiography was performed as previously described[164, 165]. Briefly, anesthetized animals were placed on a controlled heating pad, and the core temperature, measured via rectal probe, was maintained at 37 °C. Transthoracic echocardiography was performed in supine position by one investigator blinded to the experimental groups. Two dimensional and M-mode echocardiographic images of long and short (mid-papillary muscle level) axis were

recorded, using a 13 MHz linear transducer (GE 12L-RS, GE Healthcare), connected to an echocardiographic imaging unit (Vivid I, GE Healthcare). The digital images were analyzed by a blinded investigator using an image analysis software (EchoPac, GE Healthcare). On two dimensional recordings of the short-axis at the mid-papillary level, left ventricular (LV) anterior (LVAWT) and posterior (LVPWT) wall thickness in diastole (index: d) and systole (index: s), left ventricular end-diastolic (LVEDD) and end-systolic diameter (LVESD) were measured. In addition, end-diastolic and end-systolic LV areas were planimetered from short and long axis two dimensional recordings. End-systole was defined as the time point of minimal left ventricular dimensions, and end-diastole as the time point of maximal dimensions. All values were averaged over three consecutive cycles. The following parameters were derived from these measurements[166]. Fractional shortening (FS) was calculated as ((LVEDD-LVESD)/LVEDD)×100. LV mass was calculated according to the following formula: [LVmass=(LVEDD+AWTd+PWTd)3-LVEDD3×]1.04×0.8+0.14.

5.5 Hemodynamic measurements, left ventricular pressure-volume analysis

After echocardiographic measurements, hemodynamic measurement was performed on Long-Evans rats as previously described[167, 168]. Briefly, rats were tracheotomized, intubated and ventilated, while core temperature was maintained at 37 °C. A median laparotomy was performed. A polyethylene catheter was inserted into the left external jugular vein. A 2-Fr microtip pressure-conductance catheter (SPR-838, Millar Instruments) was inserted into the right carotid artery and advanced into the ascending aorta. After stabilization for 5 min, mean arterial blood pressure (MAP) was recorded. After that, the catheter was advanced into the LV under pressure control. After stabilization for 5 min, signals were continuously recorded at a sampling rate of 1,000/s using a Pressure-Volume (P-V) conductance system (MPVS-Ultra, Millar Instruments) connected to the PowerLab 16/30 data acquisition system (AD Instruments), stored and displayed on a personal computer by the LabChart5 Software System (AD Instruments). After positioning the catheter baseline P-V loops were registered. With the use of a special P-V analysis program (PVAN, Millar Instruments), LV end-systolic pressure (LVESP),

LV end-diastolic pressure (LVEDP), the maximal slope of LV systolic pressure increment (dP/dtmax) and diastolic pressure decrement (dP/dtmin), time constant of LV pressure decay (τ; according to the Glantz method), ejection fraction (EF) stroke work (SW) and LV maximal power were computed and calculated. Stroke volume (SV) and cardiac output (CO) were calculated and corrected according to *in vitro* and *in vivo* volume calibrations using the PVAN software. Total peripheral resistance (TPR) was calculated by the following equation: TPR=MAP/CO. In addition to the above parameters, P-V loops recorded at different preloads can be used to derive other useful systolic function indexes that are less influenced by loading conditions and cardiac mass[169, 170]. Therefore, LV P-V relations were measured by transiently compressing the inferior vena cava (reducing preload) under the diaphragm with a cotton-tipped applicator. The slope of the LV end-systolic P-V relationship (ESPVR; according to the parabolic curvilinear model), preload recruitable stroke work (PRSW), and the slope of the dP/dtmax - end-diastolic volume relationship (dP/dtmax-EDV) were calculated as load-independent indexes of LV contractility. The slope of the LV end-diastolic P-V relationship (EDPVR) was calculated as a reliable index of LV stiffness[170]. At the end of each experiment, 100 μL of hypertonic saline were injected intravenously, and from the shift of P-V relations, parallel conductance volume was calculated by the software and used for the correction of the cardiac mass volume. The volume calibration of the conductance system was performed as previously described[170].

5.6 Adipokine array from rat plasma

Adipokine array was performed from 1 mL plasma from Long-Evans rats according to manufacturer's instructions (Proteome Profiler Rat Adipokine Array Kit, R&D Systems).

5.7 Biochemical measurements

Serum cholesterol, high density lipoprotein (HDL) and triglyceride levels were measured in Long-Evans rats and glucose, cholesterol and triglyceride levels were measured from plasma of NORM and CHOL Wistar rats by colorimetric assays (Diagnosticum) as previously described[171]. Plasma leptin (Invitrogen), TIMP

metallopeptidase inhibitor 1 (TIMP-1; R&D System) and angiotensin-II (Phoenix pharmaceuticals) were measured by enzyme-linked immunosorbent assay (ELISA) according to manufacturer's instructions. Urea, glutamate oxaloacetate transaminase (GOT), glutamate pyruvate transaminase (GPT), low density lipoprotein (LDL), C-reactive protein (CRP), cholesterol, uric acid and creatinine were measured by automated clinical laboratory assays (Diagnosticum).

5.8 Histology

Heart, liver and pancreas samples from Long-Evans rats were fixed in 4% neutral-buffered formalin. After 24 hours, samples were washed with phosphate buffered saline (PBS) and stored in 70% ethanol in PBS until embedded in paraffin. Samples were stained with hematoxylin-eosin (HE) and Masson's trichrome (MA) staining. Left ventricle samples were analyzed to examine histopathological differences and evaluate cardiomyocyte hypertrophy and fibrosis. The level of fibrosis was measured on MA-stained LV sections, and transverse transnuclear width (cardiomyocyte diameter) was assessed on longitudinally oriented cardiomyocytes on HE-stained LV sections by a Zeiss microscope (Carl Zeiss). Digital images were acquired using an imaging software (QCapture Pro 6.0, QImaging) at 20× magnification. Quantification of cardiomyocyte diameter and fibrosis was performed with ImageJ Software (v1.48, NIH, Bethesda). Liver samples were evaluated for hepatic steatosis/fibrosis and scored as previously described [172].

5.9 Nitrotyrosine immunostainig of left ventricular samples

Nitrotyrosine levels were also investigated from Long-Evans rat left ventricles. After embedding and cutting 5 μm thick sections, heat-induced antigen epitope retrieval was performed (95 °C, 10 min, in citrate buffer with a pH of 6.0). Sections were stained with rabbit polyclonal anti-nitrotyrosine antibody (5 μg/mL, Cayman Chemical) by using the ABC-kit of Vector Laboratories (Burlingame) according to the manufacturer's protocol. Nitrotyrosine-stained sections were counterstained with hematoxylin. Specific staining was visualized and images were acquired using a BX-41 microscope (Olympus).

5.10 Quantitative RT-PCR

Total RNA was isolated from Long-Evans rat LV tissue with ReliaprepTM RNA Tissue Miniprep kit (Promega) according to the manufacturer's instructions. cDNA was synthesized using Tetro cDNA Synthesis Kit (Bioline) according to the manufacturer's protocol. PCR reaction was performed with iQ SYBR Green Supermix (Bio-Rad), or TaqMan Universal PCR MasterMix (Thermo Fisher Scientific) and 3 nM forward and reverse primers for collagen type 1 and 3 (COL1 and COL3), atrial natriuretic peptide (ANP), brain natriuretic peptide (BNP) (Integrated DNA Technologies), assay mixes for α-myosin heavy chain (α-MHC, assay ID: Rn00691721_g1), β-myosin heavy chain (β-MHC, assay ID: Rn00568328_m1), TNF-α (assay ID: Rn99999017_m1) and interleukin-6 (IL-6, assay ID: Rn01410330_m1, Thermo Fisher Scientific) were used. Beta-2 microglobulin (B2M) or glyceraldehyde-3-phosphate dehydrogenase (GAPDH; reference gene; assay ID: Rn01775763_g1) were used as reference genes. Quantitative real-time PCR was performed with the StepOnePlus Real-Time PCR System (Thermo Fisher Scientific). Expression levels were calculated using the cycle threshold (CT) comparative method ($2^{-\Delta CT}$).

5.11 Measurement of pancreatic insulin

Freeze clamped and pulverized pancreas samples from Long-Evans rats were used to determine pancreatic insulin content. Analysis was performed with Insulin (I-125) IRMA Kit (Izotop Kft) according to the manufacturer's instructions.

5.12 Electron microscopy

Left ventricular tissue samples (1×1 mm) from Long-Evans rats were placed in modified Kranovsky fixative (2% paraformaldehyde, 2.5 % glutaraldehyde, 0.1 M Na-cacodylate buffer, pH 7.4 and 3mM $CaCl_2$). After washing in cacodylate buffer, samples were incubated in 1% osmium tetroxide in 0.1 M PBS for 35 min. Then samples were washed in buffer several times for 10 minutes and dehydrated in an ascending ethanol series, including a step of uranyl acetate (1%) solution in 70% ethanol to increase contrast. Dehydrated blocks were transferred to propylene oxide before being placed into

Durcupan resin. Blocks were placed in thermostat for 48 h at 56 °C. From the embedded blocks, 1 μm-thick semithin and serial ultrathin sections (70 nm) were cut with a Leica ultramicrotome, and mounted either on mesh, or on Collodion-coated (Parlodion, Electron Microscopy Sciences) single-slot copper grids. Additional contrast was provided to these sections with uranyl acetate and lead citrate solutions, and they were examined with a JEOL1200EX-II electron microscope. Areas of subsarcolemmal (SSM), interfibrillar mitochondria (IFM) and lipid droplets were measured by free hand polygon selection in iTEM Imaging Platform.

5.13 Mitochondrial enzyme activity measurements

Fresh myocardial samples were homogenized from Long-Evans rats in 1/30 weight per volume Chappel-Perry buffer (100 mM KCl, 5 mM $MgCl_2$, 1 mM EDTA, 50 mM Tris, pH: 7.5) supplemented with 15 mg/L trypsine-inhibitor, 15.5 mg/L benzamidine, 5 mg/L leupeptin and 7 mg/L pepstatin A. All enzyme activities were measured as duplicates with a photometer (Cary 50 Scan UV-Visible Spectrophotometer, Varian). Before adding substrate or cofactor, the reaction mix was incubated at 30 °C for 10 min (except for cytochrome c oxidase). Enzyme activities were expressed relative to citrate synthase activity or total protein levels (measured with Bicinchoninic Acid assay). The activity of rotenone-sensitive NADH:ubiquinone-oxidoreductase (Complex I) was measured at 340 nm in the presence of 1 mM EDTA, 2.5 mM KCN, 1 μM antimycin A and 20 μM rotenone after adding coenzyme Q and NADH to a final concentration of 60 μM. The activity of NADH:cytochrome c-oxidoreductase (Complex I+III) was measured at 550 nm as the antimycin A- and rotenone-sensitive fraction of total NADH-cytochrome c oxidoreductase in the presence of 0.1 mM EDTA, 3 mM KCN and 0.1% cytochrome c after adding NADH to a final concentration of 0.2 mM. The activity of succinate:cytochrome c-oxidoreductase (Complex II+III) was measured at 550 nm in the presence of 0.1 mM EDTA, 2.5 mM KCN, 0.1% bovine serum albumin and 4 mM succinate after adding cytochrome c to a final concentration of 0.1%. The activity of succinate-dehydrogenase was measured at 600 nm in the presence of 0.1 mM EDTA, 2.5 mM KCN, 0.1% bovine serum albumin and 2 mM succinate after adding 2,6-dichloroindophenol and phenazine-methosulfate to a final concentration of 34.9 μM and 1.625 mM, respectively. The activity of cytochrome c-oxidase was measured at 550 nm

in the presence of 0.08% reduced cytochrome c. The activity of citrate-synthase was measured at 412 nm in the presence of 0.1% triton-X 100, 0.1 mM 5,5'-dithiobis (2-nitrobenzoic acid), and 0.1 mM acetyl-coenzyme A after adding oxalacetate to a final concentration of 0.5 mM.

5.14 Preparation of isolated mitochondria

SSM and IFM fractions from Long-Evans and Wistar rat as well as C57Bl6J mouse left ventricles were isolated as described previously[147] with minor modification as shown in Figure 7. From both mouse and rat hearts, right ventricles (RVs) were taken as control tissue. This protocol follows essentially that published by Palmer *et al.*[142], and is referred to as the common protocol. All steps were performed at 4 °C. Briefly, left ventricular tissues were washed in buffer A (100 mM KCl, 50 mM 3-[N-Morpholino]-propanesulfonic acid (MOPS), 5 mM $MgSO_4$, 1 mM ATP, 1 mM EGTA, pH 7.4), weighed and subsequently minced with scissors in 10 mL buffer A per grams of tissue. Then, tissues were disrupted with a Polytron tissue homogenizer (Ika T25-Digital, 3 times 15 sec) and the homogenates were centrifuged for 10 min at 1000×g. The supernatants (containing SSM) were divided into 2 groups. One portion of SSM was used without nagarse and protease inhibitor treatment (SSM). Another portion of SSM was treated with 8 U/g of nagarse (SSM+N; Bacterial type XXIV) at 4 °C for 1 min. Sediments of the first centrifugation (containing IFM) were resuspended in buffer A (10 mL/g tissue) and were treated with 8 U/g of nagarse for 1 min. Then, 1 mM phenylmethylsulfonyl fluoride (PMSF) was added to one portion of IFM (IFM+N+I), whereas another portion was without PMSF (IFM+N). All mitochondrial samples were disrupted with a Potter-Elvejhem tissue homogenizer and were centrifuged for 10 min at 1000×g. The resulting supernatants were centrifuged for 10 min at 8000×g to collect the SSM and IFM. The mitochondria were resuspended in buffer A, and were centrifuged at 8000×g for 10 min, and finally resuspended in buffer B (in mM: sucrose 250; HEPES 10; EGTA 1; pH 7.4). The concentration of nagarse was the same as used in our previous studies[147, 173] and PMSF was added after 1 min incubation to modify only one parameter at a time. For Western blot analysis, mitochondria were further purified by layering them on top of a 30% Percoll solution in isolation buffer and subsequent ultracentrifugation at 35.000×g for 30 min at 4 °C. The lower mitochondrial band was collected, washed twice in isolation

Buffer B by centrifugation at 10.300×g for 10 min, and the purified mitochondria were stored at -80 °C.

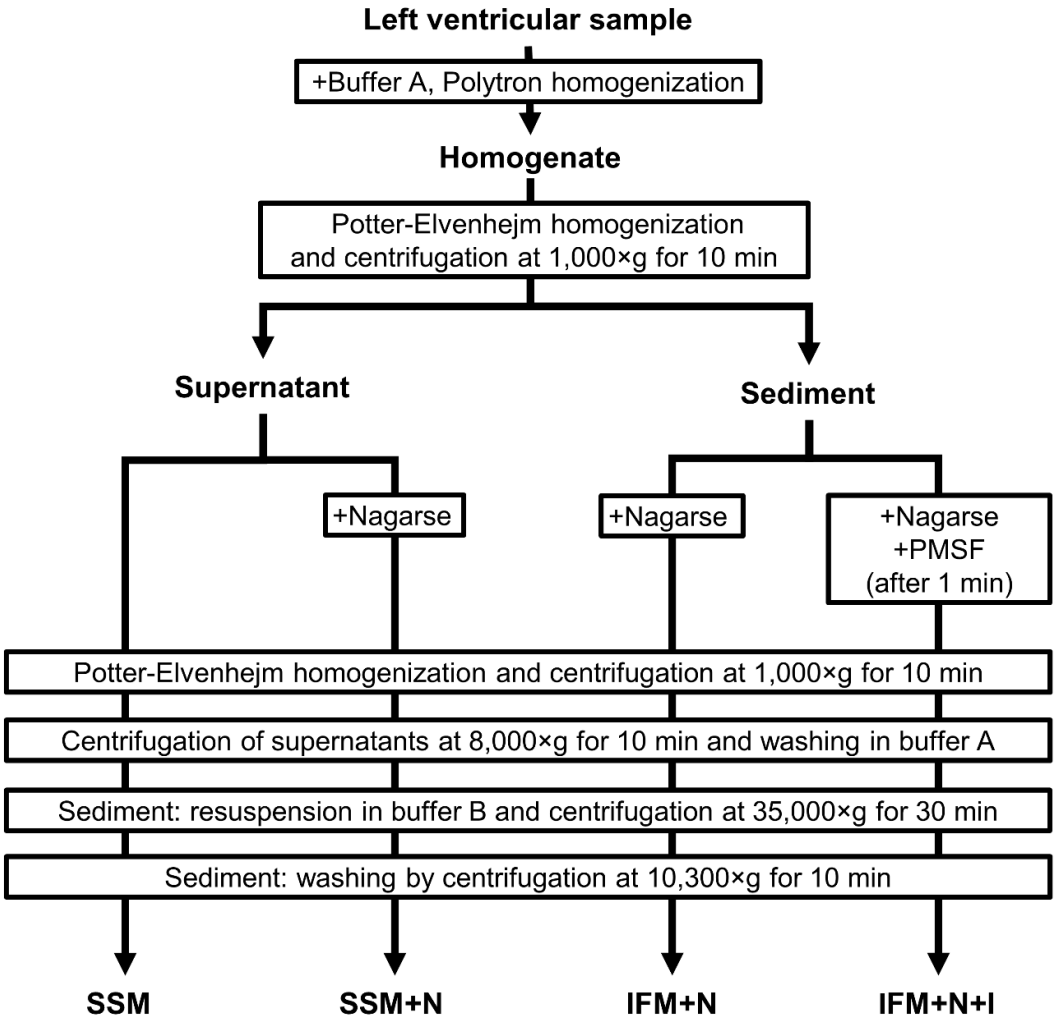

Figure 7. Schematic representation demonstrating the isolation of mitochondrial subfractions from Wistar rat and C57Bl6J mouse hearts.
PMSF, phenylmethylsulfonyl fluoride; SSM, subsarcolemmal mitochondria; SSM+N, subsarcolemmal mitochondria+nagarse; IFM+N, interfibrillar mitochondria+nagarse; IFM+N+I, interfibrillar mitochondria+nagarse+inhibitor (PMSF).

5.15 Measurement of mitochondrial respiration

Long-Evans rat cardiac mitochondria: protein concentration of SSM and IFM samples was determined by biuret method[174]. Mitochondrial oxygen consumption was measured by high-resolution respirometry with Oxygraph-2K (Oroboros Instruments) a Clark-type O_2 electrode for 40 min. The mitochondrial protein content was 0.1 mg/mL in the measurements. Measuring mitochondrial respiration followed the substrate-uncoupler-inhibitor titration (SUIT) protocol. Mitochondria were energized with 5 mM glutamate and 5 mM malate. Mitochondrial respiration was initiated with 2 mM adenosine diphosphate (ADP). Cytochrome c (4 μM), succinate (5 mM), rotenone (1 μM) and carboxyatractyloside (CAT; 2 μM) were used as indicated. Measurements were performed in an assay medium containing 125 mM KCl, 20 mM HEPES, 100 μM EGTA, 2 mM K_2HPO_4, 1 mM $MgCl_2$ and 0.025% BSA. Data were digitally recorded using DatLab4 software.

C57Bl6J mouse cardiac mitochondria: mitochondrial oxygen consumption was measured from samples obtained after the 8,000×g centrifugation; the subsequent ultracentrifugation step necessary to obtain pure mitochondria was omitted. Oxygen consumption of 100 μg/mL SSM, SSM+N, IFM+N, and IFM+N+I was measured with a Clark-type oxygen electrode (Oxygen meter 782, Strathkelvin) at 25 °C in incubation buffer (containing in mM: 125 KCl, 10 Tris (titrated with MOPS), 1.2 Pi (titrated with Tris), 1.2 $MgCl_2$, 0.02 EGTA (titrated with Tris), pH 7.4). Complex I-mediated respiration was analyzed in the presence of 5 mM glutamate and 2.5 mM malate, whereas complex II-mediated respiration was measured in the presence of 5 mM succinate and 2 μM rotenone. After recording of basal oxygen consumption, respiration was stimulated by the addition of 40 μM ADP. Oxygen consumption was expressed in nmol $O_2 \times min^{-1} \times mg\ protein^{-1}$).

5.16 Measurement of mitochondrial membrane potential

To detect mitochondrial membrane potential from Long-Evans rat left ventricles, we used the fluorescent, cationic dye, safranine O (2 μM) which can bind to the protein possessing negative charge in the inner mitochondrial membrane depending on the mitochondrial membrane potential. The excitation/emission wavelengths were 495/585

nm. Fluorescence was recorded at 37 °C by Hitachi F-4500 spectrofluorimeter (Hitachi High Technologies). The reaction medium was the following: 125 mM KCl, 20 mM HEPES, 100 μM EGTA, 2 mM K_2HPO_4, 1 mM $MgCl_2$ and 0.025% BSA.

5.17 Detection of H_2O_2 formation in mitochondria

H_2O_2 production of SSM and IFM from Long-Evans left ventricles was assessed by Amplex UltraRed fluorescent dye method[175]. Horseradish peroxidase (2.5 U/mL) and Amplex UltraRed reagent (1 μM), then 0.05 mg/mL mitochondria were added to the incubation medium. H_2O_2 formation was initiated by the addition of 5 mM glutamate and 5 mM malate or 5 mM succinate and fluorescence was detected at 37 °C with Deltascan fluorescence spectrophotometer (Photon Technology International). The excitation wavelength was 550 nm and the fluorescence emission was detected at 585 nm. A calibration signal was generated with known quantities of H_2O_2 at the end of each experiment.

5.18 Measurement of Ca^{2+} - uptake in mitochondria

The free Ca^{2+} concentration at each added concentration of Ca^{2+} was calculated and measured from Long-Evans rat left ventricles. Ca^{2+} uptake by mitochondria was followed by measuring Calcium-Green-5N (100 nM) fluorescence at 505 nm excitation and 535 emission wavelengths at 37 °C using a Hitachi F-4500 spectrofluorimeter (Hitachi High Technologies). The reaction medium was the following: 125 mM KCl, 20 mM HEPES, 100 μM EGTA, 2 mM K_2HPO_4, 1 mM $MgCl_2$ and 0.025% BSA.

5.19 Western blot of left ventricle lysates and isolated mitochondria fractions

Freeze clamped left ventricles from rats and mice were pulverized under liquid nitrogen and homogenized with TissueLyser LT (Qiagen) in homogenization buffer containing (in mmol/L): 20 Tris-HCl, 250 sucrose, 1.0 EGTA, 1.0 dithiothreitol, or in radioimmunoprecipitation assay buffer (Cell Signaling Technology), supplemented with 1 mM PMSF (Roche), 0.1 mM sodium fluoride, 200 mM sodium orthovanadate and

complete protease inhibitor cocktail (Roche) with TissueLyser LT (Qiagen, Venlo, Netherlands) to obtain LV soluble protein fraction or LV whole cell lysate. Purified mitochondria were lysed in 1× NP40 buffer (25 mM Tris, 150 mM NaCl, 1 mM EDTA, 1% NP-40, 5% glycerol, pH 7.4) or 1× Cell lysis buffer (Cell Signaling Technology) supplemented with 1× PhosStop and Complete inhibitors (Roche) as well as 1 μM neocuproine. Concentration of proteins was assessed with Lowry's assay or Bicinchoninic Acid Assay kit (Thermo Fisher Scientific).

For tropomyosin oxidation analysis, tissue samples were homogenized in ice-cold PBS, pH 7.2 containing an antiprotease mixture (Complete, Roche) and 5 mM EDTA. Just before use, the protein samples were stirred under vacuum and bubbled with argon to maximally reduce the oxygen tension. The protein suspension was centrifuged at 12,000×g for 10 min at 4°C. The resulting pellet was resuspended in sample buffer (2% SDS, 5% glycerol, 1% β-mercaptoethanol, 125 mM Tris-HCl, pH 6.8) and denatured by 10 min boiling. This procedure referred to as reducing condition was compared with the non-reducing condition obtained without the addition of β-mercaptoethanol. To avoid artifacts due to the oxidation of thiol groups *in vitro*, non-reducing conditions were performed in the presence of 1 mM N-ethylmaleimide.

Protein samples were resolved on precast 4–20% Criterion TGX gels (Bio-Rad) or bis-tris gels depending on the protein of interest and transferred to nitrocellulose or Immun-Blot PVDF membranes (Bio-Rad). Quality of transfer was verified with Ponceau S staining. Membranes were blocked with 5% nonfat milk (Bio-Rad) or 2-5% bovine serum albumin (BSA; Santa Cruz Biotechnology) or fish skin gelatin in Tris-buffered saline with 0.05% Tween 20 (TBS-T) for 0.5-2 hours. Membranes were incubated with primary antibodies in 1-5% nonfat milk or BSA in TBS-T: anti-tropomyosin (Tm) anti-phospho-phospholamban (PLB-Ser^{16}), p-PLB (Thr^{17}), anti-sarco/endoplasmic reticulum Ca^{2+}-ATPase II (SERCA2A) from Badrilla, anti-apoptosis regulator Bcl-2, anti-receptor-interacting serine/threonine-protein kinase 1 (RIP1), anti-receptor-interacting serine/threonine-protein kinase 3 (RIP3) anti-mixed lineage kinase domain-like protein (MLKL) from Sigma, anti-caspase-3 from Novus Biologicals, anti-heat shock protein-60 (HSP-60), anti-HSP-70, anti-HSP-90, anti-B-cell lymphoma 2 (Bcl-2), anti-caspase-3, anti-CaMKIIδ, anti-Parkin from Santa Cruz Biotechnology, anti-Shc, anti-dynamin-like protein 1 (DLP1), anti-OPA1 from BD Biosciences, anti-mitofusin-2 (MFN2) from

Abcam, anti-phospho-CaMKIIδ (Thr^{287}) anti-phospho-HSP-27 (Ser^{82}), anti-HSP-27, anti-apoptosis regulator Bax, anti- SQSTM1/p62, anti- LC3 A/B, anti-Beclin-1, anti-Bcl-2/adenovirus E1B 19 kDa protein-interacting protein 3 (BNIP3), anti-phospho-acetyl-CoA carboxylase (ACC-Ser^{79}), anti-ACC, anti-phospo-Akt (Thr^{308}), anti-phospo-Akt (Ser^{473}), anti-Akt, anti-phospho-AMPKα (Thr^{172}), anti-AMPKα, anti-phospho-mTOR (Ser^{2448}), anti-mTOR, anti-phospho-ribosomal S6 ($Ser^{235/236}$), anti-ribosomal S6, anti-phospho-glycogen synthase kinase-3 beta (GSK3β-Ser^{9}), anti-GSK3β, anti-NBR1, anti-Class-III PI3K, anti-run domain Beclin-1-interacting and cysteine-rich domain-containing protein (Rubicon), anti-ras-related protein Rab-7a (RAB7), and GAPDH from Cell Signaling Technology or anti-Actin from Sigma as loading controls.

For isolated mitochondria the following primary antibodies were used in 5% nonfat milk in TBS-T: anti-OPA1 and anti-human/rat SHC antibodies (p66shc) from BD Biosciences, anti-SQSTM1/p62, anti-LC3 A/B and anti-Bcl-2/adenovirus E1B 19 kDa protein-interacting protein 3 (BNIP3) from Cell Signaling Technology, anti-mitofusin-1 (MFN1), anti-mitofusin-2 (MFN2), anti-Parkinson disease protein 7 (protein deglycase DJ-1, also termed PARK7) from Abcam, anti-Cx43 from Sigma and anti-voltage-dependent anion-selective channel protein (VDAC) Acris Antibodies GmbH and anti-cytochrome c oxidase subunit 4 (COX4) from Cell Signaling Technology as loading controls. To demonstrate the purity of isolated mitochondria, Organelle Detection Western Blot Cocktail (Abcam) was used which contained anti-sodium potassium ATPase (Na^+/K^+-ATPase), anti-ATP5A and anti-GAPDH antibodies for mitochondria samples from Long-Evans rats and anti-SERCA2A, anti-Na^+/K^+-ATPase (Merck Millipore) and anti-GAPDH (HyTest) were used for mitochondria samples from C57Bl6J mice and Wistar Han rats. To demonstrate that the presence of extramitochondrial (contaminating) proteins is not masked by a too short exposition of the Western blot membranes, representative images are shown for different expositions times (short, medium, and long exposure), which yield in either weak, medium, or strong (saturated signals, Figure 21*D*). After washing and incubation with the respective secondary antibodies, signals were detected with enhanced chemiluminescence kit (Clarity Western ECL Substrate, Bio-Rad, or SuperSignal West Pico or Femto Chemiluminescent Substrate, Thermo Fisher Scientific) and visualized by Chemidoc XRS+ gel documentation system (Bio-Rad,) and analyzed by Image Lab 4.1 (Bio-Rad,) or

ScionImage software (Scion Corporation). For the analysis of tropomyosin oxidation, the density of the additional band with higher molecular weight reflecting the formation of disulfide cross-bridges was normalized to densitometric values of the respective tropomyosin monomer. Antibodies against phosphorylated epitopes were removed with Pierce Stripping Buffer (Thermo Fisher Scientific) before incubation with antibodies detecting the total protein.

5.20 Statistical analysis

Values are expressed as *mean±standard error of mean* (SEM). Statistical analysis was performed between groups by *unpaired two-tailed t-test* or by *Mann-Whitney U-test*. Data on mitochondrial protein levels of MFN1, MFN2, DJ-1, p66shc, and Cx43 in mouse and rat SSM and IFM+N were normalized to VDAC and compared by *unpaired two-tailed Student's t-test* or *one-way ANOVA* with *LSD post hoc test*. Mitochondrial oxygen consumption data was evaluated by *one-way ANOVA* with *LSD post hoc test* or by *Kruskal-Wallis analysis* with *Dunn's post hoc test* in case of dataset with non-normal distribution. GraphPad Prism 6 software was used for statistical analyses. A $p<0.05$ value was considered significant.

6 Results

6.1 Effect of high-cholesterol diet in Wistar rats

6.1.1 Elevated serum cholesterol level in hypercholesterolemic rats

We examined body weight at the 12th week of the diet and found no significant difference between groups (NORM: 551.5±13.0 g vs. CHOL: 529.4±12.2 g; $p<0.05$). Serum cholesterol, triglyceride and glucose parameters were measured in control and cholesterol-fed rats to assess the state of lipid- and glucose homeostasis. After the feeding period, serum cholesterol level was elevated, although serum triglyceride and glucose levels were unchanged in CHOL group as compared to the NORM group, evidencing hypercholesterolemia in CHOL animals (Table 2), in addition, cholesterol-fed animals displayed an altered lipoprotein pattern after 12 weeks of feeding, as shown previously by lipid electrophoresis[159].

***Table 2. Plasma triglycerides, cholesterol, glucose levels in NORM and CHOL groups**. Plasma cholesterol level was significantly elevated after 12 weeks of feeding in CHOL animals. NORM, normocholesterolemic; CHOL, hypercholesterolemic. Data are mean±SEM; NORM (n=9) vs. CHOL (n=9); *: p<0.05.*

	NORM	CHOL
Glucose (mmol/L)	5.32±0.14	5.23±0.09
Cholesterol (mmol/L)	2.89±0.22	4.09±0.62*
Triglycerides (mmol/L)	2.17±0.03	2.26±0.05

6.1.2 Hypercholesterolemia downregulates autophagy

In order to establish whether hypercholesterolemia influences autophagy we measured cardiac expression of autophagy markers by Western blot. Hearts of cholesterol-fed animals exhibited a decrease in LC3-II, Beclin-1, Rubicon, and RAB7 (Figure 8, *B-F*), consistent with downregulation of autophagy initiation and vesicle traffic despite upregulation of the Class-III PI3K involved in autophagy initiation (Figure 8*F*). No difference in the expression of markers of autophagic clearance NBR1 and SQSTM1/p62 proteins was detected between groups (Figure 8, *G-H*). These results suggest that both

early and late phases of autophagy were attenuated in the heart of hypercholesterolemic rats.

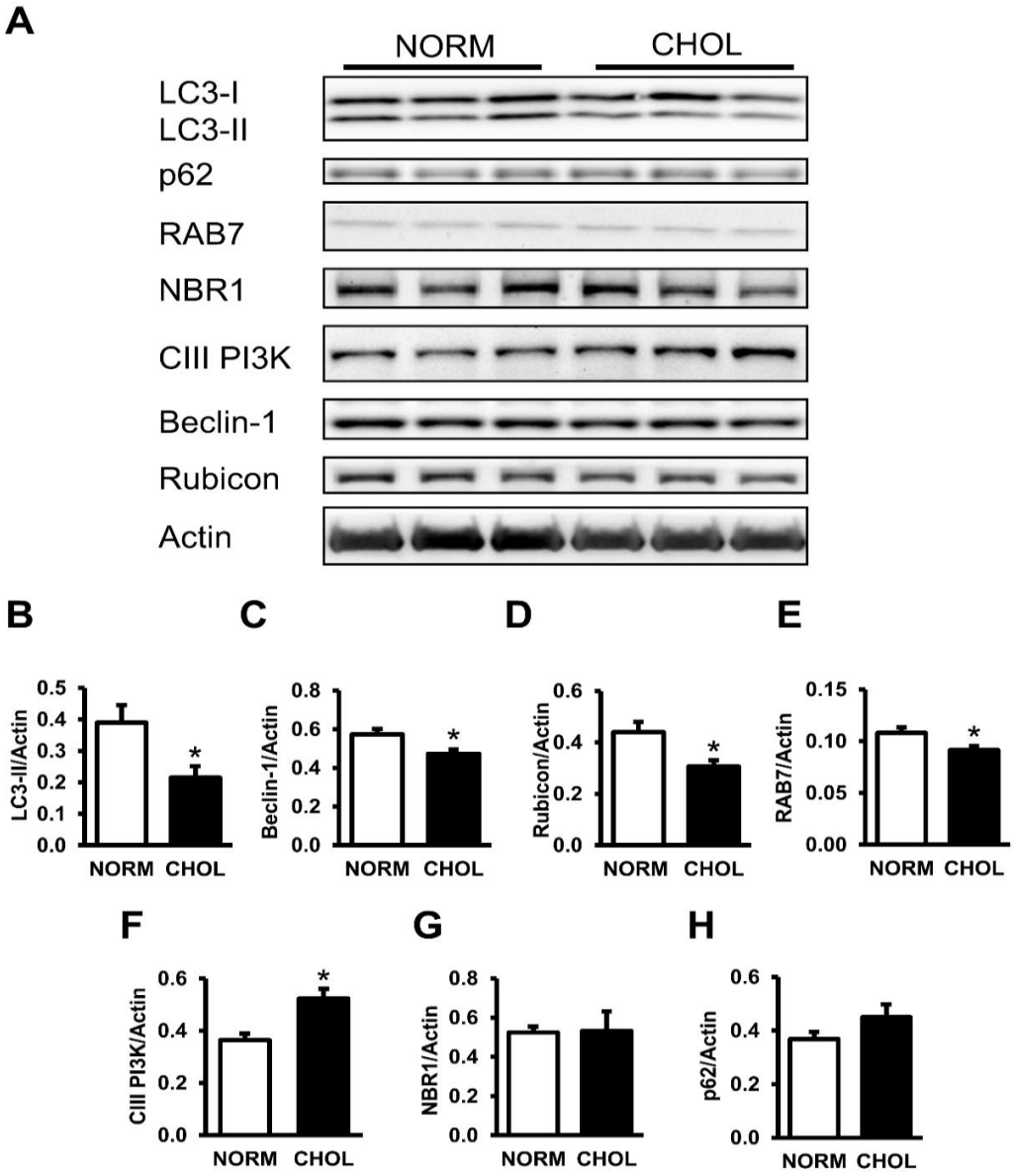

Figure 8. Hypercholesterolemia downregulated cardiac autophagy.
*Representative Western blots for autophagy-related proteins in the left ventricle of NORM and CHOL rats (A). Quantification of LC3-I/II, Beclin-1, Class III PI3K, NBR1, SQSTM1/p62, RAB7 and Rubicon protein expressions as normalized to Actin (B-H). NORM, normocholesterolemic; CHOL, hypercholesterolemic; CIII PI3K, class-III phosphoinositide 3-kinase; NBR1, neighbor of BRCA1 gene 1; LC3, microtubule-associated protein light chain 3; RAB7, ras-related protein Rab-7a; Rubicon, run domain Beclin-1-interacting and cysteine-rich domain-containing protein; SQSTM1/p62, sequestosome 1. Data are presented as mean±SEM; NORM (n=4) vs. CHOL (n=5); *: p<0.05.*

6.1.3 Hypercholesterolemia activates mTOR in the heart

In order to investigate whether hypercholesterolemia affects mTOR pathway, we measured the phosphorylation of mTOR and ribosomal S6 proteins. Our results showed that there was no significant difference in the expressions or phosphorylations of Akt and mTOR protein between groups; however, phosphorylation of ribosomal S6, a surrogate marker of mTOR complex activity, was elevated in CHOL group (Figure 9, *B-E*). These results indicate that mTOR activity was upregulated in hypercholesterolemia.

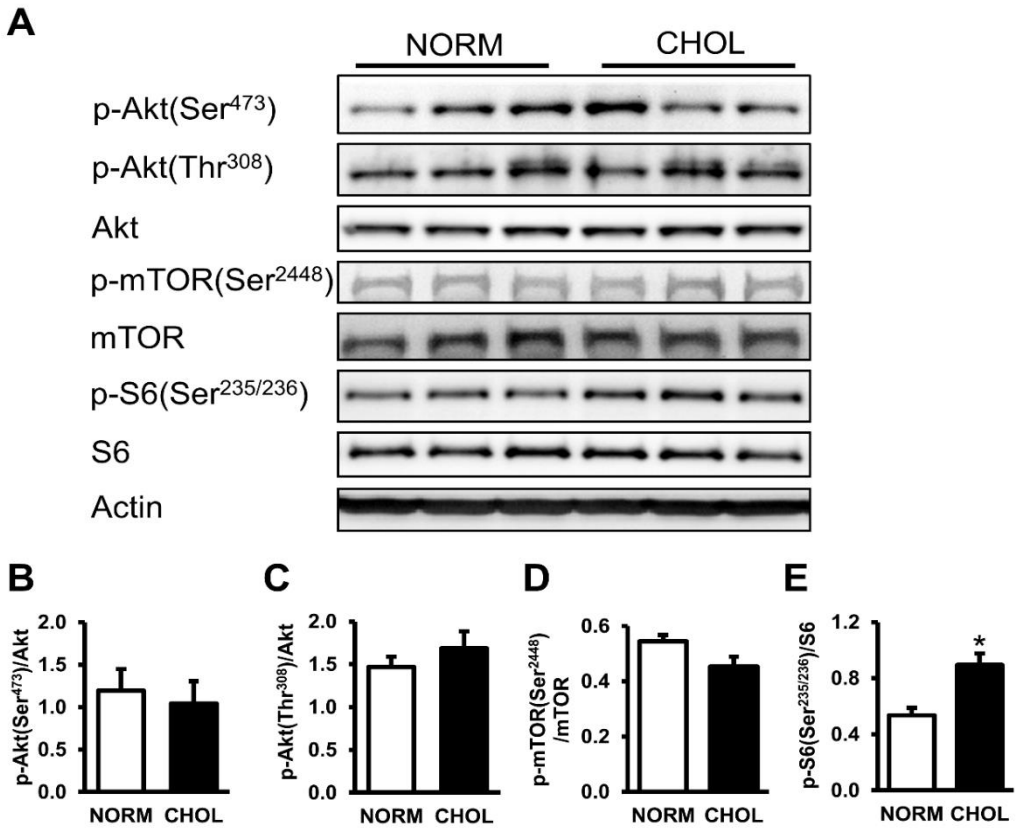

Figure 9. Hypercholesterolemia activated mTOR pathway.
*Representative Western blots for mTOR pathway-related proteins in the left ventricle of NORM and CHOL rats (A). Quantification of phospho-Akt (Ser^{473}; Thr^{308}), phospho-mTOR (Ser^{2448}), and phospho-S6 (Ser$^{235/236}$) protein expressions as normalized to the corresponding total proteins (B-E). NORM, normocholesterolemic; CHOL, hypercholesterolemic; mTOR, mechanistic target of rapamycin; S6, ribosomal S6 protein. Data are presented as mean±SEM; NORM (n=4) vs. CHOL (n=5); *: p<0.05.*

6.1.4 Apoptosis but not necroptosis is elevated in hypercholesterolemia

We also investigated whether decreased autophagy in hypercholesterolemia is associated with altered apoptotic and necroptotic pathways. Expression of apoptotic marker cleaved caspase-3 was significantly increased, while Bcl-2/Bax protein expression ratio was unchanged (Figure 10, *A-C*). Furthermore, expression of RIP1, RIP3 and MLKL proteins, major markers of necroptosis, were unchanged (Figure 10, *D-G*). These results suggest that hypercholesterolemia upregulates apoptosis but not necroptosis in the heart.

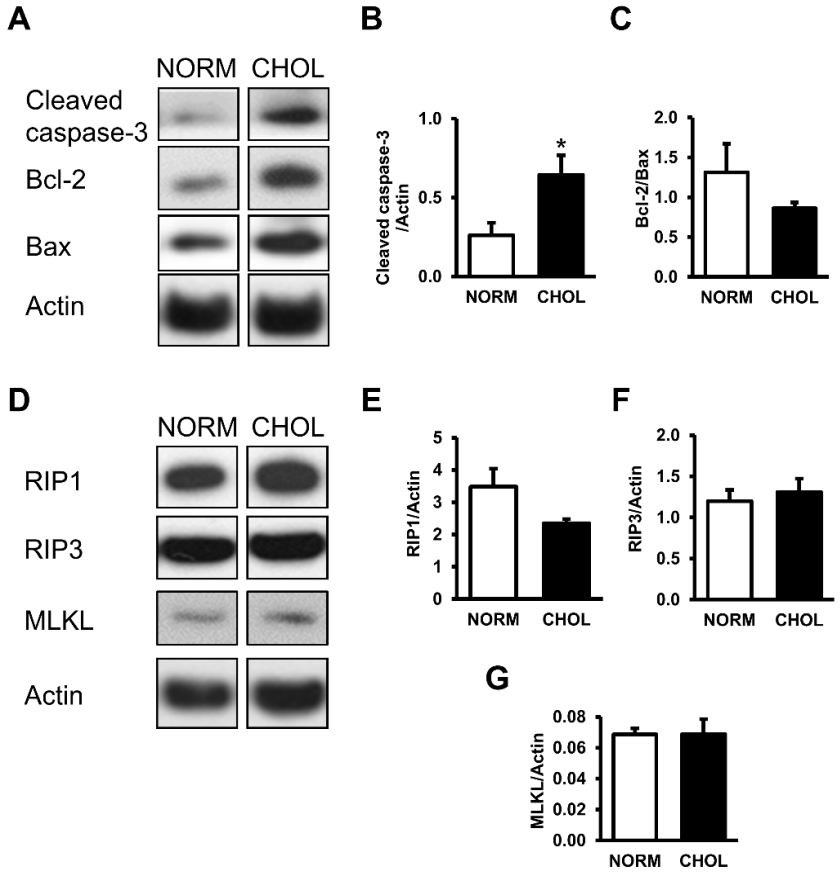

Figure 10. Hypercholesterolemia activated apoptosis, but had no effect on cardiac necroptosis.

*Representative Western blots for apoptosis-related protein expressions (A). Quantification of cleaved caspase-3 expression normalized to Actin and ratio of Bcl-2 to Bax (B-C). Representative Western blots for necroptosis-related proteins (D). Quantification of RIP1, RIP3, MLKL and cleaved caspase-3 as normalized to Actin protein expression (E-G). NORM, normocholesterolemic; CHOL, hypercholesterolemic; Bax, Bcl-2-associated X protein; RIP1-3, receptor-interacting serine/threonine-protein kinase 1 and 3; MLKL, mixed lineage kinase domain-like protein. Data are presented as mean±SEM; NORM (n=5) vs. CHOL (n=5); *: p<0.05.*

6.2 Effect of high-fat diet and streptozotin treatment in Long-Evans rats

6.2.1 Moderately increased adiposity in prediabetic animals

To determine the effect of high-fat diet and the single, low dose STZ injection, we measured body weight, fat tissue volumes and plasma lipid parameters. We found that body weights of the prediabetic animals were moderately but statistically significantly elevated from week 9 as compared to the control group, and that this difference reached 18% at the end of the diet period (Figure 11, *A-B*). At week 20, plasma leptin level was significantly increased in prediabetes, however, CRP level was decreased, plasma cholesterol, HDL cholesterol and triglyceride levels, and parameters of liver and kidney function were unchanged (Table 3). To characterize prediabetes-induced changes in further obesity-related molecules, we performed an adipokine array measurement, which revealed that the circulating level of TIMP-1 might be influenced by prediabetes, however, we could not confirm these results by ELISA (Table 3). CT scan showed that body fat volume of prediabetic rats was substantially increased at the end of the diet (Figure 11, *C-D*). Epididymal fat tissue weight, which is an indicator of total body adiposity, was increased in the prediabetic group, however, the weight of interscapular brown adipose tissue was not changed (Figure 11, *G-H*). Histological score analysis of HE- and MA-stained liver samples evidenced the development of hepatic steatosis in the prediabetic group (CON: 0.5±0.3 vs. PRED: 2.25±0.5; $p<0.05$), however, no signs of hepatic fibrosis was detected (Figure 11*H*). Furthermore, electron microscopy showed an increased number of lipid droplets in the myocardium of prediabetic animals as compared to controls (Figure 11, *E-F*). These results demonstrated a moderately increased adiposity, hepatic and cardiac fat deposits without signs of hyperlipidemia in the prediabetic group.

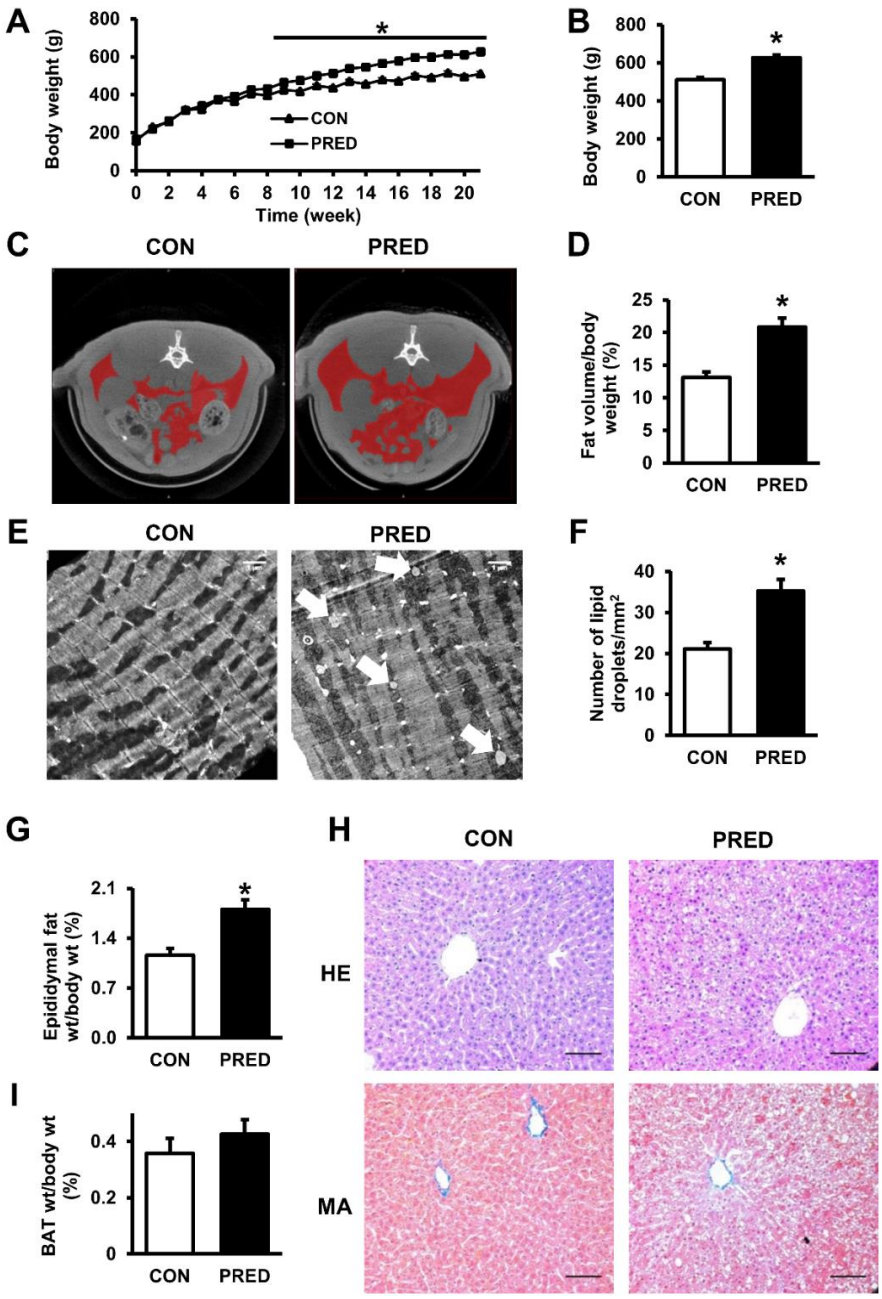

Figure 11. High-fat feeding with a single low dose STZ treatment increase adiposity. *Changes in body weight during the experiment (A) and body weight data after 21 weeks (B); n=19. Axial representative CT slice from the middle of 4th lumbal spine. Red color indicates the segmented VOIs showing the volume of fat in the CON and PRED rats (C). Whole body fat volume to body weight ratio at week 20; n=3 (D). Representative transmission electron micrographs of myocardial lipid droplets (E; white arrows) and number of lipid droplets in CON and PRED cardiomyocytes (F). Magnification 7,500×; scale bar 1 µm; n=5. Epididymal fat tissue (G) and BAT (I) weight to body weight ratios; n=19. HE and MA staining of liver sections (H). Magnification 200×; scale bar 100 µm; n=4. CON, control; PRED, prediabetic; VOIs, Volume-of-Interests; HE, hematoxylin-eosin; MA, Masson's trichrome; BAT, interscapular brown adipose tissue. Data are presented as mean±SEM; (*: p<0.05).*

Table 3. Plasma parameters at week 21.
CON, control; PRED, prediabetic; ANG II, angiotensin II; TIMP1, TIMP metallopeptidase inhibitor 1; HDL, high-density lipoprotein; LDL, low-density lipoprotein; GOT, glutamate oxaloacetate transaminase; GPT, glutamate pyruvate transaminase; CRP, C-reactive protein. Data are presented as mean±SEM for 12 rat per group (: p<0.05).*

	CON	PRED
Plasma leptin (ng/mL)	2.51±0.33	5.91±0.60*
Plasma ANG II (ng/mL)	7.6±1.32	8.05±1.56
Plasma TIMP-1 (ng/mL)	4.19±0.39	4.76±0.51
Plasma cholesterol (mmol/L)	1.88±0.06	1.72±0.08
HDL cholesterol (mmol/L)	2.75±0.14	2.75±0.10
Plasma triglyceride (mmol/L)	1.20±0.10	1.31±0.09
LDL cholesterol (mmol/L)	0.44±0.02	0.47±0.03
Total Cholesterol (mmol/L)	1.61±0.05	1.51±0.08
GOT (U/L)	82±15	58±4
GPT (U/L)	50±14	49±5
Uric acid (mmol/L)	24±4	16±1
Creatinine (µmol/L)	46±3	40±3
CRP (mg/L)	109.56±1.24	94.96±3.87*

6.2.2 Impaired glucose tolerance, insulin resistance, and sensory neuropathy evidence disturbed carbohydrate metabolism in prediabetes

We aimed to characterize the glucose homeostasis in our rat model of prediabetes. At week 20 of the diet, fasting blood glucose levels were slightly elevated in prediabetes from week 10, however, remained in the normoglycemic range (Figure 12, *A*-*B*). OGTT and ITT demonstrated impaired glucose tolerance and insulin resistance in the prediabetic group (Figure 12, *C*-*F*), however, there was no difference in pancreatic insulin content (Figure 12*G*), or in pancreatic islet morphology (Figure 12*H*) between groups. These results demonstrate prediabetic conditions (as was defined by World Health Organization, see above) in the present model and evidence that type 1 diabetes did not develop due to the STZ treatment. Sensory neuropathy is a well-accepted accompanying symptom of diabetes[176]. Accordingly, here we have found a decrease in the mechanical hind limb withdrawal threshold at week 15 (CON: 48±1g vs. PRED: 42±2g; $p<0.05$) of diet in the PRED, which indicates a moderate sensory neuropathy in this model of prediabetes.

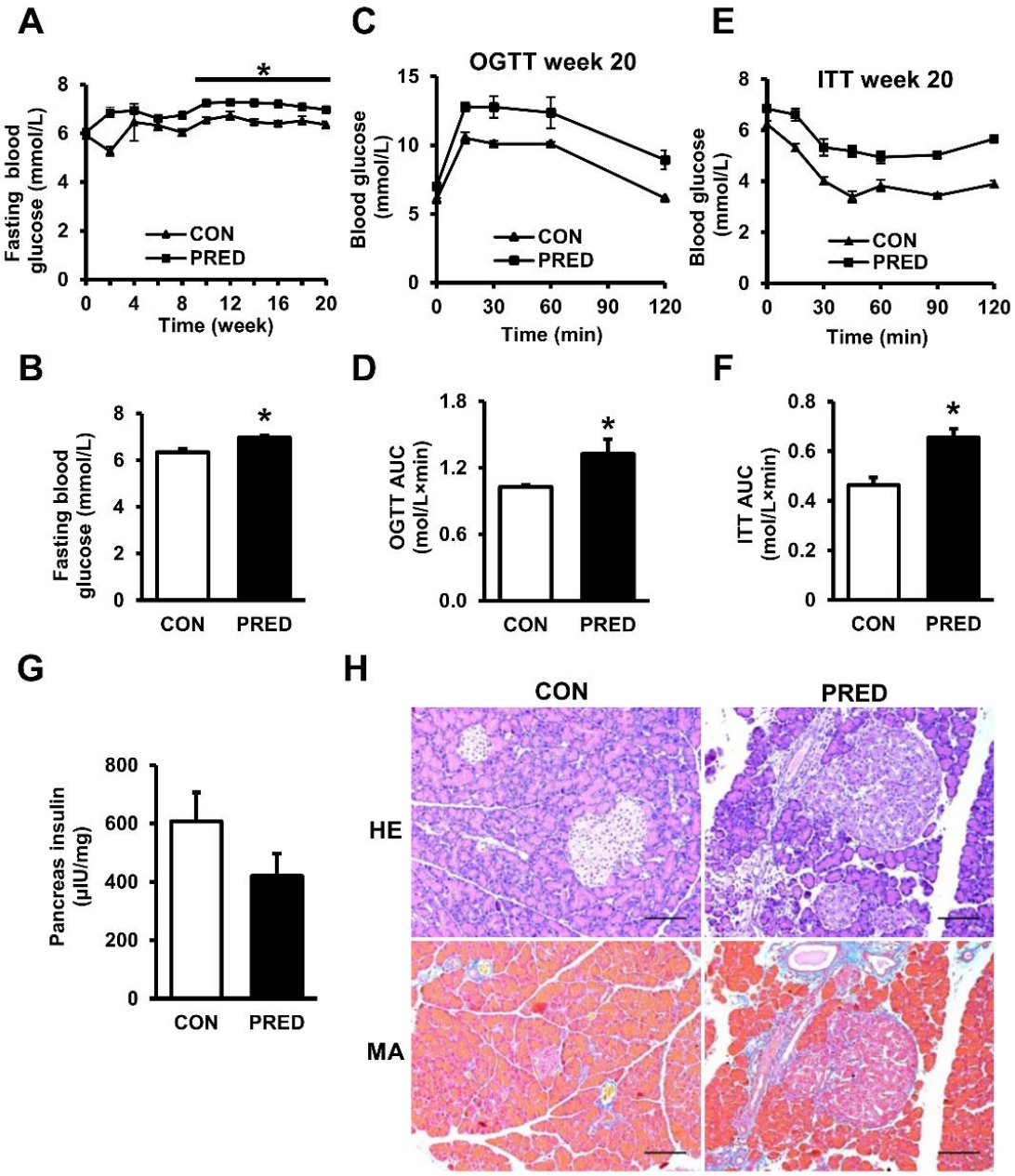

Figure 12. Alterations in glucose homeostasis indicate the development of a prediabetes in streptozotocin-treated and high-fat-fed rats at week 21.

Fasting blood glucose levels during the experiment (A) and at week 20 (B); n=19. OGTT (C-D) and ITT (E-F) results at week 20 of the diet; n=6. Insulin content of pancreas at week 21 (G); n=4. HE and MA staining of pancreas sections (H). Magnification 200×; scale bar 100 μm; n=4. CON, control; PRED, prediabetic; OGTT, oral glucose tolerance test; ITT, insulin tolerance test; HE, hematoxylin-eosin; MA, Masson's trichrome. Data are presented as mean±SEM (: p<0.05).*

6.2.3 Diastolic dysfunction and hypertrophy in prediabetes with no sign of fibrosis

To determine the cardiac effect of prediabetes, we measured morphological and functional parameters of the hearts. Heart weights were significantly increased (Figure 13*A*), however, heart weight/body weight ratio was decreased in prediabetes (CON: 0.27±0.01% vs. PRED: 0.24±0.01%; $p<0.05$), plausibly due to obesity. Left ventricular (LV) mass, left ventricular anterior wall thickness, systolic (LVAWTs), left ventricular posterior wall thickness, systolic (LVPWTs) and left ventricular posterior wall thickness, diastolic (LVPWTd) were increased in prediabetic group as assessed with echocardiography, however, other cardiac dimensional parameters were unchanged (Table 4). The slope of end-diastolic pressure-volume relationship (EDPVR), which is a very early and sensitive marker of diastolic dysfunction, was significantly elevated in prediabetes, although other hemodynamic parameters, including blood pressure, were unchanged evidencing the lack of systolic dysfunction or hypertension (Table 5, Figure 13*B*). To uncover the molecular background of the observed mild diastolic dysfunction, we performed measurements on the common mechanistic contributors of heart failure[177]. On hematoxylin-eosin-stained LV sections increased cardiomyocyte diameter was detected in prediabetes (Figure 13, *C-D*). To characterize components affecting diastolic function, we analyzed MHC expression. Interestingly, the gene expression of β-MHC was decreased, and α-MHC also showed a tendency of decrease ($p=0.17$), the ratio of which resulted in a strong tendency to decrease in prediabetes. No increase in ANP or BNP gene expressions (Figure 13, *G-H*) or in angiotensin-II level (Table 3) was detected in prediabetes. To evaluate the extent of fibrosis, MA-stained LV sections were analyzed, which revealed no difference between groups (Figure 13*E*). Similarly, we found that gene expression of type I (COL1) and III (COL3) collagen isoforms were unchanged in the left ventricle (Figure 13*F*). These results indicate that mild diastolic dysfunction developed in prediabetic animals which was associated with a mild hypertrophy (increased LV mass and anterior and posterior LV wall thickness, increased cardiomyocyte diameter) without signs of fibrosis.

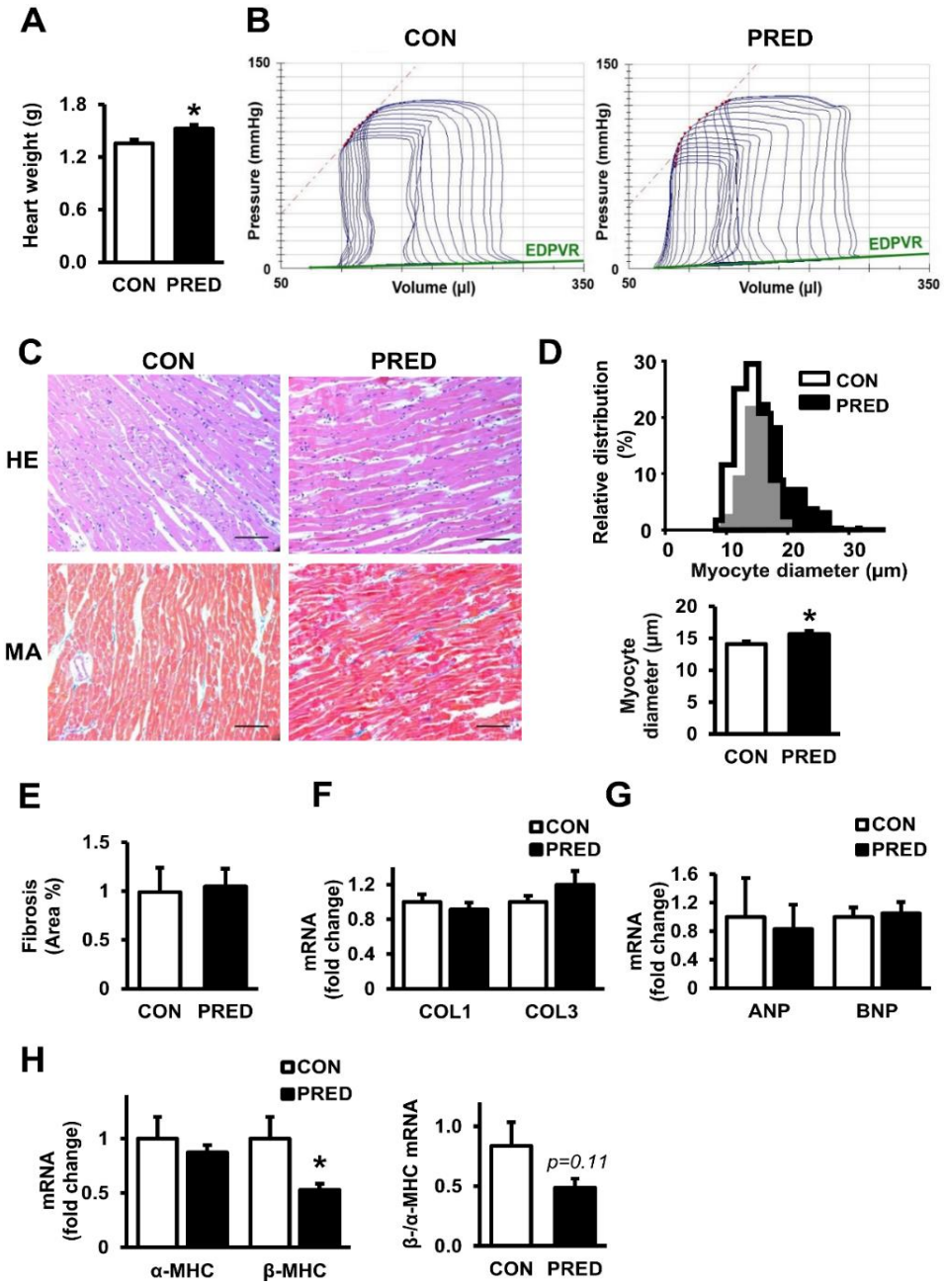

Figure 13. Characterization of cardiac function, myocardial morphology and fibrosis in prediabetic rats.

Quantification of heart weights after 21 weeks (A); n=19. Representative pressure-volume loops and slope of EDPVR in CON and PRED group (B). HE and MA staining of myocardial sections (C) and quantification of cardiomyocyte diameter (D) and level of fibrosis (E) in CON and PRED rats. Magnification 200×; scale bar 100 µm; n=6-8. Quantification of COL1, COL3 (F), ANP, BNP (G), α-MHC, β-MHC gene expressions and α- to β-MHC ratio (H) in CON and PRED group; n=9. CON, control; PRED, prediabetic; EDPVR, end diastolic pressure-volume relationship; HE, hematoxylin-eosin; MA, Masson's trichrome; COL1-3, collagen type I and III; ANP, atrial natriuretic peptide; BNP, brain natriuretic peptide; α-MHC, alpha-myosin heavy chain; β-MHC, beta-alpha-myosin heavy chain. Data are presented as mean±SEM (: p<0.05).*

Table 4. Characterization of cardiac morphology and function in prediabetes by means of echocardiography.

CON, control, PRED, prediabetic; LV mass, left ventricular mass; LVAWTd, left ventricular anterior wall thickness, diastolic; LVAWTs, left ventricular anterior wall thickness, systolic; LVPWTd, left ventricular posterior wall thickness, diastolic; LVPWTs, left ventricular posterior wall thickness, systolic; LVEDD, left ventricle end-diastolic diameter; LVESD, left ventricle end-systolic diameter; FS%, fractional shortening %; HR, heart rate. Data are presented as mean±SEM for 10 rat per group (: p<0.05).*

	CON	**PRED**
LV mass (g)	1.01±0.04	1.22±0.07*
LVAWTd (mm)	1.89±0.12	2.07±0.12
LVAWTs (mm)	2.86±0.17	3.42±0.11*
LVPWTd (mm)	1.86±0.07	2.05±0.04*
LVPWTs (mm)	2.72±0.12	3.25±0.15*
LVEDD (mm)	7.71±0.22	7.75±0.17
LVESD (mm)	4.93±0.22	4.96±0.31
FS (%)	36.0±2.2	37.4±3.8
HR (1/min)	335±13	348±10

Table 5. Characterization of left ventricular (LV) hemodynamics in vivo in prediabetes by means of pressure-volume analysis.
CON, control; PRED, prediabetic; MAP, mean arterial pressure; LVESP, left ventricular end-systolic pressure; LVEDP, left ventricular end-diastolic pressure; LVEDV, left ventricular end-diastolic volume; LVESV, left ventricular end-systolic volume; SV, stroke volume; CO, cardiac output; EF, ejection fraction; SW, stroke work; dP/dtmax, maximal slope of LV systolic pressure increment; dP/dtmin, maximal slope of LV diastolic pressure decrement; τ, time constant of LV pressure decay; TPR, total peripheral resistance; ESPVR, end-systolic pressure-volume relationship; EDPVR, end-diastolic pressure-volume relationship; PRSW, preload recruitable stroke work; dP/dtmax-EDV, the slope of the dP/dtmax-end-diastolic volume relationship. Data are presented as mean±SEM for 10 rat per group (: p<0.05).*

	CON	**PRED**
MAP (mmHg)	110.1±7.3	113.6±6.1
LVESP (mmHg)	116.6±5.6	120.0±6.8
LVEDP (mmHg)	4.4±0.4	4.0±0.2
LVEDV (µL)	292.8±14.5	280.2±9.6
LVESV (µL)	130.7±6.9	127.5±4.5
SV (µl)	162.1±9.1	152.8±7.7
CO (mL/min)	59.5±3.2	56.6±2.3
EF (%)	55.3±1.3	54.4±1.3
SW (mmHg·mL)	14.5±0.5	13.6±0.6
dP/dtmax (mmHg/s)	7226±487	7387±401
dP/dtmin (mmHg/s)	-8198±680	-8551±545
τ (Glantz) (ms)	12.6±0.3	12.1±0.4
TPR [(mmHg·min)/mL]	1.90±0.19	2.00±0.12
Slope of ESPVR (mmHg/µL)	2.68±0.12	2.71±0.06
Slope of EDPVR (mmHg/µL)	0.026±0.001	0.037±0.004*
PRSW (mmHg)	100.5±5.2	98.9±4.1
Slope of dP/dtmax-EDV [(mmHg/s)/µL)]	34.3±2.3	35.2±2.2
Maximal power (mW)	91.8±8.2	98.2±12.5

6.2.4 Elevated reactive oxygen species formation in cardiac subsarcolemmal mitochondria in prediabetic rats

To investigate whether cardiac mitochondrial disturbances contribute to the observed diastolic dysfunction, mitochondrial morphology and enzyme activity were analyzed

from left ventricles of prediabetic rats. Our electron microscopy results showed that there is no major difference in the number of interfibrillar mitochondria (IFM) between the groups (Figure 14, *A-B*). However, area (CON: 0.43±0.01 vs. PRED: 0.39±0.01 μm^2; $p<0.05$), perimeter (CON: 2.69±0.02 vs. PRED: 2.63±0.03 μm; $p<0.05$) and sphericity (CON: 0.35±0.01 vs. PRED: 0.31±0.01; $p<0.05$) of IFM are decreased in PRED group. Previous studies indicated that IFM and subsarcolemmal mitochondria (SSM) are affected by diabetes differentially[178, 179]. Therefore, we analyzed our EM imagery containing SSM and found no difference in SSM size, perimeter, or sphericity (data not shown), although, the statistical power of these analyses was not high enough (n=2 for CON and n=4 for PRED). Furthermore, we have not seen any major difference in mitochondrial oxygen consumption, enzyme activities (Table 6-7), Ca-uptake, or membrane potential (Figure 15-16). However, we have found that hydrogen-peroxide production was increased in the cardiac SSM fraction with glutamate-malate as a substrate (Figure 14*C*), although, there was no difference when succinate was used as substrate. Interestingly, there was no increase in reactive oxygen species (ROS) production of the IFM isolated from LV supported either with glutamate-malate or with succinate (Figure 14, *D-F*). As leukocytes are one of the main sources of ROS, inflammatory mediators were measured. We could not find significant difference in TNF-α (CON: 1±0.27 vs. PRED: 0.59±0.07; ratio normalized to GAPDH; $p>0.05$) and IL-6 (CON: 1±0.27 vs. PRED: 0.69±0.14; ratio normalized to GAPDH; $p>0.05$) mRNA expressions between groups, which evidence that in our model prediabetes does not elicit cardiac or systemic inflammation. Furthermore, we have not seen any difference in other markers of oxidative stress: the expression of p66Shc and tropomyosin oxidation between groups (Figure 17, *B-E*). It is known that reactive nitrogen species have important role in deteriorated contractile- and endothelial function in diabetes[180, 181], therefore, we analyzed whether nitrative stress is influenced in prediabetes. Nitrotyrosine immunohistology indicated that protein nitrosylation is increased in prediabetes (Figure 17*A*). As CaMKIIδ has been proposed to be activated in oxidative stress-associated conditions [182], we measured the levels of the active forms of the kinase which might affect the contractility and relaxation capacity of the heart[183]. The phosphorylation of CaMKIIδ and of its target PLB on Thr^{17} was not changed by prediabetes (Figure 18, *A-C*). Similarly, there was no change in the protein expression of SERCA2A in our model of prediabetes

as compared to control animals (Figure 18*E*). On the other hand, the level of p-Ser^{16}-PLB showed a tendency for downregulation in prediabetes (p=0.08; Figure 18*D*).

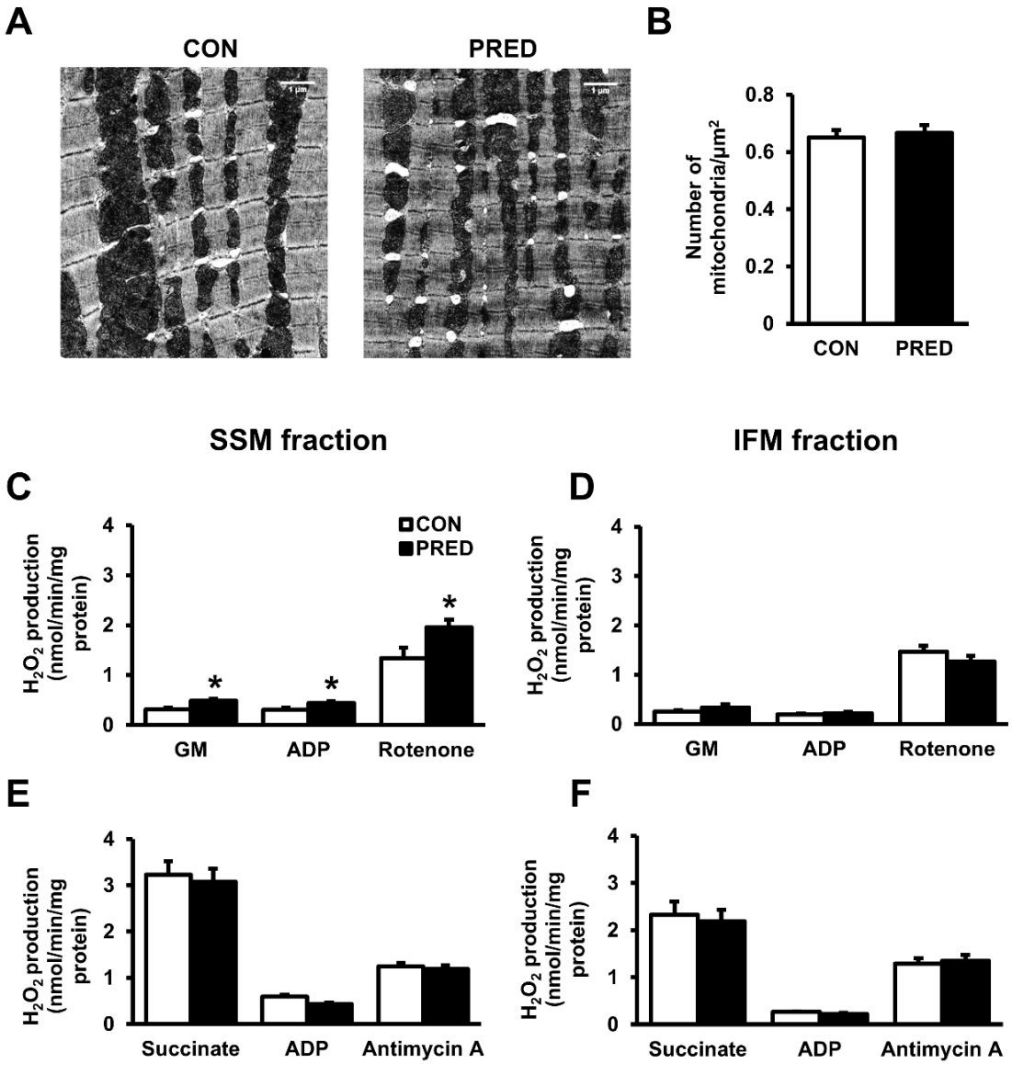

Figure 14. Mitochondrial morphology and function in prediabetes at week 21. *Representative transmission electron micrographs (A) and number of IFM (B) in the left ventricle. Magnification 12,000×, scale bar 1 µm. Quantification of H_2O_2 production in SSM (C) and IFM (D) with glutamate-malate as substrate (GM). Quantification of H_2O_2 production in SSM (E) and IFM (F) with succinate as substrate. CON, control; PRED, prediabetic; IFM, interfibrillar mitochondria; SSM, subsarcolemmal mitochondria; ADP, adenosine diphosphate. Data are presented as mean±SEM, n=5-9 per group (*: p<0.05).*

Table 6. Quantification of cardiac mitochondria enzyme activity in left ventricle.
CON, control; PRED, prediabetic. Data are presented as mean±SEM for 5-9 rat per group (: p<0.05).*

	CON	PRED
Citrate-synthase activity (U/mg protein)	223.12±9.98	220.44±8.32
NADH:Ubiquinone-Oxidoreductase activity (U/mg protein)	40.52±2.55	36.48±2.99
NADH:Cytochrome c-Oxidoreductase activity (U/mg protein)	7.85±1.18	8.47±1.31
Succinate:Cytochrome-c-Oxidoreductase activity (U/mg protein)	21.09±1.49	23.57±1.61
Succinate-Dehydrogenase activity (U/mg protein)	84.06±5.83	80.09±3.42
Cytochrome-c-Oxidase activity (U/mg protein)	38.74±3.15	40.36±2.33

Table 7. Quantification of mitochondrial oxygen consumption.
CON, control; PRED, prediabetic; SSM, subsarcolemmal mitochondria; IFM, interfibrillar mitochondria; ADP, adenosine diphosphate; CAT, carboxyatractyloside. Data are presented as mean±SEM for 9 rat per group (: p<0.05).*

	CON	PRED	CON	PRED
	SSM (pmol/mL)s	SSM (pmol/mL)s	IFM (pmol/mL)s	IFM (pmol/mL)s
Glutamate-malate	25.08±3.6	21.06±3.53	58.6±19.31	61.78±21.41
ADP	203.31±32.57	194.03±42.16	304.23±25.75	287.9±22.35
Cytochrome c	260.8±28.27	287.06±54.91	335.96±25.79	345.41±28.17
Succinate	306.2±25.19	289.74±23.23	367.76±15.74	393.56±18.82
Rotenone	143.12±18.19	139.7±23.64	238.4±18.44	220.73±16.19
CAT	105.95±8.89	106.5±12.22	159.78±6.86	156.6±8.03

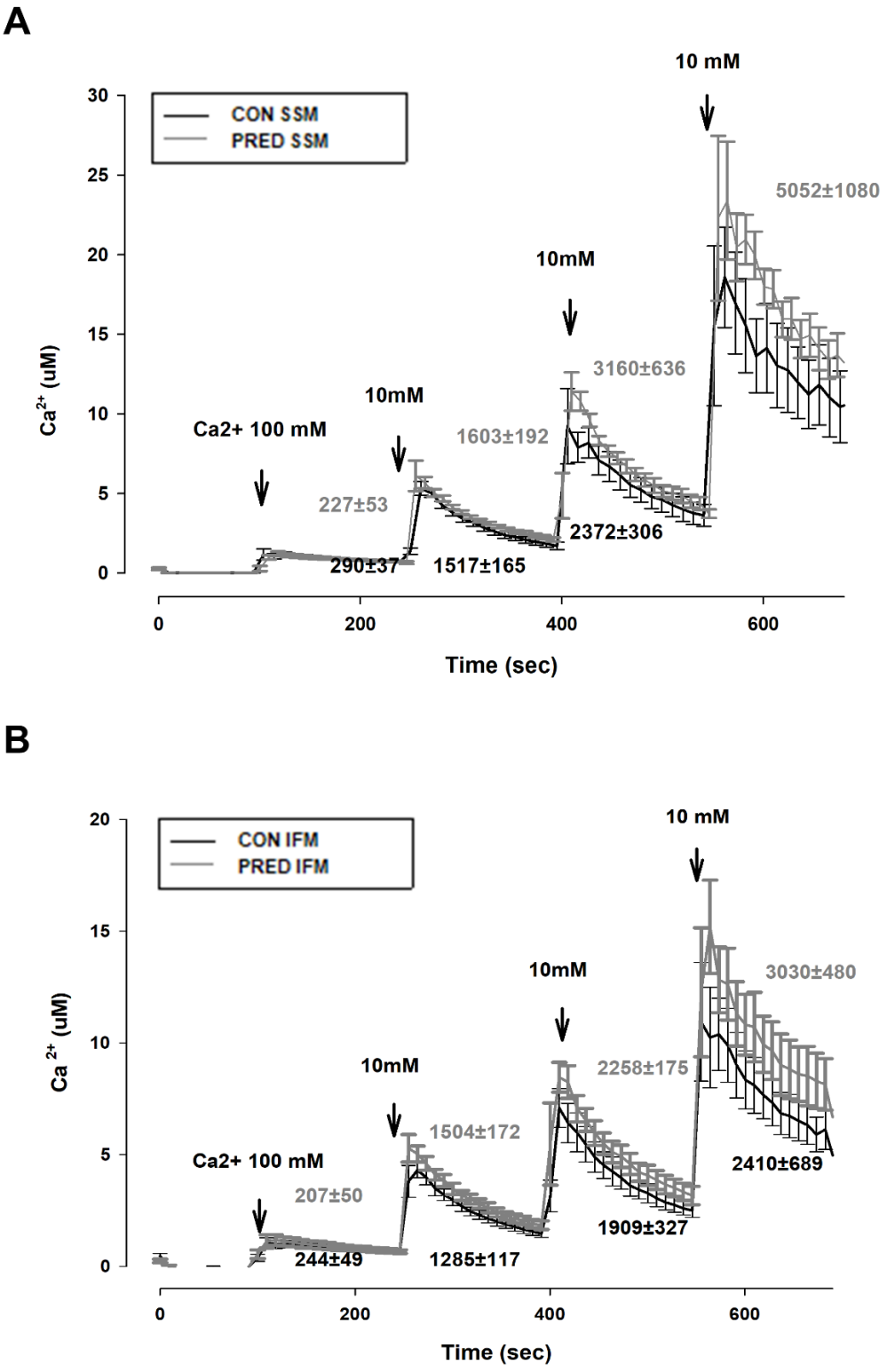

Figure 15. Characterization of mitchondrial Ca^{2+} uptake in prediabetes.
No changes were observed in Ca^{2+} uptake in SSM (A) and IFM (B). CON, control; PRED, prediabetic; SSM, subsarcolemmal mitochondria; IFM, interfibrillar mitochondria. Data are presented as mean±SEM, n=8 per group.

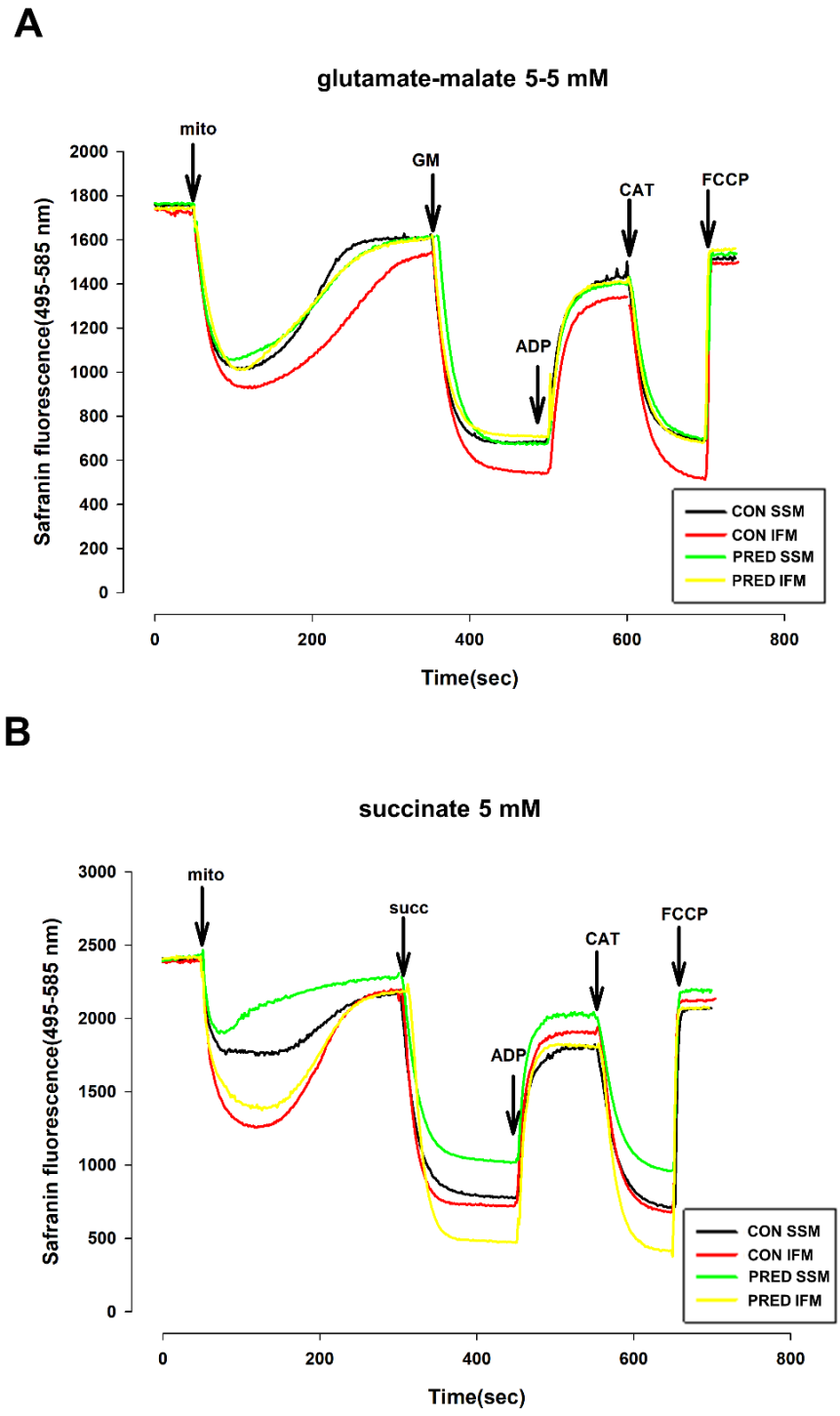

Figure 16. Characterization of mitochondrial membrane potential in prediabetes.
No changes in mitochondrial membrane potential with glutamate-malate (A) and succinate (B) substrates in prediabetes. CON, control; PRED, prediabetic; SSM, subsarcolemmal mitochondria; IFM, interfibrillar mitochondria; ADP, adenosine-diphosphate; CAT, carboxyatractyloside; FCCP, carbonyl cyanide-4-(trifluoromethoxy)phenylhydrazone. Data are presented as mean±SEM, n=8 per group.

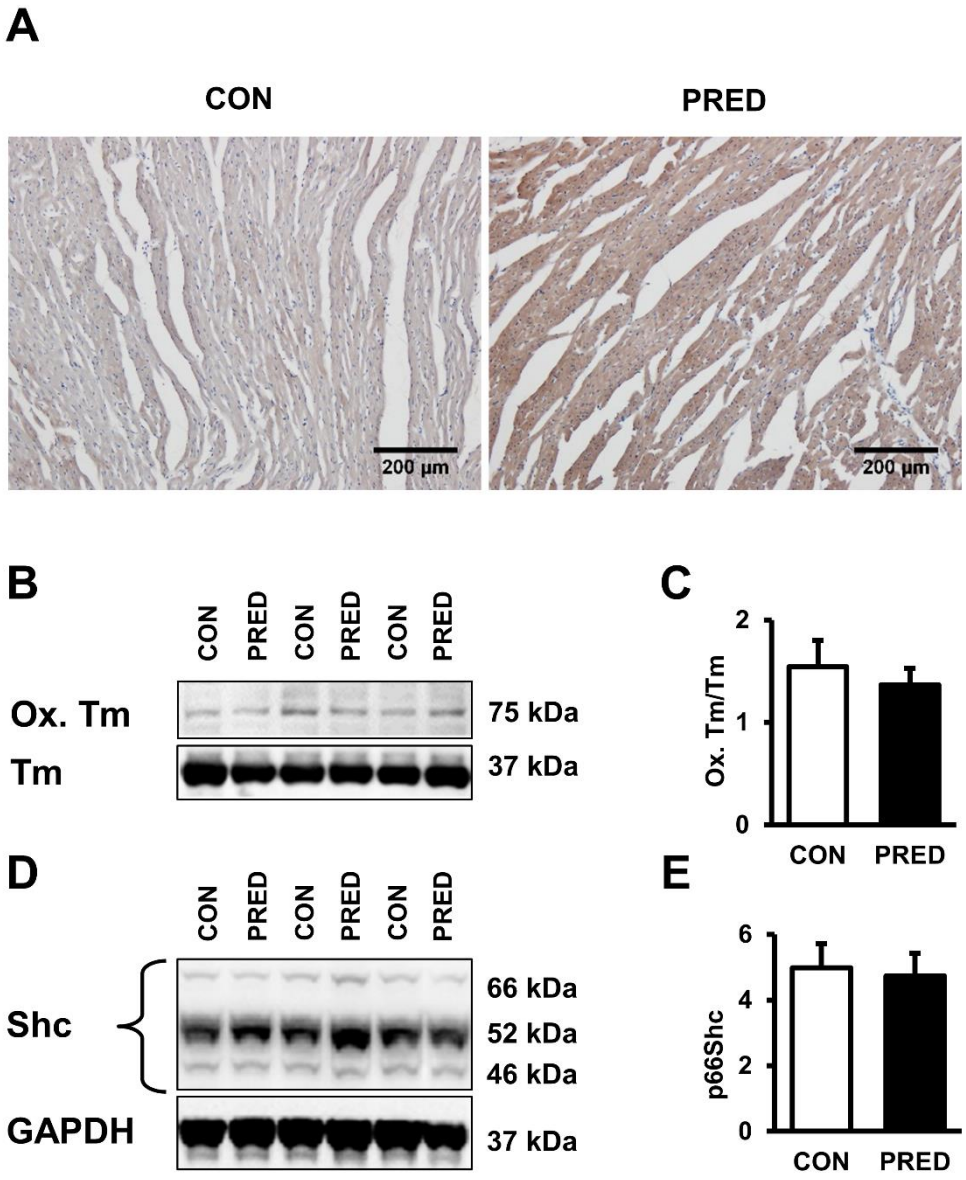

Figure 17. Characterization of oxidative and nitrative stress in prediabetes. *Representative immunostaining of nitrotyrosine in the left ventricle (A), magnification 200×; scale bar 200 µm. Representative Western blots (B) and quantification (C) of tropomyosin oxidation. Representative Western blots (D) and quantification (E) of cardiac p66Shc expression. CON, control; PRED, prediabetic; Tm, tropomyosin; Ox. Tm, oxidized tropomyosin; GAPDH, glyceraldehyde 3-phosphate dehydrogenase. Data are presented as mean±SEM, n=6-8 per group.*

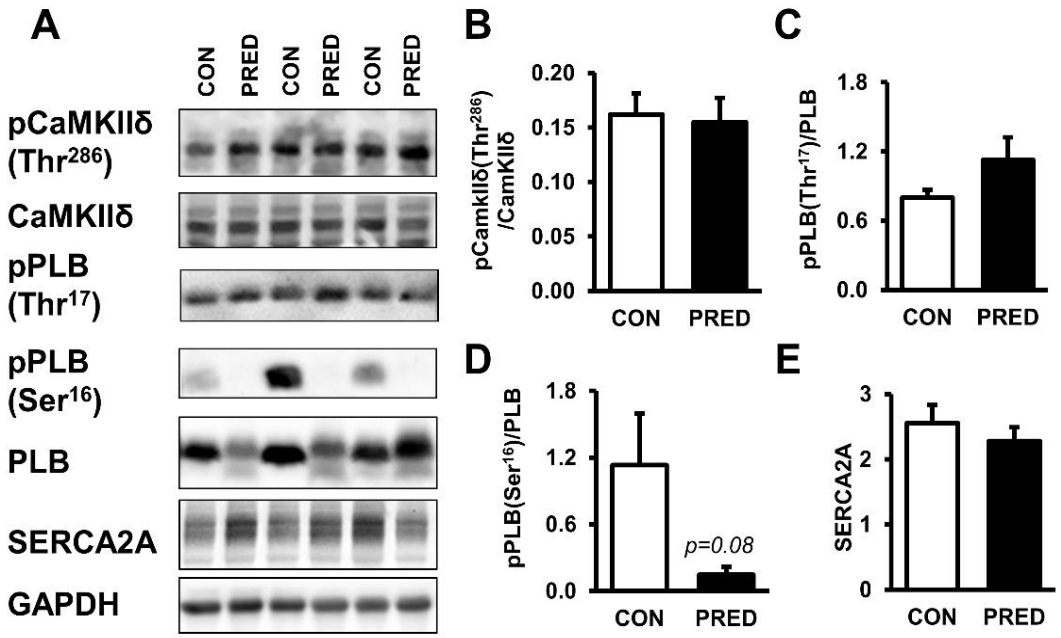

Figure 18. Characterization of major proteins of calcium homeostasis in prediabetes. *Representative Western blots (A) and quantification of CaMKIIδ (B) and PLB phosphorylation on Thr[17] (C) and Ser[16] (D), and SERCA2A (E) expression. CON, control; PRED, prediabetic; GAPDH, glyceraldehyde 3-phosphate dehydrogenase; CaMKIIδ, Ca^{2+}/calmodulin-dependent protein kinase II; SERCA2A, sarco/endoplasmic reticulum Ca^{2+} ATPase II; PLB, phospholamban. Data are presented as mean±SEM, n=6-8 per group.*

6.2.5 Alterations in cardiac mitofusin-2 expression and mitophagy in prediabetes

To investigate the effect of cardiac mitochondrial dynamics, auto- and mitophagy in prediabetes, we analyzed protein expression changes. Cardiac expression of the mitophagy-related protein, BNIP3 was decreased in the prediabetic group in left ventricle lysates, however, other auto- and mitophagy-related proteins such as Beclin-1, LC3-II, SQSTM1/p62 and Parkin were unchanged (Figure 19*A*; Table 8). Upstream modulators of autophagy such as ACC, Akt, AMPKα, GSK3β and ribosomal S6 protein (a surrogate marker of mTOR complex activity) were also measured, however, expression or phosphorylation of these proteins were not different between groups (Figure 19*A*; Table 8). Furthermore, the expression of a mitochondrial fusion-related protein, MFN2 was elevated, however, expression of DLP1 and OPA1 proteins were unchanged in whole left ventricle lysates in the prediabetic group (Figure 19*B*; Table 8). Nonetheless, we measured the expression of mitochondrial dynamics- and mitophagy-related proteins

from SSM and IFM isolated from left ventricles. No difference was found in the expression of OPA1, LC3-II, SQSTM1/p62 in isolated cardiac SSM and IFM between groups (Figure 19, *C-D*; Table 8). Our results indicate that mitochondrial dynamics and autophagy/mitophagy were not modulated substantially by prediabetes, however, the upregulation of MFN2 (increased mitochondrial fusion, tethering to endoplasmic reticulum) and the downregulation of BNIP3 (decreased mitophagy) may implicate early changes in mitochondrial homeostasis, which might lead to the accumulation of dysfunctional mitochondria.

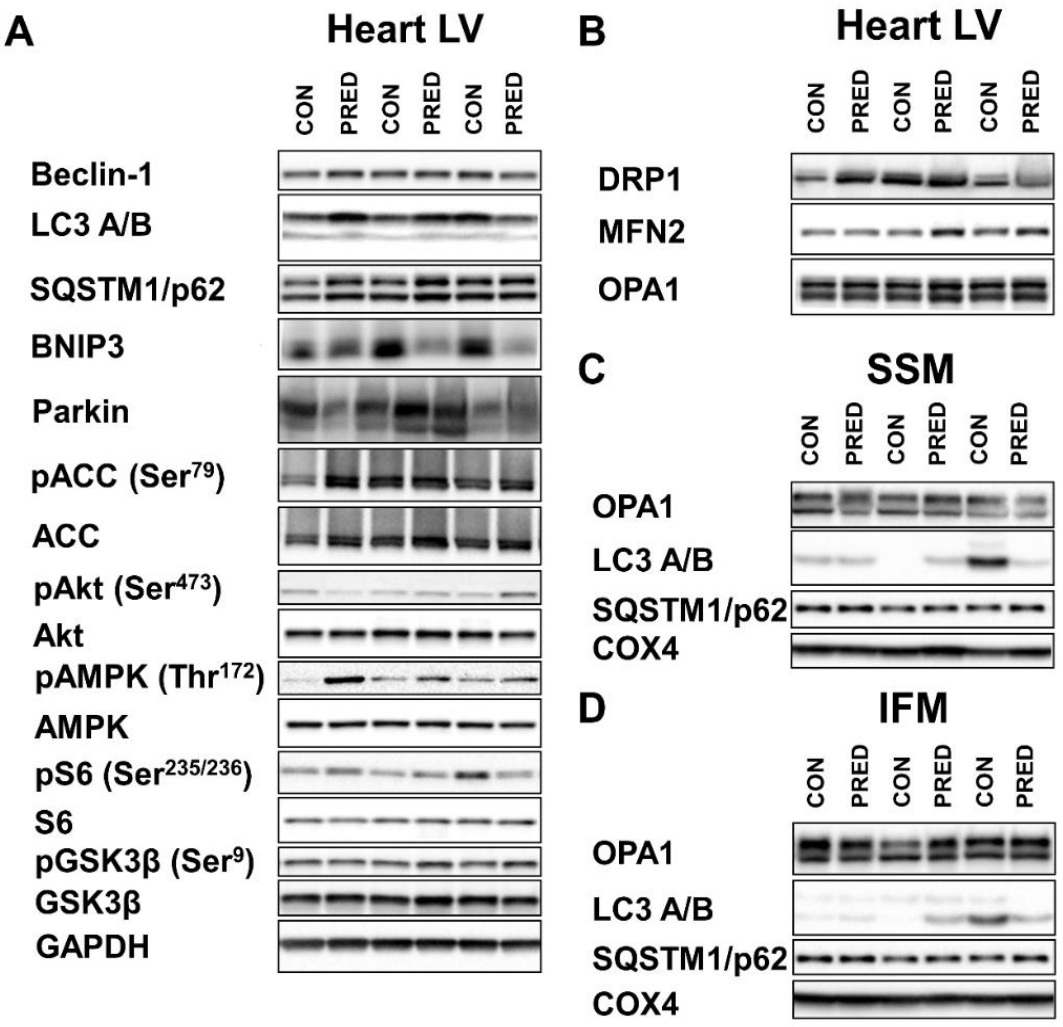

Figure 19. Cardiac expression of mitochondrial dynamics-, autophagy/mitophagy-and insulin signaling pathway-related proteins in prediabetes.

Representative Western blots of autophagy/mitophagy-related proteins and upstream modulators of autophagy (A), mitochondrial fission- and fusion-related protein (B) in whole left ventricles. Representative Western blots of mitochondrial dynamics- and mitophagy-related proteins in isolated SSM (C) and IFM (D). CON, control; PRED, prediabetic; LV, left ventricle; SSM, subsarcolemmal mitochondria; IFM, interfibrillar mitochondria; GAPDH, glyceraldehyde 3-phosphate dehydrogenase; DLP1, dynamin-like protein 1; MFN2, mitofusin-2; OPA1, optic atrophy 1 protein; COX4, cytochrome c oxidase subunit 4, mitochondrial; LC3, 1 microtubule-associated protein 1 light chain 3; SQSTM1/p62, sequestosome 1; BNIP3, Bcl-2/adenovirus E1B 19 kDa protein-interacting protein 3; ACC, Acetyl-CoA carboxylase; AMPKα, AMP-activated protein kinase α; GSK3β, glycogen synthase kinase-3 beta.

Table 8. Quantification of mitochondrial dynamics- and mitophagy-related protein expressions in isolated mitochondrial fractions and whole left ventricles (see Figure 19). *CON, control; PRED, prediabetic; LV, left ventricle; BNIP3, Bcl-2/adenovirus E1B 19 kDa protein-interacting protein 3; GAPDH, glyceraldehyde 3-phosphate dehydrogenase; MFN2, mitofusin-2; OPA1, optic atrophy 1; DLP1, dynamin-like protein 1; COX4, cytochrome c oxidase subunit 4, mitochondrial; LC3, 1 microtubule-associated protein 1 light chain 3; SQSTM1/p62, sequestosome 1, ACC, Acetyl-CoA carboxylase; AMPKα, AMP-activated protein kinase α; GSK3β, glycogen synthase kinase-3 beta. Data are presented as mean±SEM for 8 rat per group (*: p<0.05).*

	CON	**PRED**
Total LV		
BNIP3/GAPDH ratio	0.59±0.03	0.44±0.02*
MFN2/GAPDH ratio	0.27±0.01	0.36±0.02*
OPA1/GAPDH ratio	1.47±0.11	1.63±0.1
DLP1/GAPDH ratio	1.16±0.08	1.34±0.14
LC3-II/GAPDH ratio	0.56±0.07	0.56±0.05
p62/GAPDH ratio	3.05±0.18	3.45±0.23
Parkin/GAPDH ratio	2.25±0.14	2.43±0.17
Beclin1/GAPDH ratio	0.81±0.07	0.82±0.07
Phospho ACC (Ser^{79})/ACC ratio	0.92±0.05	1.0±0.09
Phospho AKT(Ser^{473})/AKT ratio	0.32±0.04	0.29±0.02
Phospho AMPK(Thr^{172})/AMPK ratio	0.12±0.02	0.21±0.06
Phospho S6($Ser^{235/236}$)/S6 ratio	2.62±1.08	2.16±0.61
Phospho GSK3β(Ser^{9})/GSK3β ratio	0.8±0.09	0.72±0.1
Subsarcolemmal mitochondria		
OPA1/COX4 ratio	1.34±0.07	1.32±0.06
LC3-II/COX4 ratio	0.22±0.1	0.25±0.04
p62/COX4 ratio	0.13±0.02	0.12±0.03
Interfibrillar mitochondria		
OPA1/COX4 ratio	1.44±0.15	1.52±0.14
LC3-II/COX4 ratio	0.22±0.09	0.29 ±0.07
p62/COX4 ratio	0.35±0.06	0.36±0.04

6.2.6 Expression of cardiac Bcl-2 decreases in prediabetes

Our investigation also aimed to explore the effect of prediabetes on apoptosis in the heart. Prediabetes did not affect the expression of pro-apoptotic caspase-3 and Bax in left ventricles. On the other hand, the anti-apoptotic Bcl-2 was downregulated in prediabetic animals. However, the Bcl-2/Bax ratio was unchanged (Figure 20*B*; Table 9).

6.2.7 No changes in cardiac HSPs in prediabetes

We also characterized the effect of prediabetes on the expression and/or phosphorylation of heat shock proteins in the left ventricle. Our results showed no differences in the expression of HSP-60, HSP-70 and HSP-90 or in either phosphorylation or expression of HSP-27 (Fig. *20A*; Table 9).

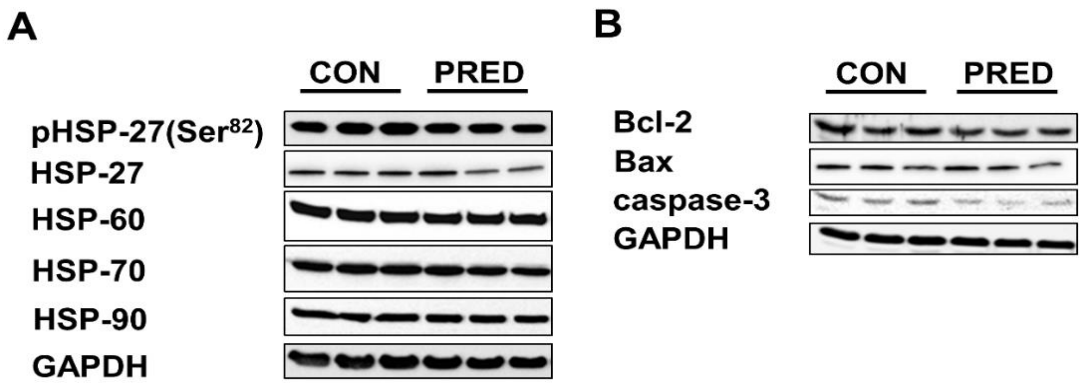

Figure 20. Cardiac expression of HSPs, and apoptosis-related proteins in prediabetes. *Representative Western blots of HSP- (A), and apoptosis-related (B) proteins in whole left ventricle. CON, control; PRED, prediabetic; HSP, heat shock protein; Bax, Bcl-2-associated X protein; GAPDH, glyceraldehyde 3-phosphate dehydrogenase.*

Table 9. Quantification of apoptosis and HSPs in whole left ventricles (see Figure 20). *CON, control; PRED, prediabetic; HSP, heat shock protein; GAPDH, glyceraldehyde 3-phosphate dehydrogenase. Data are presented as mean±SEM for 8 rat per group (*: p<0.05).*

Total LV	**CON**	**PRED**
Bcl-2/GAPDH ratio	0.23±0.01	0.20±0.003*
Bcl-2/Bax ratio	0.15±0.02	0.15±0.02
caspase-3/GAPDH ratio	0.05±0.001	0.04±0.003
Phospho HSP-27(Ser^{82})/HSP-27 ratio	0.34±0.05	0.28±0.02
HSP-60/GAPDH ratio	0.85±0.02	0.84±0.02
HSP-70/GAPDH ratio	0.53±0.01	0.51±0.01
HSP-90/GAPDH ratio	0.46±0.01	0.50±0.02

6.3 Detection and quantification of proteins in cardiac mitochondrial subpopulations

6.3.1 Differential amounts of proteins in mouse and rat cardiac SSM and IFM

To examine the amounts of proteins in cardiac subsarcolemmal (SSM) and interfibrillar (IFM) mitochondria, inner (connexin-43 - Cx43) and outer mitochondrial membrane (mitofusin 1 - MFN1, mitofusin 2 - MFN2, voltage-dependent anion-selective channel - VDAC) proteins as well as p66shc as a marker for the intermembrane space were measured. Mitochondrial sublocalization of DJ-1 has not been definitely established yet, since the protein has been found within the intermembrane space and the matrix[184], but also within the outer membrane and matrix [185]. The analyzed mitochondrial preparations were not contaminated with proteins of other cell compartments, which was shown by the absence of immunoreactivity for marker proteins of the sarcolemma, sarcoplasmic reticulum, and cytosol (Figure 21). The presence of perinuclear mitochondria (PNM) in SSM or IFM was not investigated due to lack of suitable methods. The signal intensity of VDAC in relation to Ponceau S staining was similar between SSM and IFM+N allowing the use of VDAC for normalization of protein data in the main study (Figure 22). The predominant localization of MFN2 in SSM was confirmed in mitochondria from Long-Evans rat hearts (Figure 23). In Wistar rats, MFN2 and Cx43 protein signals were higher in SSM samples, while intensities of MFN1 and p66shc protein signals were not different between SSM and IFM+N, and DJ-1 protein signal was

higher in IFM+N as compared to those in SSM (Figure 24). Similarly, in mitochondria obtained from mouse hearts, signal intensities for MFN2 and Cx43 were lower, while that of DJ-1 were higher in IFM+N as compared to SSM, and there were no significant differences in MFN1 and p66shc signals between groups (Figure 25).

These results suggest that mitochondrial proteins might have different expression patterns in cardiac SSM and IFM+N fractions.

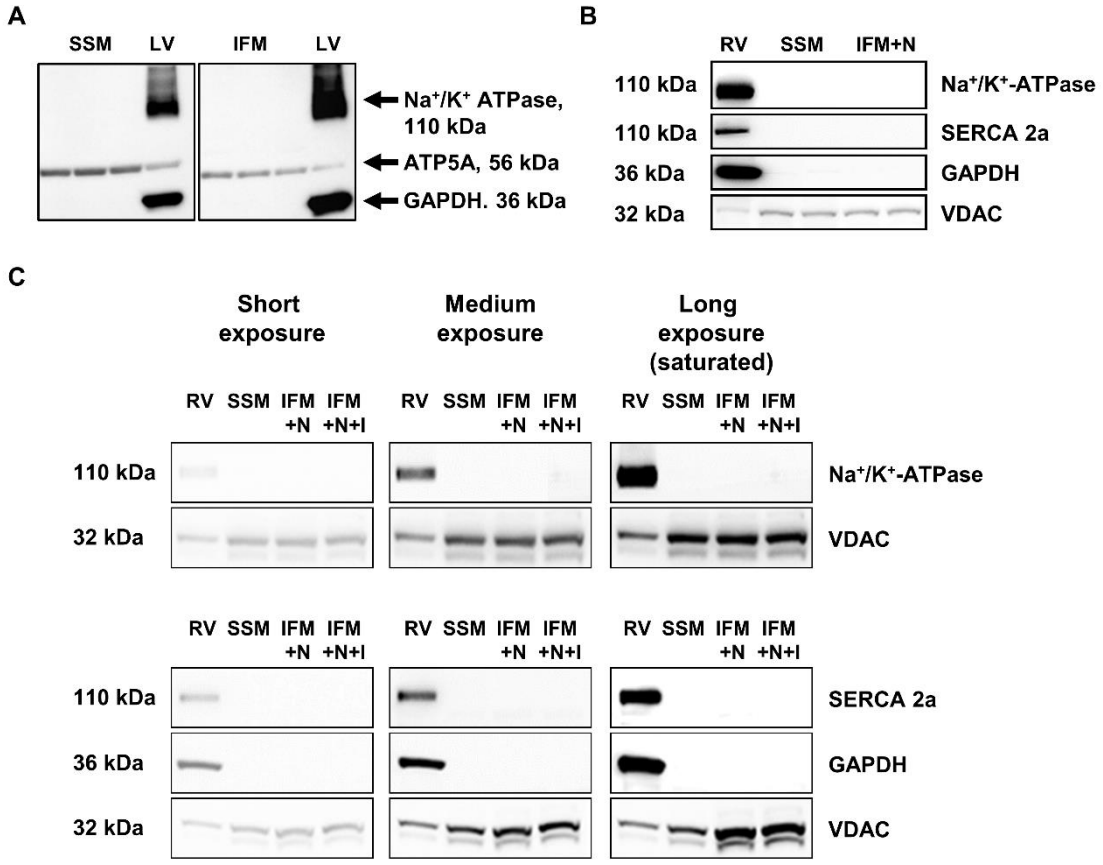

Figure. 21. Organelle markers demonstrated the purity of isolated mitochondria.
Western blot analysis for Na^+/K^+-ATPase, ATP5A and GAPDH on cardiac SSM and IFM isolated from Long-Evans rats (A) and SERCA 2a, Na^+/K^+-ATPase and GAPDH were used for cardiac SSM and IFM isolated from Wistar Han rats (B). Different protein signal exposures between mitochondrial subfractions in C57Bl6J mouse hearts (C). SSM, subsarcolemmal mitochondria, IFM+N, interfibrillar mitochondria treated with nagarse, GAPDH, glyceraldehyde 3-phosphate dehydrogenase; ATP5A, ATP synthase subunit alpha; SERCA 2a, sarco/endoplasmic reticulum Ca^{2+}ATPase II; VDAC, voltage-dependent anion-selective channel protein. SSM (n=8) vs. IFM+N (n=8) from Long-Evans rats (pilot study), SSM (n=4) vs. IFM+N (n=4) from Wistar Han rats and SSM (n=9-10) vs. IFM+N (9-10) and IFM+N+I (n=9-10) from C57Bl6J mice.

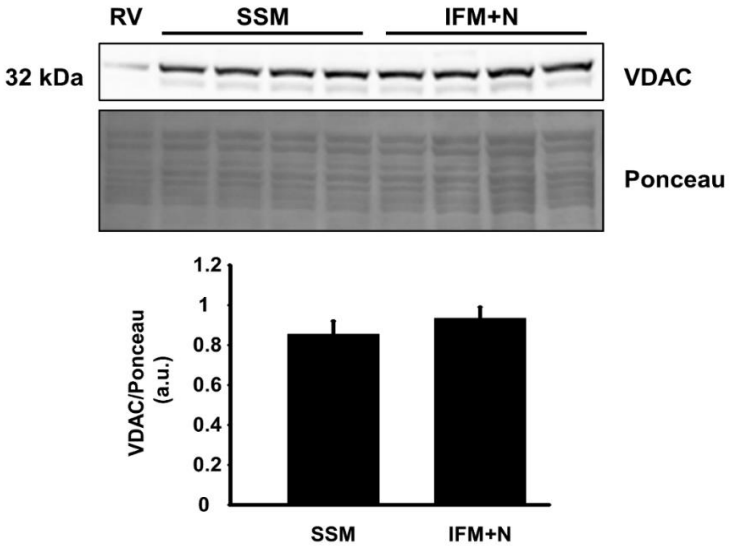

Figure 22. Presence of VDAC protein in SSM and IFM+N.
Western blot analysis was performed on total mouse right ventricular (RV) protein extracts and on mouse left ventricular SSM and IFM+N for the mitochondrial marker protein VDAC. Ponceau staining of the transferred proteins is also shown (upper panel). SSM, subsarcolemmal mitochondria; IFM+N, interfibrillar mitochondria treated with nagarse; VDAC, voltage-dependent anion-selective channel protein. Immunoreactive VDAC signals in SSM and IFM+N were normalized to respective Ponceau staining (lower panel). SSM (n=4) vs. IFM+N (n=4); mean±SEM; p=ns.

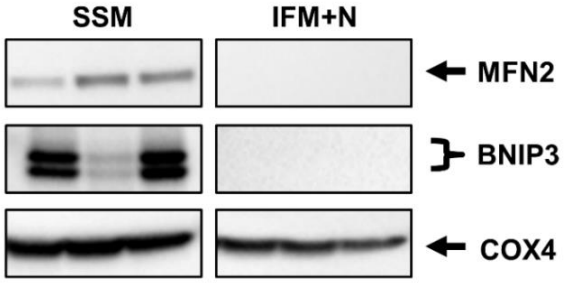

Figure 23. Different protein signal intensities between mitochondrial subfractions.
Representative Western blot pictures for MFN2 and Bnip3 proteins showed different signal intensities in cardiac SSM compared to IFM+N in a pilot study from Long-Evans rats. SSM, subsarcolemmal mitochondria; IFM+N, interfibrillar mitochondria treated with nagarse; MFN2, mitufusin 2; BNIP3, Bcl-2/adenovirus E1B 19 kDa protein-interacting protein 3; COX4, cytochrome c oxidase subunit 4 isoform 1. SSM (n=8) vs. IFM+N (n=8).

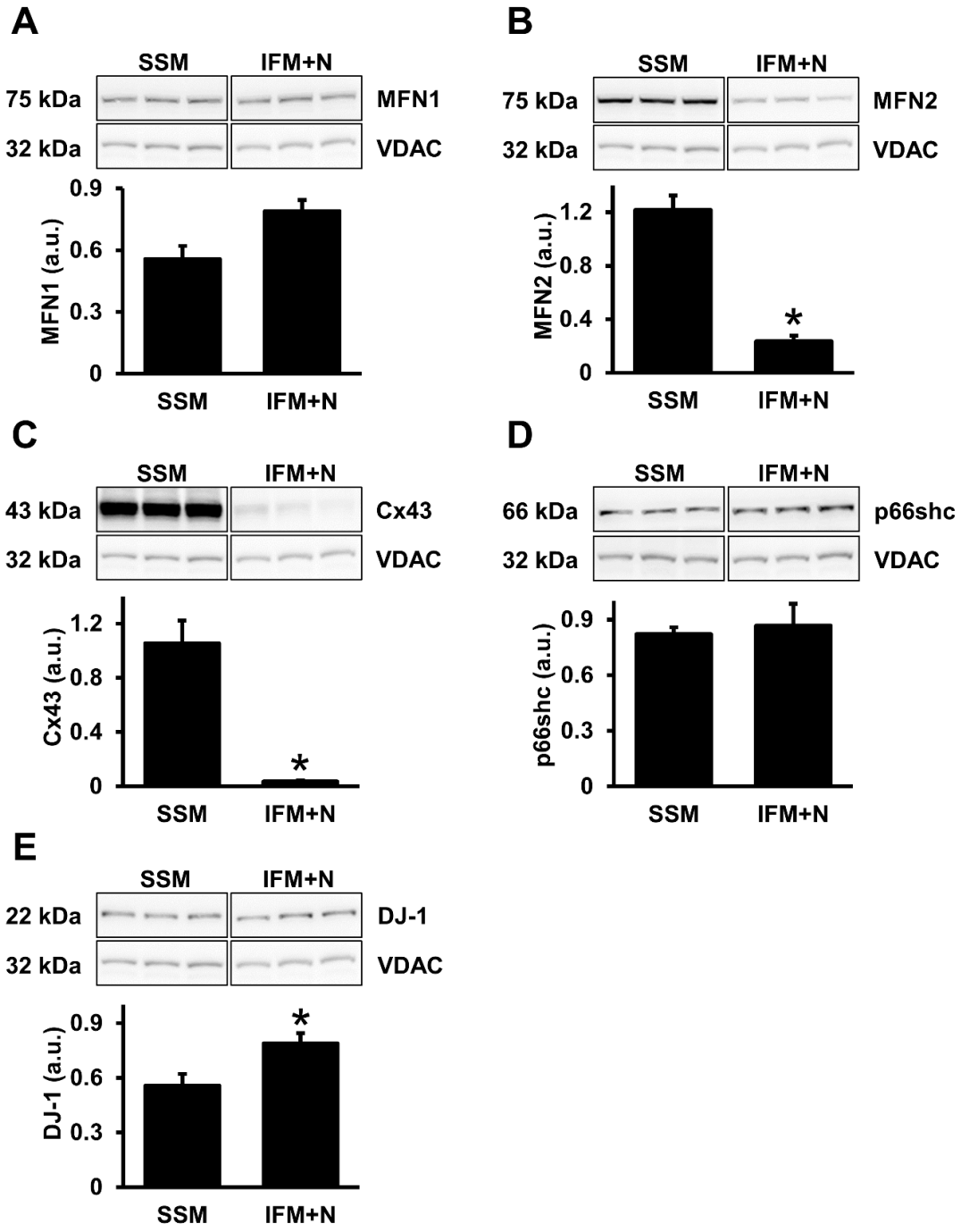

Figure 24. Presence of MFN1, MFN2, Cx43, p66shc and DJ-1 in rat cardiac SSM and IFM+N.

*Representative Western blot analysis and quantification of MFN1 (A), MFN2 (B), Cx43 (C), p66shc (D) and DJ-1 (E) in Wistar rat cardiac SSM and IFM+N. Respective protein amounts were normalized to those of VDAC. SSM, subsarcolemmal mitochondria; IFM+N, interfibrillar mitochondria treated with nagarse; MFN1-2, mitufusin 1-2; Cx43, connexin-43; DJ-1, protein deglycase DJ-1 (Parkinson disease protein 7); VDAC, voltage-dependent anion-selective channel protein. SSM (n=4) vs. IFM+N (n=4); mean±SEM; *: p<0.05.*

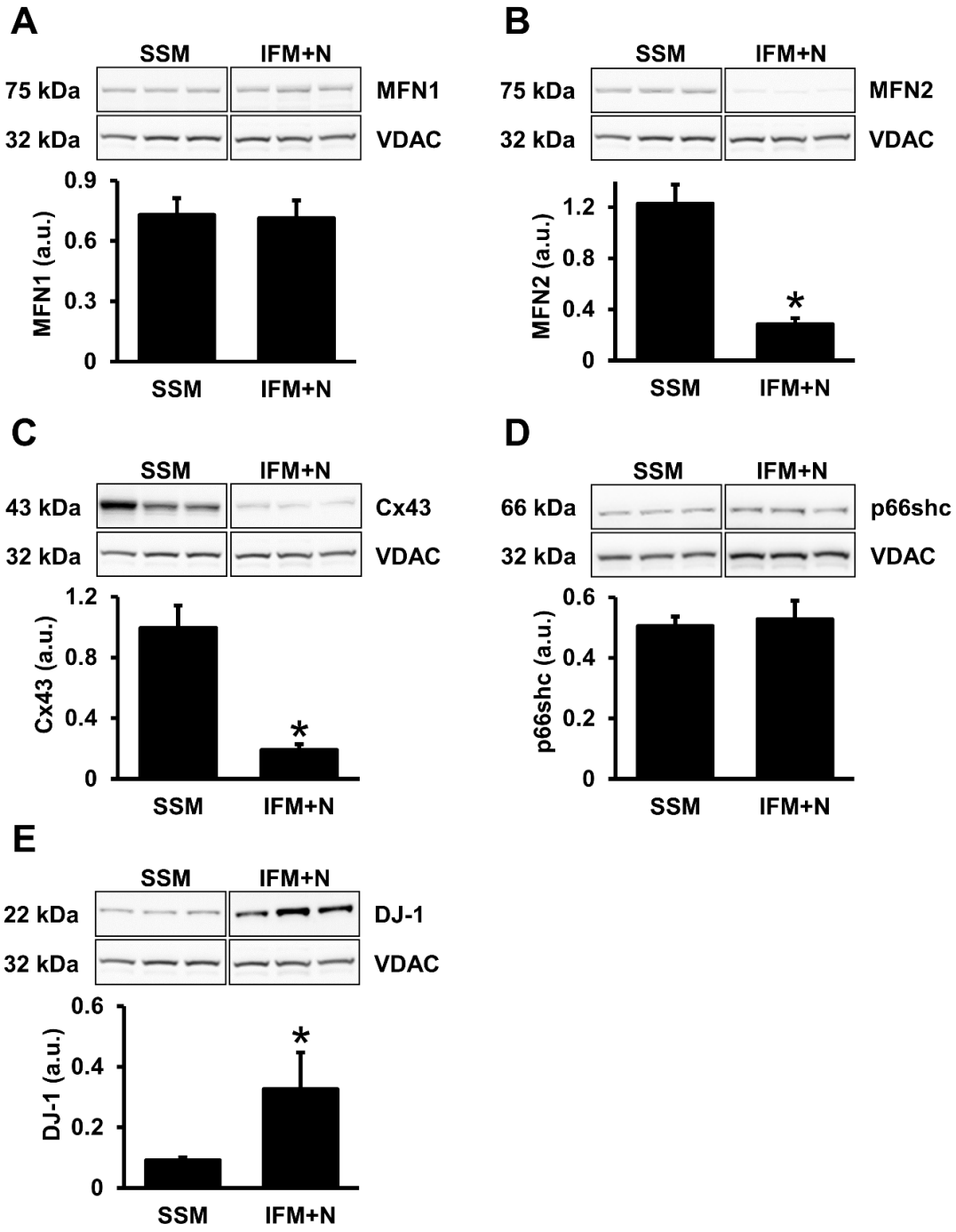

Figure 25. Presence of MFN1, MFN2, Cx43, p66shc and DJ-1 in mouse cardiac SSM and IFM+N.

*Representative Western blot analysis and quantification of MFN1 (A), MFN2 (B), Cx43 (C), p66shc (D) and DJ-1 (E) in C57Bl6J mouse cardiac SSM and IFM+N. Respective protein amounts were normalized to those of VDAC. SSM, subsarcolemmal mitochondria; IFM+N, interfibrillar mitochondria treated with nagarse; MFN1-2, mitofusin 1-2; Cx43, connexin-43; DJ-1, protein deglycase DJ-1 (Parkinson disease protein 7); VDAC, voltage-dependent anion-selective channel protein. SSM (n=4) vs. IFM+N (n=4); mean±SEM; *: $p<0.05$.*

6.3.2 Nagarse treatment influences protein signals in SSM and IFM from mouse hearts

To investigate the impact of enzymatic treatment on mitochondrial proteins of the mouse heart, similarly to the standard isolation method of IFM (common protocol), nagarse was added to SSM as well (SSM+N). Nagarse treatment of SSM resulted in decreased signal intensities of MFN1, MFN2, and Cx43, as shown by Western blot analysis (Figure 26, *A-C*). In contrast, nagarse treatment had no effect on the amount of p66shc in SSM, whereas the level of DJ-1 slightly – but significantly – increased in SSM+N compared to SSM (Figure 26, *D-E*). To study the role of the enzymatic digestion by nagarse on protein signals in IFM, two strategies were followed: 1) as described in the common protocol, nagarse was added to the sample containing the IFM, incubated for 1 min, samples were homogenized and then the activity of the enzyme was stopped by centrifugation and washing of the released IFM (IFM+N); 2) nagarse was added to the sample containing the IFM, incubated for 1 min, then the activity of the enzyme was stopped by addition of PMSF and samples were then processed as under 1) (IFM+N+I, Figure 7). When comparing both protocols, nagarse inhibition by PMSF had no influence on signals of Cx43, DJ-1, p66shc, and MFN1, whereas it significantly increased the signal intensity of MFN2 to that measured in SSM.

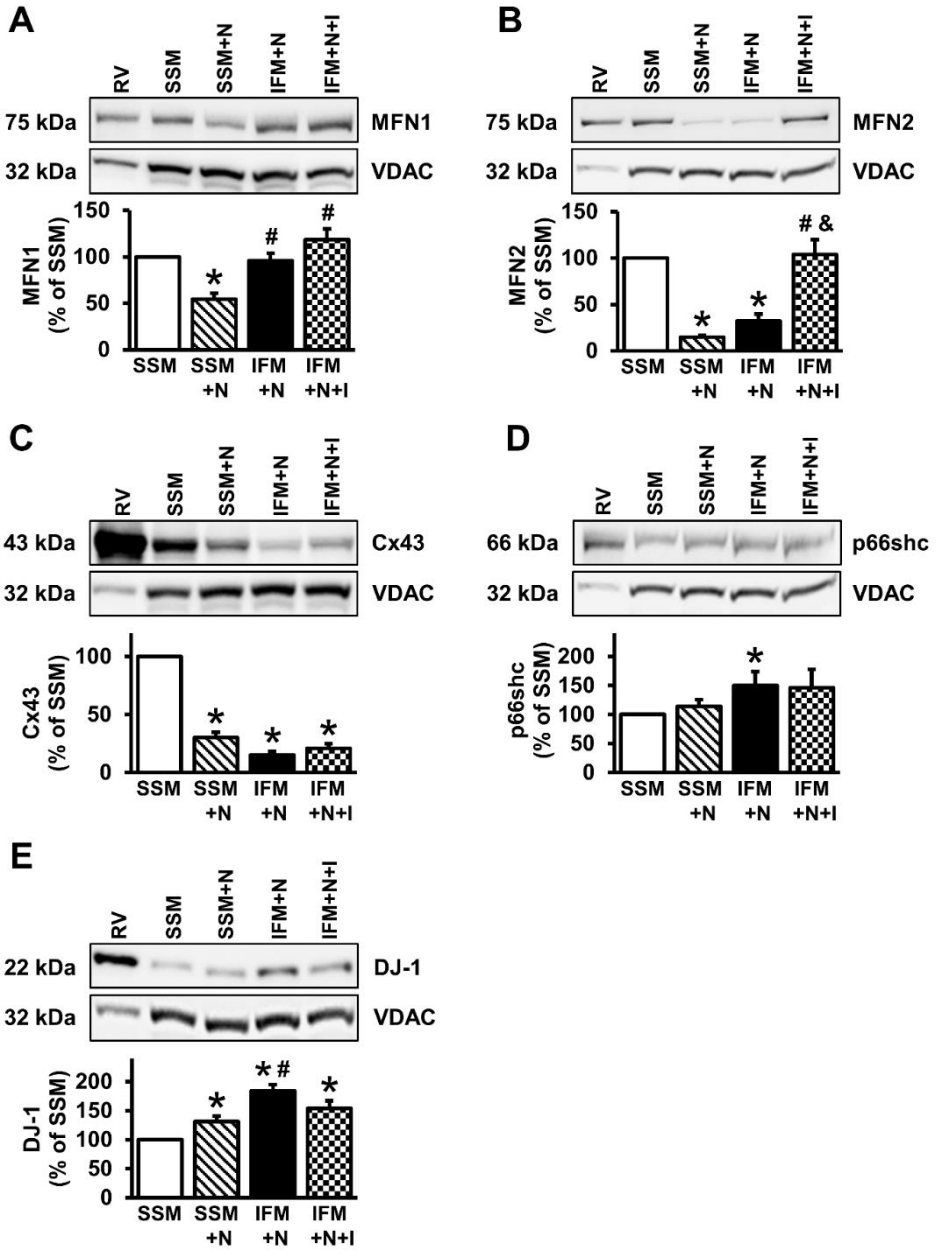

Figure 26. Effects of nagarse and its inhibition on the amounts of MFN1, MFN2, Cx43, p66shc, and DJ-1 in mouse SSM and IFM.

*Western blot analysis for MFN1 (A), MFN2 (B), Cx43 (C), p66shc (D) and DJ-1 (E) on mouse SSM and IFM isolated according to the common protocol (SSM, IFM+N), on SSM treated with nagarse (SSM+N) and on IFM, in which the nagarse was inhibited after 1 minute incubation (IFM+N+I). Total mouse right ventricular (RV) protein extracts were used as control. Lower panels show the quantification of MFN1, MFN2, Cx43, p66shc and DJ-1 in SSM, SSM+N, IFM+N, and IFM+N+I normalized to VDAC in % of the respective SSM controls. SSM, subsarcolemmal mitochondria; IFM, interfibrillar mitochondria; MFN1-2, mitofusin 1-2; Cx43, connexin-43; DJ-1, protein deglycase DJ-1 (Parkinson disease protein 7); VDAC, voltage-dependent anion-selective channel protein. SSM (n=8-10) vs. IFM (n=8-10); mean±SEM; *,#,&: p<0.05 *: vs. SSM; #: vs. SSM+N; &: vs. IFM+N.*

6.3.3 Nagarse treatment has no effect on respiration of mitochondrial subfractions

To investigate the enzymatic effect of nagarse on mitochondrial function, mitochondrial oxygen consumption was measured. Our results showed that nagarse treatment had no effect on either basal or ADP-stimulated oxygen consumption by complex I or complex II compared to untreated SSM. However, a tendency towards a higher complex I-mediated oxygen consumption was observed after nagarse treatment in SSM (p=0.098, Figure 27). Mitochondrial respiration was similar in IFM+N and IFM+N+I demonstrating that PMSF-treatment had no deleterious effect on mitochondrial function.

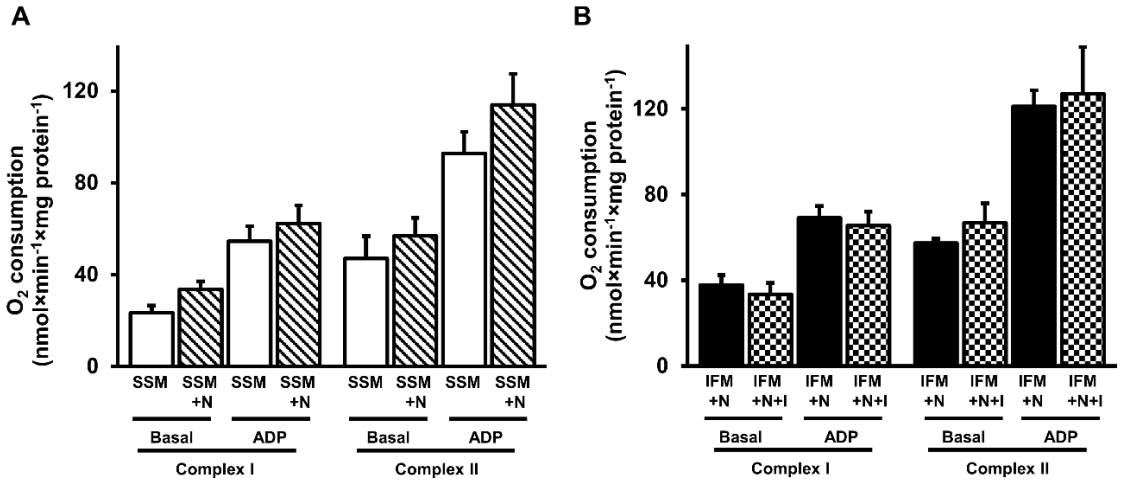

Figure 27. Nagarse had no effect on oxygen consumption in mitochondrial subfractions. *Mitochondrial oxygen consumption by complex I and complex II was measured in mouse SSM (A) and IFM (B) isolated according to the common protocol (SSM, IFM+N), in SSM treated with nagarse (SSM+N), and in IFM, in which nagarse was inhibited after 1 minute incubation (IFM+N+I). Data are presented as mean±SEM; n=6 per group; p=ns.*

Pictures and quantitative data of phospho- and total form of ACC found in Figure 19*A* and Table 8 have not yet been published previously. The results that are not derived from my own work will not be used in the doctoral dissertation of another authors.

7 Discussion

7.1 Hypercholesterolemia modulates cardiac mTOR and autophagy

7.1.1 Hypercholesterolemia increases mTOR activity and attenuates autophagy in rat heart

In this thesis, we showed that hypercholesterolemia downregulates cardiac autophagy and activates mTOR pathway (for schematic representation see Figure 28). Autophagy-related pathways were previously studied in various swine models of mixed hyperlipidemia, which presented somewhat divergent results. Sellke *et al.*[84] studied swine models of mixed hyperlipidemia where they applied regional cardiac ischemia and assessed autophagy in non-ischemic myocardium. They demonstrated that cardiac mTOR activity was significantly elevated while autophagy marker LC3-II was diminished in hyperlipidemic Yucatan pigs. These findings are in good alignment with our results shown here, however, another study showed that hyperlipidemia decreased expression of Beclin-1, but not of LC3-II in Yorkshire swine[186], while in Ossabaw swine hyperlipidemia elevated cardiac LC3-II and Beclin-1 proteins[187]. Similarly to these findings, the status of cardiac autophagy in other metabolic disorders was also found to be unclear. Recently we showed that diet-induced obesity leads to decreased induction of autophagy in response to fasting in mice involving altered expression of numerous proteins related to metabolic pathways [85], which is in parallel to our current findings. In contrast, Hsu *et al.* demonstrated that metabolic syndrome induced by high-fat feeding increased cardiac LC3-II and SQSTM1/p62 in mice[188]. In addition, we found an increased expression in Class-III PI3K expression in hypercholesterolemia, however, no similar data has published yet, thus, this phenomenon needs further investigation.

Overall, these reports and our current findings demonstrate that complex metabolic disorders might modulate cardiac mTOR pathway and autophagy differentially depending on the animal model applied, and they also highlight that focused studies are necessary to decipher the role of specific metabolic pathways on autophagy.

7.1.2 Hypercholesterolemia increases apoptosis, but not necroptosis in rat heart

Our results demonstrated that apoptosis was upregulated by hypercholesterolemia in the rat heart. We assessed an increased cleaved caspase-3 activation, however, the balance of pro- and anti-apoptotic Bcl-2 proteins was unaffected by hypercholesterolemia. Similarly, Cheng *et al.* reported that 8 weeks of cholesterol-enriched diet induced cardiac apoptosis in hamsters, associated with increased expression of BH3 interacting-domain death agonist (BID) and Bax[98]. These results correlate well with findings of Zhu *et al.* who showed that 12 weeks of hypercholesterolemic diet elevated cardiac expression of Bax, decreased Bcl-x_L but did not affect caspase-3 in swine[189]. Furthermore, Hsu *et al.* demonstrated that cardiac cleaved Poly (ADP-ribose) polymerase (PARP) was increased in obese C57BL/6 mice on a high fat diet[188]. On the contrary, Osipov *et al.* showed that hyperlipidemia did not exacerbate cardiac apoptosis after I/R in a Yucatan swine model based on the findings of decreased cleaved PARP and no difference in activation of caspase-3[97]. Hypercholesterolemia has also been shown to modulate apoptosis in other tissue types. For example, Perales *et al.* showed upregulated Bax expression in vascular smooth muscle cells exposed to 25-hydroxycholesterol[190]. Therefore, the majority of these results demonstrate that there is a strong relationship between increased cardiac apoptosis and hypercholesterolemia, although different models of hypercholesterolemia display varying constellations of altered apoptotic markers.

Although several publications report elevated cardiac apoptosis in hypercholesterolemia, data on cardiac necroptosis is scarce. Thus we assessed the first time the status of necroptosis *in vivo* in hypercholesterolemia. Here we demonstrate that the expression of major markers of necroptosis are not modulated in the heart of cholesterol-fed rats. However, in a similar model of hypercholesterolemia, cardiac expression of RIP3 mRNA was increased[191], although no other measures of necroptosis were assessed. Nevertheless, these findings demonstrate that the effect of hypercholesterolemia on cardiac necroptosis needs further investigation.

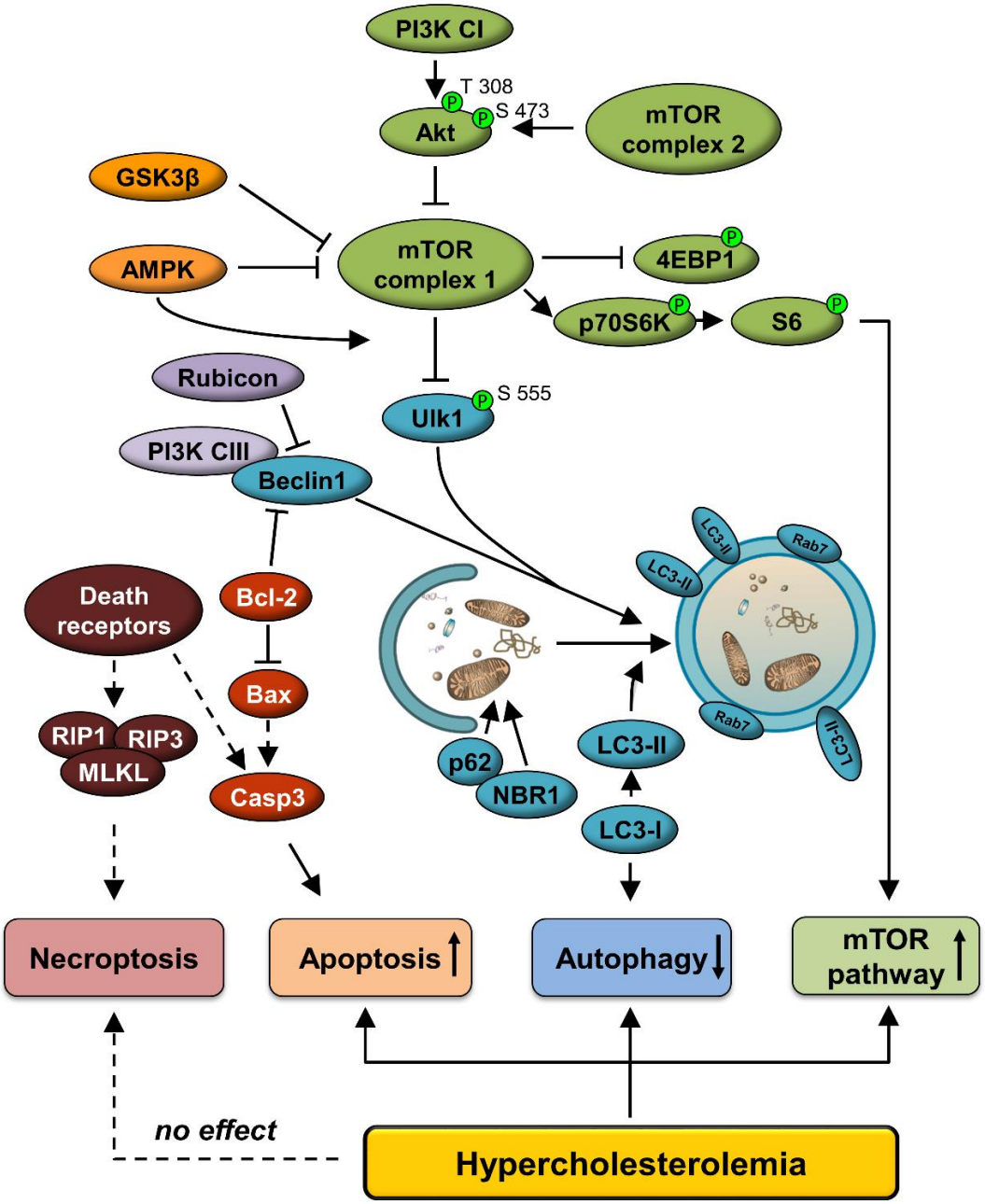

Figure 28. Schematic representation of the cardiac effect of hypercholesterolemia on autophagy, apoptosis, necroptosis and mTOR pathways.

PI3K CI-III, class I-III phosphoinositide 3-kinase; NBR1, neighbor of BRCA1 gene 1; AMPKα, AMP-activated protein kinase α; GSK3β, glycogen synthase kinase-3 beta; ULK1, unc-51-like kinase 1; LC3, microtubule-associated protein light chain 3; RAB7, ras-related protein Rab-7a; Rubicon, run domain Beclin-1-interacting and cysteine-rich domain-containing protein; SQSTM1/p62, sequestosome 1; mTOR, mechanistic target of rapamycin; P70S6K, ribosomal protein S6 kinase beta-1; S6, ribosomal S6 protein; 4EBP1; eIF-4E binding protein 1; Casp3, caspase 3; Bax, Bcl-2-associated X protein; RIP1-3, receptor-interacting serine/threonine-protein kinase 1 and 3; MLKL, mixed lineage kinase domain-like protein.

7.2 Prediabetes induced diastolic dysfunction by mild mitochondrial oxidative stress and impaired mitophagy

7.2.1 Prediabetes induces mild diastolic dysfunction and hypertrophy without fibrosis

This setting allowed us to investigate cardiac consequences of a moderate metabolic derangement, prediabetes, rather than of a severely disturbed glucose and lipid homeostasis, such as seen in genetically modified models of diabetes, e.g. in *db/db* or *ob/ob* mice[192, 193]. Since it has been reported that left ventricular (LV) hypertrophy had a higher prevalence in patients with diabetes, and that 40-75% of patients with type 1 or type 2 diabetes mellitus presented with diastolic dysfunction[194, 195], we aimed to investigate whether cardiac function is affected by prediabetes. Previously it has been shown that diastolic dysfunction was developed in several pathological condition, however, the underlying mechanisms are still not clearly understood[177]. Here we demonstrated that the deterioration of diastolic function and sensory neuropathy occurs well before overt diabetes develops, which is accompanied by early signs of cardiac hypertrophy. These findings are in agreement with previous reports showing that neuropathy might precede the development of a full-fledged diabetes[196], and that high-fat diet-induced prediabetes increased heart weights and decreased contractile function, as assessed by a diminished aortic output[51, 197]. However, in contrast to our report, plasma triglycerides and insulin levels were elevated in these studies, highlighting that substantial difference can be observed between different diet-induced models and stages of prediabetes[51]. Furthermore, it has been described that obesity promoted the hypertrophy-inducing effect of diabetes regardless of hypertension[198], which could be attributed to adipokines, such as leptin and resistin[199, 200]. Similarly, here we evidenced that even mild obesity (only 18% increase in body weight was observed) with an elevated leptin level is sufficient to induce hypertrophy even without impairment of fasting plasma glucose and lipid levels or hypertension, which is in agreement with previous reports[51, 197]. Furthermore, it has been shown recently that, high-fat diet did not resulted in cardiac hypertrophy but induced diastolic dysfunction in rats, which was prevented by monosaturated fat canola oil[201]. However, clinical data seem to contradict these findings, since no increase in the prevalence of LV hypertrophy was observed in overweight prediabetic patients with impaired fasting glucose and impaired glucose tolerance[202].

Mechanistic studies on how obesity abrogates cardiac function are scarce. Increased myocardial triglyceride content is associated with diastolic dysfunction in *ob/ob* mice[203], which is well in line with our findings that the number of lipid particles increased in the myocardium in prediabetes. Although microRNA-451 has been demonstrated to promote cardiac hypertrophy and diminished contractile reserves in mice on high-fat diet[204], further studies are warranted to describe the relationship between cardiac dysfunction and the disturbed cardiac lipid metabolism in prediabetes. Interestingly, unlike in genetic models of prediabetes[205], diet-induced prediabetes did not result in an elevation in classical molecular markers of hypertrophy or conventional signs of fibrosis in the heart as expected in case of hypertrophy. Moreover, this is the first evidence on decreased beta-myosin heavy chain (β-MHC) in prediabetes. Although the vast majority of publications evidence an increase in β-MHC in diabetes[206, 207], a small number of studies indicate a downregulation of MHC expression in animals with diverse cardiac or metabolic challenges. For instance, in cardiomyocytes from STZ-treated rats, total MHC expression was significantly decreased[208]. Furthermore, a recent publication also found that cardiac β-MHC gene expression was decreased after 2 months of high-fat, high-glucose feeding in diabetic male Wistar rats[209]. These results indicate that although in most cardiometabolic derangements expression of the slow MHC isoform increases, in certain conditions, such as in prediabetes, a general suppression of MHC expression might be present. The reduction in MHC expression might also contribute to the observed cardiac dysfunction in prediabetes; however, to uncover its significance and mechanism, further experiments are warranted.

7.2.2 Prediabetes induces mild elevation of oxidative stress in cardiac subsarcolemmal mitochondria

Oxidative stress has a major role in the development of diabetic cardiomyopathy[36, 210]; however, it has not been well described whether it is responsible for the decreased cardiac function in prediabetes. Here we found an elevated hydrogen peroxide production in SSM, increased nitrotyrosine formation and an elevated cardiac expression of mitofusin 2 (MFN2).

These findings are in agreement with previous reports, where elevated oxidative stress, such as seen in our model of prediabetes, leads to an increase in MFN2 in rat vascular

smooth muscle cells[211], and its robust overexpression induced apoptotic cell death in neonatal rat cardiomyocytes[212]. Similarly, in another study, high-fat diet induced oxidative stress and MFN2 overexpression in the liver of C57BL/6 mice after 16 weeks[213]. However, in a previous study on diet-induced prediabetes, no sign of cardiac mitochondrial oxidative stress was evidenced in male Wistar rats after 16 weeks[51], which may implicate that mitochondrial oxidative stress might not be present in all models and stages of prediabetes and that it might not be the primary driving force of prediabetes-induced cardiac functional alterations.

It is well-established that mitochondria, especially the mitochondrial electron transport chain is one of the main source of ROS, however, several other intracellular components can produce ROS in mitochondria[111]. For instance, it is known that p66Shc translocation to mitochondria can increase the formation of ROS[214], and NADPH oxidase 4 (NOX4) and monoamine oxidase (MAO) also have important role in mitochondrial ROS production[215, 216]. Based on the increased mitochondrial hydrogen peroxide production with glutamate-malate substrate, we showed that elevated mitochondrial oxidative stress might have been generated by respiratory complex I in prediabetic rat SSM. We could not detect differences with succinate substrate between mitochondrial subfractions, therefore, we concluded that respiratory complex II is not responsible for ROS production. Although here we observed a moderately increased ROS production in SSM, no difference can be seen in mitochondrial oxygen consumption between normal and prediabetic mitochondria (see Table 7), evidencing no impairment in mitochondrial redox chains. Although, a recent study also showed that no changes were observed in mitochondrial respiratory activity in high-fructose fed rat hearts, cardiac activity of sirtuin 1, which has important role in the mitochondrial lipid metabolism, was decreased. Furthermore, they showed that oxidation level of cardiac mitochondria was increased after 6 weeks of diet, which indicated an increased activity of cardiac mitochondria for fatty acid oxidation[217]. It is currently unknown what mechanism leads to the increased ROS production exclusively in SSM in prediabetes. In mice on high-fat diet, cardiac mitochondrial ROS production was elevated, and similarly to our results, mitochondrial oxygen consumption did not change substantially, while a significant amount of cardiac lipid accumulation was observed[218], however, the source of ROS has not been identified in this study either. In agreement with our experiments, a recent study indicated that long-

term high-fat diet increased cardiac mitochondrial ROS production; however, high-fat feeding decreased mitochondrial membrane potential in prediabetic Wistar rats. Elsewhere, high-fat, high-sucrose diet also increased cardiac superoxide level in a rat model of metabolic syndrome (JCR rats) after 12 weeks[219]. Thus, to reveal the direct connection between elevated ROS production, mitochondrial-, and cardiac dysfunction, further studies are warranted.

Although widely-used antidiabetic and antioxidant drugs such as metformin or Coenzyme Q_{10} can reduce the negative cardiovascular effect of diabetes and prediabetes[220-223], molecular mechanism and efficiency of these drugs in antioxidant therapy is still not clear. Vildagliptin, a dipeptidyl peptidase-4 inhibitor, restored high-fat diet-induced mitochondrial ROS production and improved mitochondrial function in prediabetic hearts[224, 225]. Furthermore, it was also shown that vildagliptin improved metabolic status and protected cardiac mitochondrial function against I/R injury in estrogen-deprived obese-insulin resistant female rats[226]. Empagliflozin, a sodium-glucose cotransporter 2 inhibitor, significantly reduced visceral adiposity, cardiac ROS production and inflammation as well as prevented cardiac hypertrophy in SHR/NDmcr-cp prediabetic rats[227].

Therefore, these drugs may regulate oxidative stress under pathological conditions, which could prevent the cardiac effect of prediabetes and could be novel therapeutic targets in the treatment of obesity or diabetes.

7.2.3 No changes in cardiac Ca^{2+} homeostasis in prediabetes

Molecular mechanisms that contribute to hypertrophy and cardiac dysfunction in prediabetes has not been investigated in detail. In our previous studies on diet-induced hypercholesterolemia or metabolic syndrome in Zucker Diabetic Fatty rats, we have shown by DNA- and miRNA microarrays that a multitude of cardiac cellular processes is modulated by these conditions[159, 228]. Similarly, we evidenced changes in several cellular processes, suggesting that hypertrophy and deteriorated diastolic function in prediabetes maybe consequences of numerous concurrent alterations in the cardiac homeostasis (see Figure 29). Characterizing active components of the contractile apparatus and Ca^{2+} homeostasis, here we observed a tendency to decrease in the Ser^{16} phosphorylation of PLB in prediabetes. In previous studies, decreased phosphorylation of PLB on Ser^{16} was

demonstrated to be associated with abnormalities in contraction and relaxation in the diabetic heart[229, 230]. This notion is further supported by the findings of Abdurrachim *et al.,* who demonstrated that phosphorylation of PLB was reduced in the heart of mice with diastolic dysfunction induced by a high-fat diet[218]. Therefore, decreased phosphorylation of PLB may also contribute to the development of early diastolic dysfunction we uncovered in prediabetes. Increased activity and expression of CaMKIIδ and reduced phosphorylation of PLB by CaMKIIδ have been found to be associated with contractile dysfunction, diabetes[183, 231], and fructose-rich diet-induced prediabetes[232]. In our model, expression and phosphorylation of CaMKIIδ, and phosphorylation of PLB on Thr^{17} were unchanged. This is in contrast with previous findings which have reported the phosphorylation of CaMKIIδ being increased in the heart of STZ-treated diabetic rats[233, 234], although, in these reports, a significant hyperglycemia was present, which was shown to facilitate the activation of CaMKIIδ[235]. Moreover, it was reported elsewhere that CaMKIIδ activity was enhanced by hyperlipidemia/obesity and this activation led to increased autophagy, mitochondrial dysfunction, endoplasmic reticulum- and oxidative stress in high-fat fed mice[236]. In another study, Esma *et al.* showed that Ca^{2+} homeostasis was impaired due to altered PLB and SERCA2a activities in rats with metabolic syndrome induced by a 16-week high-sucrose drinking-water diet[237].

Tropomyosin is prone to loss of function by oxidative modifications that are associated with the severity of heart failure in humans[238, 239]. Our results showed that, oxidized tropomyosin content of the heart was not modulated by prediabetes. These data suggest that neither the CaMKIIδ pathway nor tropomyosin oxidation are responsible for the diastolic dysfunction observed in prediabetes.

7.2.4 Apoptosis is not modulated by prediabetes in cardiomyocytes

Apoptosis is considered to be one of the hallmarks of diabetic cardiomyopathy and it is induced by oxidative stress in diabetes[36, 105]. It has been described that experimental diabetes induces upregulation of pro-apoptotic, and downregulation of anti-apoptotic proteins[103, 240]. In this thesis, a modest downregulation of Bcl-2 was shown, however, no change in Bcl-2/Bax ratio, and in caspase-3 expression was detected in prediabetic animals. Previously it was demonstrated that high-fat diet resulted in cardiac injury via induction of apoptosis and inhibition of autophagy[241]. A recent study showed that

apoptosis was elevated due to the increased cardiac Bax and decreased Bcl-2 expressions, however, vildagliptin treatment improved the anti-apoptotic capability of cardiac tissue in high-fat fed prediabetic rats[224]. This research group also demonstrated that fibroblast growth factor 21 has similar efficacy for cardioprotection than vildagliptin via its anti-apoptotic mechanism in prediabetic rats[242]. Thus, our data suggest an early dysregulation of pro- and anti-apoptotic proteins in prediabetes; however, they do not evidence a gross induction of apoptosis in prediabetes. These data suggest that apoptosis induction has no effect in prediabetes.

7.2.5 Early sign of altered mitochondrial fusion and mitophagy in prediabetes

Here we demonstrate an early dysregulation of mitochondrial fusion and mitophagy first in the literature, as evidenced by an elevated MFN2 and an attenuated BNIP3 expression in prediabetes; however, other canonical markers of autophagy, mitophagy and apoptosis were unaffected. Similarly, right atrial myocardial samples of type-2 diabetic patients presenting no signs of overt cardiomyopathy the expression of the majority of mitochondrial dynamics- and autophagy-related proteins was not elevated, except for that of Atg5 and MFN1[243]. Furthermore, impaired autophagy resulted in endothelial dysfunction in patients with diabetes via unchanged LC3 and higher SQSTM1/p62 protein levels[244]. Recently, it was shown that autophagy was suppressed due to elevated mTOR activity distinct from IGF-1-Akt signaling; however, inhibition of ERK signaling abolished the mTOR activation and autophagy suppression in *ob/ob* mouse hearts[245]. It was previously demonstrated that altered glucose homeostasis has negative effect on cardioprotective interventions[246]. Indeed, our previous study demonstrated that acute hyperglycemia with no preceding diabetes abolished cardioprotection via overactivation of cardiac mTOR pathway, however, autophagy is not modulated in rats[247]. Despite our findings, Xie *et. al.* presented that acute hyperglycemia decreased the level of autophagic flux which is associated with suppressed diastolic function and impaired mitochondrial energy signaling in rat cardiomyocytes[248]. Therefore, we can assume that only major disturbances in glucose and lipid homeostasis, such as seen in untreated patients or in genetic models of diabetes, might be a powerful enough signal to extensively modulate cardiac autophagy, mitophagy, or mitochondrial dynamics, which might result in grossly deteriorated cardiac function. Moreover,

experimental systemic sensory neuropathy by itself has been previously shown to cause diastolic dysfunction and global gene expression changes in the rat heart[48, 49]. Therefore, the observed prediabetes-induced sensory neuropathy might also contribute to the diabetic cardiomyopathy.

Furthermore, our findings demonstrate the first time that prediabetes does not modulate cardiac expression of HSP-60, HSP-70 and HSP-90 and phosphorylation or expression of HSP-27. In contrast, in STZ-induced diabetes, increased levels of HSP-70 has been detected in the rat heart[249], and increased level of circulating HSP-60 found in diabetic patients[250], suggesting that in advanced stages of diabetes HSPs might be involved in the development of cardiac dysfunction. However, our data suggests no role of HSPs in prediabetes in the heart.

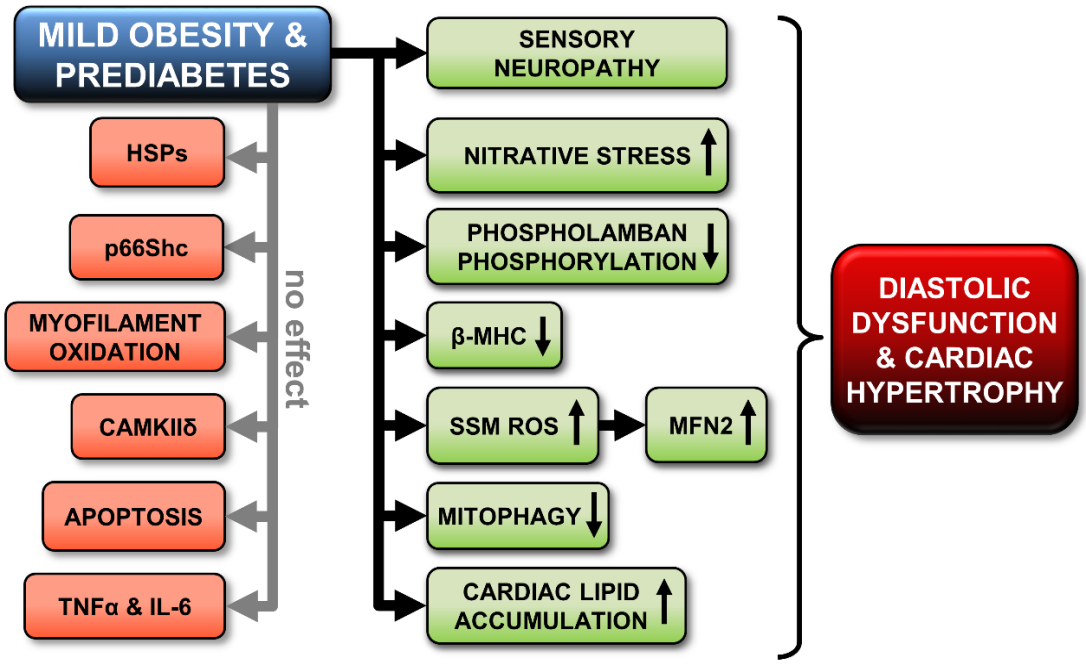

Figure 29. Schematic representation of the cardiac effects of prediabetes.
SSM, subsarcolemmal mitochondria; ROS, reactive oxygen species; HSP, heat shock protein; CAMKIIδ, Ca^{2+}/calmodulin-dependent protein kinase II; TNFα, tumor necrosis factor alpha; IL-6, interleukin-6; MFN2, mitofusin 2; β-MHC, beta-alpha-myosin heavy chain.

7.3 Detection of mitochondrial proteins is influenced by mitochondrial isolation with nagarse

Here we evidence that nagarse, a bacterial protease commonly used for isolation of IFM, significantly influences the detection of MFN2 in this mitochondrial subfraction. Differential protease sensitivity of SSM proteins was also evidenced: whereas detection of MFN1, MFN2, DJ-1 and Cx43 was influenced by nagarse that of p66shc was not. Furthermore, we also demonstrated that mitochondrial respiration was not influenced by nagarse treatment.

The effect of protease treatment on mitochondrial proteins and on mitochondrial function has been investigated previously. Studies indicated that nagarse reduced palmitoyl-coenzyme A synthetase activity in cardiac mitochondria[251], and partial breakdown of mitochondrial proteins were reported in rat brain[252] and gastrocnemius muscle[253] after nagarse treatment. The effect of protease treatment on proteins of different mitochondrial subfractions has also been investigated. Kras and colleagues found that nagarse decreased the total protein concentration of SSM samples isolated from striated muscles, which suggests that certain proteins in the SSM fraction might be partially degraded by nagarse[156]. In contrast to the reduced protein yield, mitochondrial respiration was significantly elevated by nagarse, indicating that nagarse treatment might remove non-mitochondrial contamination or damaged mitochondria, although, specific protein levels were not investigated in this study[156]. However, our present data indicate no significant effect of enzymatic digestion on mitochondrial respiration; there was only a tendency for oxygen consumption being increased following nagarse treatment. Therefore, the effect of nagarse on mitochondrial function might need further investigation.

In this thesis, we assessed signal intensities of proteins from different mitochondrial compartments in control and nagarse-treated SSM. When a protease is added to intact mitochondria, it is reasonable to assume that first proteins of the outer mitochondrial membrane are digested, and indeed, the mitochondrial signals of MFN1 and MFN2 were reduced. However, VDAC signals were unaffected. The VDAC-antibody used in the present study is directed against amino acids forming the β barrels 12 and 13 of the protein, which –among other residues – form the wall of the VDAC channel and are

therefore presumably inaccessible for the nagarse. Cx43 is present in the inner mitochondrial membrane, but its C-terminus – which is detected by the antibody used in the present study – is directed towards the intermembrane space[147] and can therefore be digested. The finding that the amount of p66shc – present in the intermembrane space[254] - was unaffected by nagarse treatment of SSM implies that the extent of protein digestion by nagarse is not in the first instance determined by the submitochondrial localization of the protein. Moreover, the accessibility of the epitope against which the respective antibody is directed seems to be important for the result of the nagarse treatment.
Although DJ-1 was recently shown to be localized at the outer mitochondrial membrane[185, 255], its distribution in the mitochondrial matrix and the translocation of the protein to this compartment has also been demonstrated[184, 185]. Whereas no precise analysis of the submitochondrial localization of DJ-1 was performed in our study, the lack of digestion by nagarse suggests a localization in other compartments than the mitochondrial outer membrane. Therefore, the cause of the elevated DJ-1 signal intensity after nagarse treatment needs further investigation. Furthermore, since the DJ-1 signal is higher in IFM+N than in both SSM and SSM+N, it is plausible that DJ-1 is present at higher levels in IFM.

Considering the differences in form and function between SSM and IFM, studies using proteomic approaches aim to identify specific proteins in mitochondrial subfractions, which are implicated in pathophysiological conditions such as diabetes[146, 256], or ischemic preconditioning[257]. A recent publication also demonstrated that nagarse was responsible for the loss of mitochondrial proteins from mouse heart, as evidenced by immunogold labelling and Western blot of Cx43 in nagarse-treated SSM[258]. However, mitochondrial preparations are not completely comparable with our samples, because this group did not perform an ultracentrifugation step during mitochondria isolation, which is necessary to isolate pure mitochondria fractions. We found that Cx43 was predominantly present within cardiac SSM. This data confirm previous results from Boengler *et al.*[147] and others in which nagarse[153, 154], or proteinase K[151] was used for IFM isolation. In mice, Sun *et al.* showed Cx43 exclusively in SSM, however, the lack of Cx43 in IFM might have been attributed to the use of trypsin digestion and a relatively short signal detection time[257]. Similarly to Cx43, MFN2 has been detected predominantly in SSM using the common protocol. To investigate whether or not this result is dependent on the digestion of IFM

proteins by nagarse, we inhibited the enzyme after a short incubation time. This inhibition increased the signal intensity of MFN2, but not that of Cx43 to the amount measured in SSM. The data therefore indicate that the use of the nagarse-based common protocol to isolate IFM results in a misinterpretation of the IFM/SSM ratio of MFN2 but not that of Cx43, which suggests that Cx43 indeed is a protein mostly resident in SSM. An even distribution of MFN2 between SSM and IFM has already been shown by isolating the IFM with trypsin[259], indicating that the protocol to isolate IFM determines the protein amount of MFN2 detected in the IFM fraction. It is interesting that despite the fact that MFN1 and MFN2 are both present in the outer mitochondrial membrane, share more than 60% amino acid sequence identity, and were investigated using antibodies directed against the carboxy-terminal parts of the proteins, only MFN2 was digested by nagarse using the common protocol. Whereas MFN1 is predominantly involved in the formation of inter-mitochondrial network[260, 261], it is known that MFN2 has multiple roles in cellular function. Chen and Dorn demonstrated that MFN2 has an essential role in the initiation of mitophagy via the Pink1 pathway[135]. Several studies proposed that in contrast to MFN1, MFN2 is not only located in the mitochondria, but also resides in the endoplasmic reticulum. Here, MFN2 has an important role in the tethering of the mitochondria and mediation of Ca^{2+}-transfer between them[262, 263]. Moreover, it was also described that overexpression of hyperplasia suppressor gene (HSG, which was renamed to MFN2) reduced vascular smooth muscle cell proliferation[264]. Furthermore, mutation of human MFN2 but not of MFN1 causes Charcot–Marie–Tooth disease type 2A[265], while mutation of MFN1 has not been associated with a human disease to date, highlighting a significant difference in function between MFN1 and MFN2, despite having a 66 or 60% homology in rats or human, respectively. Furthermore, it was demonstrated that MFN1 has a 100-fold stronger GTP-dependent mitochondrial homotypic tethering activity and an 8-fold higher GTPase activity than MFN2[261]. Although the distinctive roles of MFN2 are well-described, it has not been studied what percentage of the protein is responsible for which function. Nevertheless, since MFN2, but not MFN1 interacts with Bax[266], and since OPA1 requires MFN1 not MFN2 to mediate fusion[260], we postulate that the differing protein-protein interactions of MFN1 and MFN2 may affect the ability of nagarse to access and to digest mitofusin proteins. However, no experimental data has been published to support this hypothesis so far. Moreover, we also demonstrated that the

presence of OPA1, which is localized in the inner mitochondrial membrane, was not different between SSM and IFM in prediabetic rat hearts, however, its nagarse-sensitivity was not assessed. Based on these findings, careful interpretation of results comparing MFN2 signals in SSM and IFM is recommended.

7.4 Limitations

Although we demonstrated that hypercholesterolemia led to altered cardiac autophagy and mTOR activity and prediabetes induced mild diastolic dysfunction, ROS production and changes in mitophagy as well as cardiac mitochondrial protein detection is influenced by nagarse enzyme, these experiments had some limitations. The investigation of hypercholesterolemic condition was performed only on male rats; therefore, we cannot exclude the possibility that sex influences the effect of hypercholesterolemia on cardiac death and survival mechanisms. Furthermore, prediabetic condition was also not analyzed in female rats. Because pathophysiological processes might substantially differ between sexes (see NIH notice NOT-OD-15-102), it cannot be excluded that performing the studies with the inclusion of both sexes might allow different conclusions to be drawn. We did not follow food consumption during the experiments. We did not investigate either the presence of autophagosomes with electron microscopy, or autophagic flux, or the phosphorylation of ribosomal S6 protein through the 90 kDa ribosomal S6 kinase, which might contribute to the phosphorylation of ribosomal S6 protein independently of the mTOR complex[267]. Another limitation is that the effects of hypercholesterolemia and prediabetes on mitochondrial dynamics, autophagy/mitophagy, apoptosis, necroptosis and mTOR signaling pathways were assessed only in the left ventricular myocardium. Furthermore, because other studies showed that MHC protein expression is influenced by certain factors such as Foxo1[268] or miR-27a[269], assessing α- and β-MHC protein levels might have helped to understand the molecular background of the mild diastolic dysfunction and hypertrophy observed in prediabetes better.

A limitation of the investigation of mitochondrial protein detection is that only Western blot was used to examine the amount of proteins in different mitochondrial subfractions. Since differential enzymatic effects of nagarse on given mitochondrial proteins cannot be excluded, non-immunological methods, e.g., mass spectrometry[270], or immunoelectron microscopy[154] might also be necessary to support our current findings on the effect of enzymatic digestion on the detection of mitochondrial proteins.

8 Conclusions

8.1 Hypercholesterolemia activates cardiac mTOR and apoptosis but downregulates autophagy

This is the first extensive analysis of cardiac autophagy and programmed cell death pathways of apoptosis and necroptosis in hypercholesterolemic rats. Here we have shown that hypercholesterolemia attenuates cardiac autophagy in parallel with the activation of mTOR pathway and an elevation of apoptosis. Moreover, hypercholesterolemia does not influence the expression of major markers of cardiac necroptosis (for schematic representation see Figure 28). This imbalance between pro-survival and death pathways might play a role in the abolition of cardioprotection in hypercholesterolemia.

Nevertheless, our results demonstrated that expression of major markers of cardiac necroptosis is not modulated by hypercholesterolemia. These findings may help to understand the cardiac effect of hypercholesterolemia and develop more effective pharmacological and/or interventional therapies.

8.2 Prediabetes induces mild diastolic dysfunction and hypertrophy by elevated mitochondrial oxidative stress

Our comprehensive analysis showed the cardiac effects of prediabetes in a non-genetic rodent model, where we assessed cardiac functions, parameters of hypertrophy, fibrosis, oxidative and nitrative stress, inflammation, mitochondrial dynamics, autophagy, mitophagy, markers of myocardial calcium handling, apoptosis and expression of HSPs. In this model of prediabetes, we evidenced an impaired glucose and insulin tolerance, increased adiposity and myocardial lipid accumulation, a mild diastolic dysfunction and sensory neuropathy despite normal fasting plasma glucose and lipid levels. We also observed elevated ROS production in the SSM, nitrative stress, elevated expression of MFN2, decreased expression of β-MHC, and phosphorylation of PLB. Furthermore, here we found early signs of dysregulated mitophagy and decreased mitochondrial size in prediabetes; however, other major markers of mitochondrial dynamics, auto- and mitophagy, inflammation, or myocardial expression of apoptotic proteins or HSPs were

not modulated by prediabetes. Since prediabetes-induced alterations can be triggered by various pathological and compensatory mechanisms, precise identification of these initial changes is difficult. Thus, further investigations might be needed to clarify these differences in prediabetes.

Taken together, our results emphasize that parallel occurrence of several abnormalities of metabolic, oxidative and contractile functions might trigger cardiac pathological changes characteristic to prediabetes well before hyperglycemia or major metabolic derangements occur, and that preventing these abnormalities might be of importance for future therapies of cardiac pathologies observed in early metabolic diseases such as prediabetes.

8.3 Nagarse treatment of cardiac subsarcolemmal and interfibrillar mitochondria accounts for inaccurate quantification of proteins

Our results demonstrate for the first time that the proteolytic activity of nagarse influences the detection of proteins in cardiac mitochondrial subfractions, which may lead to the misinterpretation of the amount of a protein in SSM over that in IFM (as shown here for MFN2). Such putative protein digestion should be taken into account when assessing the distribution of mitochondrial proteins with nagarse-based isolation protocols. Furthermore, the modification of the common protocol by the inhibition of nagarse after a short incubation yields pure mitochondrial preparations without effects on their respiratory capacity. Therefore, nagarse inhibition with PMSF represents a valuable tool to avoid artificial degradation of mitochondrial proteins and helps to prevent inaccurate protein quantification in studies aiming to characterize the localization of specific proteins in mitochondrial subpopulations.

Therefore, we recommend assessing mitochondrial proteins and function in IFM+N+I in studies comparing IFM and SSM and in case differential signal intensities of mitochondrial proteins are observed in SSM and IFM subfractions.

9 Summary

Although severe metabolic derangements such as diabetes or morbid obesity deteriorate cardiac function significantly, little is known on cardiovascular effects of more frequent metabolic diseases such as prediabetes or hypercholesterolemia.

Therefore our aim was to assess the status of cardiac autophagy, mechanistic target of rapamycin (mTOR), apoptosis and necroptosis pathways in a hypercholesterolemic rat model. We also aimed to characterize a diet-induced prediabetes rat model and investigate its effect on the cardiovascular system, as well as to examine whether the most commonly used method for the isolation of interfibrillar mitochondria affect the detection of mitochondrial proteins in cardiac mitochondrial subfractions.

The cardiac effect of hypercholesterolemia was examined in a cholesterol-rich diet-fed male Wistar rat model, where cardiac autophagy decreased, apoptosis and mTOR activity increased but necroptosis was unchanged. In our next study, prediabetes was induced in male Long-Evans rats by a single low-dose streptozotocin treatment with high-fat diet and cardiac activity effect of prediabetes was studied. The development of prediabetes was evidenced by increased body weight and plasma leptin levels and the development of impaired glucose and insulin tolerance. This prediabetic state induced mild diastolic dysfunction and hypertrophy, which could be associated with increased cardiac mitofusin 2 expression, increased nitrative- and mitochondrial oxidative stress, increased level of cardiac lipid droplets and altered mitophagy in the heart. We also found that isolation involving nagarse digestion affects signal intensity of mitofusin 2 and connexin-43 in cardiac mitochondrial subpopulations. Therefore, we concluded that detection of certain mitochondrial proteins requires increased caution with this method.

Our results describe early metabolic derangements on the cardiovascular system, which may have an important role in the simultaneous occurrence of altered signaling pathways, oxidative and contraction functions and other multiple abnormalities. These studies aid us to better understand the complexity of metabolic diseases and to develop more efficient therapies of cardiometabolic diseases in the future.

10 Összefoglalás

Habár különböző metabolikus betegségek, mint a diabétesz vagy a súlyos elhízás jelentősen károsítják a szív működését, más gyakoribb anyagcsere-betegségek úgymint a prediabétesz vagy a hiperkoleszterolémia kardiovaszkuláris rendszerre kifejtett hatása kevésbé ismert. Ezért célul tűztük ki a kardiális autofágia, mTOR, apoptózis és nekroptózis útvonalak állapotának vizsgálatát hiperkoleszterolémiás patkánymodellben, valamint karakterizálni egy diéta-indukált prediabéteszes patkánymodellt és megvizsgálni annak kardiovaszkuláris rendszerre kifejtett hatását. Továbbá megvizsgáltuk, vajon a szívben található interfibrilláris mitokondriumok izolálásához hagyományosan használt bakteriális eredetű nagárz enzim hatással van-e a mitokondriális proteinek kimutatására a mitokondrium-szubfrakciókban.

A hiperkoleszterolémia szívre gyakorolt hatását koleszterin gazdag diétán tartott hím Wistar patkánymodellben vizsgáltuk, ahol a kardiális autofágia csökkent, míg az apoptózis és mTOR aktivitás megemelkedett, azonban a nekroptózis nem változott. A következő vizsgálatunkban prediabéteszes állapotot hoztunk létre egyszeri, alacsony dózisú streptozotocin kezeléssel és magas zsírtartalmú diétával Long-Evans patkánymodellben, ahol a prediabétesz szívműködésre kifejtett hatását vizsgáltuk. A prediabéteszes állapot kialakulását a testsúly és a plazma leptin szint emelkedése, valamint a glukóz és inzulin intolerancia kialakulása bizonyította. A prediabétesz enyhe diasztolés diszfunkciót és hipertrófiát hozott létre, mely összefüggésbe hozható volt a kardiális mitofuzin 2 expresszió, nitratív-, illetve mitokondriális oxidatív stressz növekedésével, lipidcseppek mennyiségének emelkedésével, valamint a megváltozott mitofágiával a szívben. Megállapítottuk továbbá, hogy a nagárzzal történő mitokondrium izolálás befolyásolja a mitofusin 2 és a connexin-43 fehérjék jelintenzitását a szívben található mitokondriális szubpopulációkban. Ezért bizonyos mitokondriális fehérjék kimutatása ezzel a módszerrel fokozott körültekintést igényel.

Eredményeink rávilágítanak a korai anyagcsere-betegségek kardiovaszkuláris rendszerre kifejtett hatására, melyben fontos szereppel bírhatnak megváltozott jelátviteli útvonalak, oxidatív és összehúzódási funkciók illetve többféle rendellenességének párhuzamos előfordulása. Ezen vizsgálatok alapján közelebb kerülhetünk a metabolikus betegségek komplexitásának megértéséhez és korszerűbb terápiájuk jövőbeni kifejlesztéséhez.

11 References

1. Ryden L, Grant PJ, Anker SD, Berne C, Cosentino F, Danchin N, Deaton C, Escaned J, Hammes HP, Huikuri H, Marre M, Marx N, Mellbin L, Ostergren J, Patrono C, Seferovic P, Uva MS, Taskinen MR, Tendera M, Tuomilehto J, Valensi P, Zamorano JL, Zamorano JL, Achenbach S, Baumgartner H, Bax JJ, Bueno H, Dean V, Deaton C, Erol C, Fagard R, Ferrari R, Hasdai D, Hoes AW, Kirchhof P, Knuuti J, Kolh P, Lancellotti P, Linhart A, Nihoyannopoulos P, Piepoli MF, Ponikowski P, Sirnes PA, Tamargo JL, Tendera M, Torbicki A, Wijns W, Windecker S, De Backer G, Sirnes PA, Ezquerra EA, Avogaro A, Badimon L, Baranova E, Baumgartner H, Betteridge J, Ceriello A, Fagard R, Funck-Brentano C, Gulba DC, Hasdai D, Hoes AW, Kjekshus JK, Knuuti J, Kolh P, Lev E, Mueller C, Neyses L, Nilsson PM, Perk J, Ponikowski P, Reiner Z, Sattar N, Schachinger V, Scheen A, Schirmer H, Stromberg A, Sudzhaeva S, Tamargo JL, Viigimaa M, Vlachopoulos C and Xuereb RG. ESC Guidelines on diabetes, pre-diabetes, and cardiovascular diseases developed in collaboration with the EASD: the Task Force on diabetes, pre-diabetes, and cardiovascular diseases of the European Society of Cardiology (ESC) and developed in collaboration with the European Association for the Study of Diabetes (EASD). *European heart journal*. 2013;34:3035-87.
2. Ferdinandy P, Hausenloy DJ, Heusch G, Baxter GF and Schulz R. Interaction of risk factors, comorbidities, and comedications with ischemia/reperfusion injury and cardioprotection by preconditioning, postconditioning, and remote conditioning. *Pharmacol Rev*. 2014;66:1142-74.
3. Szilvassy Z, Ferdinandy P, Szilvassy J, Nagy I, Karcsu S, Lonovics J, Dux L and Koltai M. The loss of pacing-induced preconditioning in atherosclerotic rabbits: role of hypercholesterolaemia. *J Mol Cell Cardiol*. 1995;27:2559-69.
4. Kupai K, Csonka C, Fekete V, Odendaal L, van Rooyen J, Marais de W, Csont T and Ferdinandy P. Cholesterol diet-induced hyperlipidemia impairs the cardioprotective effect of postconditioning: role of peroxynitrite. *American journal of physiology Heart and circulatory physiology*. 2009;297:H1729-35.
5. Reiner Z. Hypertriglyceridaemia and risk of coronary artery disease. *Nature reviews Cardiology*. 2017.

6. Panagiotakos DB, Pitsavos C, Skoumas Y, Lentzas Y, Papadimitriou L, Chrysohoou C and Stefanadis C. Abdominal obesity, blood glucose and apolipoprotein B levels are the best predictors of the incidence of hypercholesterolemia (2001-2006) among healthy adults: the ATTICA study. *Lipids in health and disease*. 2008;7:11.
7. Dawber TR, Meadors GF and Moore FE, Jr. Epidemiological approaches to heart disease: the Framingham Study. *American journal of public health and the nation's health*. 1951;41:279-81.
8. Sakakura K, Nakano M, Otsuka F, Ladich E, Kolodgie FD and Virmani R. Pathophysiology of atherosclerosis plaque progression. *Heart, lung & circulation*. 2013;22:399-411.
9. Bergheanu SC, Bodde MC and Jukema JW. Pathophysiology and treatment of atherosclerosis : Current view and future perspective on lipoprotein modification treatment. *Netherlands heart journal : monthly journal of the Netherlands Society of Cardiology and the Netherlands Heart Foundation*. 2017;25:231-242.
10. D'Annunzio V, Donato M, Buchholz B, Perez V, Miksztowicz V, Berg G and Gelpi RJ. High cholesterol diet effects on ischemia-reperfusion injury of the heart. *Canadian journal of physiology and pharmacology*. 2012;90:1185-96.
11. Huang Y, Walker KE, Hanley F, Narula J, Houser SR and Tulenko TN. Cardiac systolic and diastolic dysfunction after a cholesterol-rich diet. *Circulation*. 2004;109:97-102.
12. Onody A, Csonka C, Giricz Z and Ferdinandy P. Hyperlipidemia induced by a cholesterol-rich diet leads to enhanced peroxynitrite formation in rat hearts. *Cardiovasc Res*. 2003;58:663-70.
13. Murry CE, Jennings RB and Reimer KA. Preconditioning with ischemia: a delay of lethal cell injury in ischemic myocardium. *Circulation*. 1986;74:1124-36.
14. Fenton RA, Dickson EW, Meyer TE and Dobson JG, Jr. Aging reduces the cardioprotective effect of ischemic preconditioning in the rat heart. *J Mol Cell Cardiol*. 2000;32:1371-5.
15. Schulman D, Latchman DS and Yellon DM. Effect of aging on the ability of preconditioning to protect rat hearts from ischemia-reperfusion injury. *American journal of physiology Heart and circulatory physiology*. 2001;281:H1630-6.

16. Galagudza MM, Nekrasova MK, Syrenskii AV and Nifontov EM. Resistance of the myocardium to ischemia and the efficacy of ischemic preconditioning in experimental diabetes mellitus. *Neuroscience and behavioral physiology*. 2007;37:489-93.

17. Kristiansen SB, Lofgren B, Stottrup NB, Khatir D, Nielsen-Kudsk JE, Nielsen TT, Botker HE and Flyvbjerg A. Ischaemic preconditioning does not protect the heart in obese and lean animal models of type 2 diabetes. *Diabetologia*. 2004;47:1716-21.

18. Yadav HN, Singh M and Sharma PL. Modulation of the cardioprotective effect of ischemic preconditioning in hyperlipidaemic rat heart. *Eur J Pharmacol*. 2010;643:78-83.

19. Gupta V, Goyal R and Sharma PL. Preconditioning offers cardioprotection in hyperlipidemic rat hearts: possible role of Dopamine (D2) signaling. *BMC cardiovascular disorders*. 2015;15:77.

20. Ma LL, Zhang FJ, Qian LB, Kong FJ, Sun JF, Zhou C, Peng YN, Xu HJ, Wang WN, Wen CY, Zhu MH, Chen G, Yu LN, Liu XB, Wang JA and Yan M. Hypercholesterolemia blocked sevoflurane-induced cardioprotection against ischemia-reperfusion injury by alteration of the MG53/RISK/GSK3beta signaling. *International journal of cardiology*. 2013;168:3671-8.

21. Giricz Z, Lalu MM, Csonka C, Bencsik P, Schulz R and Ferdinandy P. Hyperlipidemia Attenuates the Infarct Size-Limiting Effect of Ischemic Preconditioning: Role of Matrix Metalloproteinase-2 Inhibition. *Journal of Pharmacology and Experimental Therapeutics*. 2006;316:154-161.

22. Gorbe A, Varga ZV, Kupai K, Bencsik P, Kocsis GF, Csont T, Boengler K, Schulz R and Ferdinandy P. Cholesterol diet leads to attenuation of ischemic preconditioning-induced cardiac protection: the role of connexin 43. *American journal of physiology Heart and circulatory physiology*. 2011;300:H1907-13.

23. Ferdinandy P, Csonka C, Csont T, Szilvassy Z and Dux L. Rapid pacing-induced preconditioning is recaptured by farnesol treatment in hearts of cholesterol-fed rats: role of polyprenyl derivatives and nitric oxide. *Molecular and cellular biochemistry*. 1998;186:27-34.

24. Stapleton PA, Goodwill AG, James ME, Brock RW and Frisbee JC. Hypercholesterolemia and microvascular dysfunction: interventional strategies. *Journal of inflammation (London, England)*. 2010;7:54.
25. (2) Classification and diagnosis of diabetes. *Diabetes care*. 2015;38 Suppl:S8-s16.
26. Diagnosis and classification of diabetes mellitus. *Diabetes care*. 2014;37 Suppl 1:S81-90.
27. Huynh K, Bernardo BC, McMullen JR and Ritchie RH. Diabetic cardiomyopathy: mechanisms and new treatment strategies targeting antioxidant signaling pathways. *Pharmacology & therapeutics*. 2014;142:375-415.
28. Golay A and Ybarra J. Link between obesity and type 2 diabetes. *Best practice & research Clinical endocrinology & metabolism*. 2005;19:649-63.
29. Barr EL, Zimmet PZ, Welborn TA, Jolley D, Magliano DJ, Dunstan DW, Cameron AJ, Dwyer T, Taylor HR, Tonkin AM, Wong TY, McNeil J and Shaw JE. Risk of cardiovascular and all-cause mortality in individuals with diabetes mellitus, impaired fasting glucose, and impaired glucose tolerance: the Australian Diabetes, Obesity, and Lifestyle Study (AusDiab). *Circulation*. 2007;116:151-7.
30. Brown A, Reynolds LR and Bruemmer D. Intensive glycemic control and cardiovascular disease: an update. *Nature reviews Cardiology*. 2010;7:369-75.
31. Eguchi K, Boden-Albala B, Jin Z, Rundek T, Sacco RL, Homma S and Di Tullio MR. Association Between Diabetes Mellitus and Left Ventricular Hypertrophy in a Multi-Ethnic Population. *The American journal of cardiology*. 2008;101:1787-1791.
32. Klein R, Klein BE, Moss SE, Davis MD and DeMets DL. Glycosylated hemoglobin predicts the incidence and progression of diabetic retinopathy. *Jama*. 1988;260:2864-71.
33. Selvin E, Marinopoulos S, Berkenblit G, Rami T, Brancati FL, Powe NR and Golden SH. Meta-analysis: glycosylated hemoglobin and cardiovascular disease in diabetes mellitus. *Annals of internal medicine*. 2004;141:421-31.
34. Effect of intensive diabetes treatment on the development and progression of long-term complications in adolescents with insulin-dependent diabetes mellitus: Diabetes Control and Complications Trial. Diabetes Control and Complications Trial Research Group. *The Journal of pediatrics*. 1994;125:177-88.

35. Intensive blood-glucose control with sulphonylureas or insulin compared with conventional treatment and risk of complications in patients with type 2 diabetes (UKPDS 33). UK Prospective Diabetes Study (UKPDS) Group. *Lancet (London, England)*. 1998;352:837-53.

36. Boudina S and Abel ED. Diabetic cardiomyopathy, causes and effects. *Reviews in endocrine & metabolic disorders*. 2010;11:31-9.

37. Voulgari C, Papadogiannis D and Tentolouris N. Diabetic cardiomyopathy: from the pathophysiology of the cardiac myocytes to current diagnosis and management strategies. *Vascular health and risk management*. 2010;6:883-903.

38. Nathan DM, Davidson MB, DeFronzo RA, Heine RJ, Henry RR, Pratley R and Zinman B. Impaired fasting glucose and impaired glucose tolerance: implications for care. *Diabetes care*. 2007;30:753-9.

39. DeFronzo RA and Abdul-Ghani M. Assessment and treatment of cardiovascular risk in prediabetes: impaired glucose tolerance and impaired fasting glucose. *The American journal of cardiology*. 2011;108:3b-24b.

40. Fonseca VA. Identification and treatment of prediabetes to prevent progression to type 2 diabetes. *Clinical cornerstone*. 2008;9:51-9; discussion 60-1.

41. Lewis CE, McTigue KM, Burke LE, Poirier P, Eckel RH, Howard BV, Allison DB, Kumanyika S and Pi-Sunyer FX. Mortality, health outcomes, and body mass index in the overweight range: a science advisory from the American Heart Association. *Circulation*. 2009;119:3263-71.

42. Definition and diagnosis of diabetes mellitus and intermediate hyperglycemia: report of a WHO/IDF consultation. *World Health Organization*. 2006:1-50.

43. Perreault L and Faerch K. Approaching pre-diabetes. *Journal of diabetes and its complications*. 2014;28:226-33.

44. Ford ES, Zhao G and Li C. Pre-diabetes and the risk for cardiovascular disease: a systematic review of the evidence. *Journal of the American College of Cardiology*. 2010;55:1310-7.

45. Grundy SM. Pre-diabetes, metabolic syndrome, and cardiovascular risk. *Journal of the American College of Cardiology*. 2012;59:635-43.

46. Selvin E, Steffes MW, Zhu H, Matsushita K, Wagenknecht L, Pankow J, Coresh J and Brancati FL. Glycated hemoglobin, diabetes, and cardiovascular risk in nondiabetic adults. *The New England journal of medicine*. 2010;362:800-11.
47. Qiao Q, Pyorala K, Pyorala M, Nissinen A, Lindstrom J, Tilvis R and Tuomilehto J. Two-hour glucose is a better risk predictor for incident coronary heart disease and cardiovascular mortality than fasting glucose. *European heart journal*. 2002;23:1267-75.
48. Zvara A, Bencsik P, Fodor G, Csont T, Hackler L, Jr., Dux M, Furst S, Jancso G, Puskas LG and Ferdinandy P. Capsaicin-sensitive sensory neurons regulate myocardial function and gene expression pattern of rat hearts: a DNA microarray study. *FASEB journal : official publication of the Federation of American Societies for Experimental Biology*. 2006;20:160-2.
49. Bencsik P, Kupai K, Giricz Z, Gorbe A, Huliak I, Furst S, Dux L, Csont T, Jancso G and Ferdinandy P. Cardiac capsaicin-sensitive sensory nerves regulate myocardial relaxation via S-nitrosylation of SERCA: role of peroxynitrite. *Br J Pharmacol*. 2008;153:488-96.
50. Jin HY, Cha YS, Baek HS and Park TS. Neuroprotective effects of Vitis vinifera extract on prediabetic mice induced by a high-fat diet. *The Korean journal of internal medicine*. 2013;28:579-86.
51. Essop MF, Anna Chan WY, Valle A, Garcia-Palmer FJ and Du Toit EF. Impaired contractile function and mitochondrial respiratory capacity in response to oxygen deprivation in a rat model of pre-diabetes. *Acta physiologica (Oxford, England)*. 2009;197:289-96.
52. Mizushige K, Yao L, Noma T, Kiyomoto H, Yu Y, Hosomi N, Ohmori K and Matsuo H. Alteration in left ventricular diastolic filling and accumulation of myocardial collagen at insulin-resistant prediabetic stage of a type II diabetic rat model. *Circulation*. 2000;101:899-907.
53. Pessin JE and Saltiel AR. Signaling pathways in insulin action: molecular targets of insulin resistance. *J Clin Invest*. 2000;106:165-9.
54. Brownlee M. Biochemistry and molecular cell biology of diabetic complications. *Nature*. 2001;414:813-20.

55. Natarajan R and Nadler JL. Lipid inflammatory mediators in diabetic vascular disease. *Arteriosclerosis, thrombosis, and vascular biology*. 2004;24:1542-8.
56. Oh WJ and Jacinto E. mTOR complex 2 signaling and functions. *Cell Cycle*. 2011;10:2305-16.
57. Fader CM, Aguilera MO and Colombo MI. Autophagy response: manipulating the mTOR-controlled machinery by amino acids and pathogens. *Amino acids*. 2015;47:2101-12.
58. Feng Z and Levine AJ. The regulation of energy metabolism and the IGF-1/mTOR pathways by the p53 protein. *Trends in cell biology*. 2010;20:427-34.
59. Troncoso R, Diaz-Elizondo J, Espinoza SP, Navarro-Marquez MF, Oyarzun AP, Riquelme JA, Garcia-Carvajal I, Diaz-Araya G, Garcia L, Hill JA and Lavandero S. Regulation of cardiac autophagy by insulin-like growth factor 1. *IUBMB life*. 2013;65:593-601.
60. Sarbassov DD, Ali SM, Sengupta S, Sheen JH, Hsu PP, Bagley AF, Markhard AL and Sabatini DM. Prolonged rapamycin treatment inhibits mTORC2 assembly and Akt/PKB. *Mol Cell*. 2006;22:159-68.
61. Yano T, Ferlito M, Aponte A, Kuno A, Miura T, Murphy E and Steenbergen C. Pivotal role of mTORC2 and involvement of ribosomal protein S6 in cardioprotective signaling. *Circ Res*. 2014;114:1268-80.
62. Suhara T, Baba Y, Shimada BK, Higa JK and Matsui T. The mTOR Signaling Pathway in Myocardial Dysfunction in Type 2 Diabetes Mellitus. *Current diabetes reports*. 2017;17:38.
63. Sciarretta S, Zhai P, Shao D, Maejima Y, Robbins J, Volpe M, Condorelli G and Sadoshima J. Rheb is a Critical Regulator of Autophagy During Myocardial Ischemia: Pathophysiological Implications in Obesity and Metabolic Syndrome. *Circulation*. 2012;125:1134-1146.
64. Sciarretta S, Zhai P, Volpe M and Sadoshima J. Pharmacological Modulation of Autophagy During Cardiac Stress. *Journal of Cardiovascular Pharmacology*. 2012;60:235-241 10.1097/FJC.0b013e3182575f61.
65. Giricz Z, Mentzer RM, Jr. and Gottlieb RA. Autophagy, myocardial protection, and the metabolic syndrome. *J Cardiovasc Pharmacol*. 2012;60:125-32.

66. Gustafsson ÅB and Gottlieb RA. Recycle or die: The role of autophagy in cardioprotection. *Journal of Molecular and Cellular Cardiology*. 2008;44:654-661.
67. Yuan H, Perry CN, Huang C, Iwai-Kanai E, Carreira RS, Glembotski CC and Gottlieb RA. LPS-induced autophagy is mediated by oxidative signaling in cardiomyocytes and is associated with cytoprotection. *American journal of physiology Heart and circulatory physiology*. 2009;296:H470-9.
68. Hamacher-Brady A, Brady NR and Gottlieb RA. Enhancing Macroautophagy Protects against Ischemia/Reperfusion Injury in Cardiac Myocytes. *Journal of Biological Chemistry*. 2006;281:29776-29787.
69. Gurusamy N, Lekli I, Mukherjee S, Ray D, Ahsan MK, Gherghiceanu M, Popescu LM and Das DK. Cardioprotection by resveratrol: a novel mechanism via autophagy involving the mTORC2 pathway. *Cardiovasc Res*. 2010;86:103-12.
70. Delbridge LMD, Mellor KM, Taylor DJ and Gottlieb RA. Myocardial stress and autophagy: mechanisms and potential therapies. *Nature reviews Cardiology*. 2017;14:412-425.
71. Mei Y, Thompson MD, Cohen RA and Tong X. Autophagy and oxidative stress in cardiovascular diseases. *Biochimica et biophysica acta*. 2015;1852:243-51.
72. Ravikumar B, Sarkar S, Davies JE, Futter M, Garcia-Arencibia M, Green-Thompson ZW, Jimenez-Sanchez M, Korolchuk VI, Lichtenberg M, Luo S, Massey DC, Menzies FM, Moreau K, Narayanan U, Renna M, Siddiqi FH, Underwood BR, Winslow AR and Rubinsztein DC. Regulation of mammalian autophagy in physiology and pathophysiology. *Physiological reviews*. 2010;90:1383-435.
73. Gustafsson AB and Gottlieb RA. Eat your heart out: Role of autophagy in myocardial ischemia/reperfusion. *Autophagy*. 2008;4:416-21.
74. Hariharan N, Zhai P and Sadoshima J. Oxidative stress stimulates autophagic flux during ischemia/reperfusion. *Antioxid Redox Signal*. 2011;14:2179-90.
75. Andres AM, Hernandez G, Lee P, Huang C, Ratliff EP, Sin J, Thornton CA, Damasco MV and Gottlieb RA. Mitophagy is required for acute cardioprotection by simvastatin. *Antioxid Redox Signal*. 2014;21:1960-73.
76. Ha T, Hua F, Liu X, Ma J, McMullen JR, Shioi T, Izumo S, Kelley J, Gao X, Browder W, Williams DL, Kao RL and Li C. Lipopolysaccharide-induced myocardial

protection against ischaemia/reperfusion injury is mediated through a PI3K/Akt-dependent mechanism. *Cardiovasc Res*. 2008;78:546-53.

77. Shiomi M, Miyamae M, Takemura G, Kaneda K, Inamura Y, Onishi A, Koshinuma S, Momota Y, Minami T and Figueredo VM. Sevoflurane induces cardioprotection through reactive oxygen species-mediated upregulation of autophagy in isolated guinea pig hearts. *J Anesth*. 2014;28:593-600.

78. Huang C, Yitzhaki S, Perry C, Liu W, Giricz Z, Mentzer R, Jr. and Gottlieb R. Autophagy Induced by Ischemic Preconditioning is Essential for Cardioprotection. *J of Cardiovasc Trans Res*. 2010;3:365-373.

79. Rohailla S, Clarizia N, Sourour M, Sourour W, Gelber N, Wei C, Li J and Redington AN. Acute, delayed and chronic remote ischemic conditioning is associated with downregulation of mTOR and enhanced autophagy signaling. *PloS one*. 2014;9:e111291.

80. Sengupta S, Peterson TR and Sabatini DM. Regulation of the mTOR complex 1 pathway by nutrients, growth factors, and stress. *Mol Cell*. 2010;40:310-22.

81. Wong PM, Puente C, Ganley IG and Jiang X. The ULK1 complex: sensing nutrient signals for autophagy activation. *Autophagy*. 2013;9:124-37.

82. Meijer AJ and Codogno P. AMP-activated protein kinase and autophagy. *Autophagy*. 2007;3:238-40.

83. Alers S, Loffler AS, Wesselborg S and Stork B. Role of AMPK-mTOR-Ulk1/2 in the regulation of autophagy: cross talk, shortcuts, and feedbacks. *Mol Cell Biol*. 2012;32:2-11.

84. Glazer HP, Osipov RM, Clements RT, Sellke FW and Bianchi C. Hypercholesterolemia is associated with hyperactive cardiac mTORC1 and mTORC2 signaling. *Cell Cycle*. 2009;8:1738-1746.

85. Andres AM, Kooren JA, Parker SJ, Tucker KC, Ravindran N, Ito BR, Huang C, Venkatraman V, Van Eyk JE, Gottlieb RA and Mentzer RM, Jr. Discordant signaling and autophagy response to fasting in hearts of obese mice: Implications for ischemia tolerance. *American journal of physiology Heart and circulatory physiology*. 2016;311:H219-28.

86. Jiang H, Cheng D, Liu W, Peng J and Feng J. Protein kinase C inhibits autophagy and phosphorylates LC3. *Biochem Biophys Res Commun*. 2010;395:471-6.

87. Scherz-Shouval R and Elazar Z. Regulation of autophagy by ROS: physiology and pathology. *Trends Biochem Sci*. 2011;36:30-8.
88. Sarkar S, Korolchuk VI, Renna M, Imarisio S, Fleming A, Williams A, Garcia-Arencibia M, Rose C, Luo S, Underwood BR, Kroemer G, O'Kane CJ and Rubinsztein DC. Complex inhibitory effects of nitric oxide on autophagy. *Mol Cell*. 2011;43:19-32.
89. Kanamori H, Takemura G, Goto K, Tsujimoto A, Mikami A, Ogino A, Watanabe T, Morishita K, Okada H, Kawasaki M, Seishima M and Minatoguchi S. Autophagic adaptations in diabetic cardiomyopathy differ between type 1 and type 2 diabetes. *Autophagy*. 2015;11:1146-60.
90. Nishida K, Yamaguchi O and Otsu K. Crosstalk between autophagy and apoptosis in heart disease. *Circ Res*. 2008;103:343-51.
91. Gustafsson AB and Gottlieb RA. Bcl-2 family members and apoptosis, taken to heart. *American journal of physiology Cell physiology*. 2007;292:C45-51.
92. Elmore S. Apoptosis: a review of programmed cell death. *Toxicologic pathology*. 2007;35:495-516.
93. Koff JL, Ramachandiran S and Bernal-Mizrachi L. A time to kill: targeting apoptosis in cancer. *International journal of molecular sciences*. 2015;16:2942-55.
94. Orogo AM and Gustafsson AB. Cell death in the myocardium: my heart won't go on. *IUBMB life*. 2013;65:651-6.
95. Konstantinidis K, Whelan RS and Kitsis RN. Mechanisms of cell death in heart disease. *Arteriosclerosis, thrombosis, and vascular biology*. 2012;32:1552-62.
96. Jouan-Lanhouet S, Riquet F, Duprez L, Vanden Berghe T, Takahashi N and Vandenabeele P. Necroptosis, in vivo detection in experimental disease models. *Seminars in cell & developmental biology*. 2014;35:2-13.
97. Osipov RM, Bianchi C, Feng J, Clements RT, Liu Y, Robich MP, Glazer HP, Sodha NR and Sellke FW. Effect of Hypercholesterolemia on Myocardial Necrosis and Apoptosis in the Setting of Ischemia-Reperfusion. *Circulation*. 2009;120:S22-S30.
98. Cheng YC, Chang MH, Tsai CC, Chen TS, Fan CC, Lin CC, Lai CH, Tsai FJ, Lin JA and Huang CY. Garlic oil attenuates the cardiac apoptosis in hamster-fed with hypercholesterol diet. *Food chemistry*. 2013;136:1296-302.

99. Zhang DW, Shao J, Lin J, Zhang N, Lu BJ, Lin SC, Dong MQ and Han J. RIP3, an energy metabolism regulator that switches TNF-induced cell death from apoptosis to necrosis. *Science (New York, NY)*. 2009;325:332-6.
100. Vandenabeele P, Declercq W, Van Herreweghe F and Vanden Berghe T. The role of the kinases RIP1 and RIP3 in TNF-induced necrosis. *Science signaling*. 2010;3:re4.
101. Ye YC, Wang HJ, Yu L, Tashiro S, Onodera S and Ikejima T. RIP1-mediated mitochondrial dysfunction and ROS production contributed to tumor necrosis factor alpha-induced L929 cell necroptosis and autophagy. *International immunopharmacology*. 2012;14:674-82.
102. Ogasawara M, Yano T, Tanno M, Abe K, Ishikawa S, Miki T, Kuno A, Tobisawa T, Muratsubaki S, Ohno K, Tatekoshi Y, Nakata K, Ohwada W and Miura T. Suppression of autophagic flux contributes to cardiomyocyte death by activation of necroptotic pathways. *J Mol Cell Cardiol*. 2017;108:203-213.
103. Amin AH, El-Missiry MA and Othman AI. Melatonin ameliorates metabolic risk factors, modulates apoptotic proteins, and protects the rat heart against diabetes-induced apoptosis. *Eur J Pharmacol*. 2015;747:166-73.
104. Chowdhry MF, Vohra HA and Galinanes M. Diabetes increases apoptosis and necrosis in both ischemic and nonischemic human myocardium: role of caspases and poly-adenosine diphosphate-ribose polymerase. *The Journal of thoracic and cardiovascular surgery*. 2007;134:124-31, 131.e1-3.
105. Varga ZV, Giricz Z, Liaudet L, Hasko G, Ferdinandy P and Pacher P. Interplay of oxidative, nitrosative/nitrative stress, inflammation, cell death and autophagy in diabetic cardiomyopathy. *Biochimica et biophysica acta*. 2015;1852:232-42.
106. Cai L and Kang YJ. Cell death and diabetic cardiomyopathy. *Cardiovascular toxicology*. 2003;3:219-28.
107. Duncan JG. Mitochondrial dysfunction in diabetic cardiomyopathy. *Biochimica et biophysica acta*. 2011;1813:1351-9.
108. Kobayashi S and Liang Q. Autophagy and mitophagy in diabetic cardiomyopathy. *Biochimica et biophysica acta*. 2015;1852:252-61.
109. Pereira L, Ruiz-Hurtado G, Rueda A, Mercadier JJ, Benitah JP and Gomez AM. Calcium signaling in diabetic cardiomyocytes. *Cell calcium*. 2014;56:372-80.

110. Wallace DC. A mitochondrial paradigm of metabolic and degenerative diseases, aging, and cancer: a dawn for evolutionary medicine. *Annual review of genetics*. 2005;39:359-407.
111. Chen YR and Zweier JL. Cardiac mitochondria and reactive oxygen species generation. *Circ Res*. 2014;114:524-37.
112. Ansley DM and Wang B. Oxidative stress and myocardial injury in the diabetic heart. *The Journal of pathology*. 2013;229:232-41.
113. Gottlieb RA. Cytochrome P450: major player in reperfusion injury. *Archives of Biochemistry and Biophysics*. 2003;420:262-267.
114. Raedschelders K, Ansley DM and Chen DD. The cellular and molecular origin of reactive oxygen species generation during myocardial ischemia and reperfusion. *Pharmacology & therapeutics*. 2012;133:230-55.
115. Ruiz-Ramirez A, Lopez-Acosta O, Barrios-Maya MA and El-Hafidi M. Cell Death and Heart Failure in Obesity: Role of Uncoupling Proteins. *Oxid Med Cell Longev*. 2016;2016:9340654.
116. Kim JA, Wei Y and Sowers JR. Role of mitochondrial dysfunction in insulin resistance. *Circ Res*. 2008;102:401-14.
117. Lesnefsky EJ, Moghaddas S, Tandler B, Kerner J and Hoppel CL. Mitochondrial dysfunction in cardiac disease: ischemia--reperfusion, aging, and heart failure. *J Mol Cell Cardiol*. 2001;33:1065-89.
118. Henze K and Martin W. Evolutionary biology: essence of mitochondria. *Nature*. 2003;426:127-8.
119. McBride HM, Neuspiel M and Wasiak S. Mitochondria: more than just a powerhouse. *Curr Biol*. 2006;16:R551-60.
120. Vasquez-Trincado C, Garcia-Carvajal I, Pennanen C, Parra V, Hill JA, Rothermel BA and Lavandero S. Mitochondrial dynamics, mitophagy and cardiovascular disease. *J Physiol*. 2016;594:509-25.
121. Gottlieb RA and Gustafsson AB. Mitochondrial turnover in the heart. *Biochimica et biophysica acta*. 2011;1813:1295-301.
122. Jornayvaz FR and Shulman GI. Regulation of mitochondrial biogenesis. *Essays in biochemistry*. 2010;47:69-84.

123. Liang H and Ward WF. PGC-1alpha: a key regulator of energy metabolism. *Advances in physiology education*. 2006;30:145-51.
124. Nishio Y, Kanazawa A, Nagai Y, Inagaki H and Kashiwagi A. Regulation and role of the mitochondrial transcription factor in the diabetic rat heart. *Annals of the New York Academy of Sciences*. 2004;1011:78-85.
125. Dong F, Li Q, Sreejayan N, Nunn JM and Ren J. Metallothionein prevents high-fat diet induced cardiac contractile dysfunction: role of peroxisome proliferator activated receptor gamma coactivator 1alpha and mitochondrial biogenesis. *Diabetes*. 2007;56:2201-12.
126. Rato L, Duarte AI, Tomás GD, Santos MS, Moreira PI, Socorro S, Cavaco JE, Alves MG and Oliveira PF. Pre-diabetes alters testicular PGC1-α/SIRT3 axis modulating mitochondrial bioenergetics and oxidative stress. *Biochimica et Biophysica Acta (BBA) - Bioenergetics*. 2014;1837:335-344.
127. Chen Y, Liu Y and Dorn GW, 2nd. Mitochondrial fusion is essential for organelle function and cardiac homeostasis. *Circ Res*. 2011;109:1327-31.
128. Hall AR, Burke N, Dongworth RK and Hausenloy DJ. Mitochondrial fusion and fission proteins: novel therapeutic targets for combating cardiovascular disease. *Br J Pharmacol*. 2014;171:1890-906.
129. Ong SB and Hausenloy DJ. Mitochondrial morphology and cardiovascular disease. *Cardiovasc Res*. 2010;88:16-29.
130. Ikeda Y, Shirakabe A, Brady C, Zablocki D, Ohishi M and Sadoshima J. Molecular mechanisms mediating mitochondrial dynamics and mitophagy and their functional roles in the cardiovascular system. *J Mol Cell Cardiol*. 2015;78:116-22.
131. Disatnik MH, Ferreira JC, Campos JC, Gomes KS, Dourado PM, Qi X and Mochly-Rosen D. Acute inhibition of excessive mitochondrial fission after myocardial infarction prevents long-term cardiac dysfunction. *Journal of the American Heart Association*. 2013;2:e000461.
132. Cereghetti GM, Stangherlin A, Martins de Brito O, Chang CR, Blackstone C, Bernardi P and Scorrano L. Dephosphorylation by calcineurin regulates translocation of Drp1 to mitochondria. *Proc Natl Acad Sci U S A*. 2008;105:15803-8.
133. Watanabe T, Saotome M, Nobuhara M, Sakamoto A, Urushida T, Katoh H, Satoh H, Funaki M and Hayashi H. Roles of mitochondrial fragmentation and reactive

oxygen species in mitochondrial dysfunction and myocardial insulin resistance. *Experimental Cell Research*. 2014;323:314-325.

134. Sciarretta S, Zhai P, Volpe M and Sadoshima J. Pharmacological modulation of autophagy during cardiac stress. *J Cardiovasc Pharmacol*. 2012;60:235-41.

135. Chen Y and Dorn GW, 2nd. PINK1-phosphorylated mitofusin 2 is a Parkin receptor for culling damaged mitochondria. *Science (New York, NY)*. 2013;340:471-5.

136. Galloway CA and Yoon Y. Mitochondrial dynamics in diabetic cardiomyopathy. *Antioxid Redox Signal*. 2015;22:1545-62.

137. Kluge MA, Fetterman JL and Vita JA. Mitochondria and endothelial function. *Circ Res*. 2013;112:1171-88.

138. Hollander JM, Thapa D and Shepherd DL. Physiological and structural differences in spatially distinct subpopulations of cardiac mitochondria: influence of cardiac pathologies. *American journal of physiology Heart and circulatory physiology*. 2014;307:H1-14.

139. Riva A, Tandler B, Loffredo F, Vazquez E and Hoppel C. Structural differences in two biochemically defined populations of cardiac mitochondria. *American journal of physiology Heart and circulatory physiology*. 2005;289:H868-72.

140. Shimada T, Horita K, Murakami M and Ogura R. Morphological studies of different mitochondrial populations in monkey myocardial cells. *Cell and tissue research*. 1984;238:577-82.

141. Kalkhoran SB, Munro P, Qiao F, Ong SB, Hall AR, Cabrera-Fuentes H, Chakraborty B, Boisvert WA, Yellon DM and Hausenloy DJ. Unique morphological characteristics of mitochondrial subtypes in the heart: the effect of ischemia and ischemic preconditioning. *Discoveries (Craiova, Romania)*. 2017;5.

142. Palmer JW, Tandler B and Hoppel CL. Biochemical properties of subsarcolemmal and interfibrillar mitochondria isolated from rat cardiac muscle. *J Biol Chem*. 1977;252:8731-9.

143. Palmer JW, Tandler B and Hoppel CL. Biochemical differences between subsarcolemmal and interfibrillar mitochondria from rat cardiac muscle: effects of procedural manipulations. *Arch Biochem Biophys*. 1985;236:691-702.

144. Fannin SW, Lesnefsky EJ, Slabe TJ, Hassan MO and Hoppel CL. Aging selectively decreases oxidative capacity in rat heart interfibrillar mitochondria. *Arch Biochem Biophys*. 1999;372:399-407.

145. Rennison JH, McElfresh TA, Okere IC, Patel HV, Foster AB, Patel KK, Stoll MS, Minkler PE, Fujioka H, Hoit BD, Young ME, Hoppel CL and Chandler MP. Enhanced acyl-CoA dehydrogenase activity is associated with improved mitochondrial and contractile function in heart failure. *Cardiovasc Res*. 2008;79:331-40.

146. Dabkowski ER, Williamson CL, Bukowski VC, Chapman RS, Leonard SS, Peer CJ, Callery PS and Hollander JM. Diabetic cardiomyopathy-associated dysfunction in spatially distinct mitochondrial subpopulations. *American journal of physiology Heart and circulatory physiology*. 2009;296:H359-69.

147. Boengler K, Stahlhofen S, van de Sand A, Gres P, Ruiz-Meana M, Garcia-Dorado D, Heusch G and Schulz R. Presence of connexin 43 in subsarcolemmal, but not in interfibrillar cardiomyocyte mitochondria. *Basic Res Cardiol*. 2009;104:141-7.

148. Ferreira RM, Vitorino R, Padrao AI, Moreira-Goncalves D, Alves RM, Duarte JA and Amado F. Spatially distinct mitochondrial populations exhibit different mitofilin levels. *Cell biochemistry and function*. 2012;30:395-9.

149. Baseler WA, Dabkowski ER, Williamson CL, Croston TL, Thapa D, Powell MJ, Razunguzwa TT and Hollander JM. Proteomic alterations of distinct mitochondrial subpopulations in the type 1 diabetic heart: contribution of protein import dysfunction. *American journal of physiology Regulatory, integrative and comparative physiology*. 2011;300:R186-200.

150. Ong SB, Hall AR and Hausenloy DJ. Mitochondrial dynamics in cardiovascular health and disease. *Antioxid Redox Signal*. 2013;19:400-14.

151. Ruiz-Meana M, Nunez E, Miro-Casas E, Martinez-Acedo P, Barba I, Rodriguez-Sinovas A, Inserte J, Fernandez-Sanz C, Hernando V, Vazquez J and Garcia-Dorado D. Ischemic preconditioning protects cardiomyocyte mitochondria through mechanisms independent of cytosol. *J Mol Cell Cardiol*. 2014;68:79-88.

152. Denuc A, Nunez E, Calvo E, Loureiro M, Miro-Casas E, Guaras A, Vazquez J and Garcia-Dorado D. New protein-protein interactions of mitochondrial connexin 43 in mouse heart. *J Cell Mol Med*. 2016;20:794-803.

153. Garcia-Nino WR, Correa F, Rodriguez-Barrena JI, Leon-Contreras JC, Buelna-Chontal M, Soria-Castro E, Hernandez-Pando R, Pedraza-Chaverri J and Zazueta C. Cardioprotective kinase signaling to subsarcolemmal and interfibrillar mitochondria is mediated by caveolar structures. *Basic Res Cardiol*. 2017;112:15.
154. Srisakuldee W, Makazan Z, Nickel BE, Zhang F, Thliveris JA, Pasumarthi KB and Kardami E. The FGF-2-triggered protection of cardiac subsarcolemmal mitochondria from calcium overload is mitochondrial connexin 43-dependent. *Cardiovascular research*. 2014;103:72-80.
155. Smith EL, Markland FS, Kasper CB, DeLange RJ, Landon M and Evans WH. The complete amino acid sequence of two types of subtilisin, BPN' and Carlsberg. *J Biol Chem*. 1966;241:5974-6.
156. Kras KA, Willis WT, Barker N, Czyzyk T, Langlais PR and Katsanos CS. Subsarcolemmal mitochondria isolated with the proteolytic enzyme nagarse exhibit greater protein specific activities and functional coupling. *Biochemistry and biophysics reports*. 2016;6:101-107.
157. Brooks GA, Brown MA, Butz CE, Sicurello JP and Dubouchaud H. Cardiac and skeletal muscle mitochondria have a monocarboxylate transporter MCT1. *Journal of applied physiology (Bethesda, Md : 1985)*. 1999;87:1713-8.
158. Koves TR, Noland RC, Bates AL, Henes ST, Muoio DM and Cortright RN. Subsarcolemmal and intermyofibrillar mitochondria play distinct roles in regulating skeletal muscle fatty acid metabolism. *American journal of physiology Cell physiology*. 2005;288:C1074-82.
159. Varga ZV, Kupai K, Szucs G, Gaspar R, Paloczi J, Farago N, Zvara A, Puskas LG, Razga Z, Tiszlavicz L, Bencsik P, Gorbe A, Csonka C, Ferdinandy P and Csont T. MicroRNA-25-dependent up-regulation of NADPH oxidase 4 (NOX4) mediates hypercholesterolemia-induced oxidative/nitrative stress and subsequent dysfunction in the heart. *J Mol Cell Cardiol*. 2013;62:111-21.
160. Mansor LS, Gonzalez ER, Cole MA, Tyler DJ, Beeson JH, Clarke K, Carr CA and Heather LC. Cardiac metabolism in a new rat model of type 2 diabetes using high-fat diet with low dose streptozotocin. *Cardiovascular diabetology*. 2013;12:136.
161. Harms M and Seale P. Brown and beige fat: development, function and therapeutic potential. *Nature medicine*. 2013;19:1252-63.

162. Bjorndal B, Burri L, Staalesen V, Skorve J and Berge RK. Different adipose depots: their role in the development of metabolic syndrome and mitochondrial response to hypolipidemic agents. *Journal of obesity*. 2011;2011:490650.
163. Orhan CE, Onal A, Uyanikgil Y and Ulker S. Antihyperalgesic and antiallodynic effect of sirolimus in rat model of adjuvant arthritis. *Eur J Pharmacol*. 2013;705:35-41.
164. Radovits T, Olah A, Lux A, Nemeth BT, Hidi L, Birtalan E, Kellermayer D, Matyas C, Szabo G and Merkely B. Rat model of exercise-induced cardiac hypertrophy: hemodynamic characterization using left ventricular pressure-volume analysis. *American journal of physiology Heart and circulatory physiology*. 2013;305:H124-34.
165. Kovacs A, Olah A, Lux A, Matyas C, Nemeth BT, Kellermayer D, Ruppert M, Torok M, Szabo L, Meltzer A, Assabiny A, Birtalan E, Merkely B and Radovits T. Strain and strain rate by speckle-tracking echocardiography correlate with pressure-volume loop-derived contractility indices in a rat model of athlete's heart. *American journal of physiology Heart and circulatory physiology*. 2015;308:H743-8.
166. Reffelmann T and Kloner RA. Transthoracic echocardiography in rats. Evalution of commonly used indices of left ventricular dimensions, contractile performance, and hypertrophy in a genetic model of hypertrophic heart failure (SHHF-Mcc-facp-Rats) in comparison with Wistar rats during aging. *Basic Res Cardiol*. 2003;98:275-84.
167. Radovits T, Korkmaz S, Matyas C, Olah A, Nemeth BT, Pali S, Hirschberg K, Zubarevich A, Gwanmesia PN, Li S, Loganathan S, Barnucz E, Merkely B and Szabo G. An altered pattern of myocardial histopathological and molecular changes underlies the different characteristics of type-1 and type-2 diabetic cardiac dysfunction. *Journal of diabetes research*. 2015;2015:728741.
168. Radovits T, Korkmaz S, Loganathan S, Barnucz E, Bomicke T, Arif R, Karck M and Szabo G. Comparative investigation of the left ventricular pressure-volume relationship in rat models of type 1 and type 2 diabetes mellitus. *American journal of physiology Heart and circulatory physiology*. 2009;297:H125-33.
169. Pacher P, Nagayama T, Mukhopadhyay P, Batkai S and Kass DA. Measurement of cardiac function using pressure-volume conductance catheter technique in mice and rats. *Nature protocols*. 2008;3:1422-34.
170. Kass D. Clinical ventricular pathophysiology: a pressure-volume view. *Warltier DC Baltimore, MD: Williams & Wilkins*. 1995:131-151.

171. Csont T, Bereczki E, Bencsik P, Fodor G, Gorbe A, Zvara A, Csonka C, Puskas LG, Santha M and Ferdinandy P. Hypercholesterolemia increases myocardial oxidative and nitrosative stress thereby leading to cardiac dysfunction in apoB-100 transgenic mice. *Cardiovasc Res*. 2007;76:100-9.
172. Kleiner DE, Brunt EM, Van Natta M, Behling C, Contos MJ, Cummings OW, Ferrell LD, Liu YC, Torbenson MS, Unalp-Arida A, Yeh M, McCullough AJ and Sanyal AJ. Design and validation of a histological scoring system for nonalcoholic fatty liver disease. *Hepatology (Baltimore, Md)*. 2005;41:1313-21.
173. Soetkamp D, Nguyen TT, Menazza S, Hirschhauser C, Hendgen-Cotta UB, Rassaf T, Schluter KD, Boengler K, Murphy E and Schulz R. S-nitrosation of mitochondrial connexin 43 regulates mitochondrial function. *Basic Res Cardiol*. 2014;109:433.
174. Bradford MM. A rapid and sensitive method for the quantitation of microgram quantities of protein utilizing the principle of protein-dye binding. *Analytical biochemistry*. 1976;72:248-54.
175. Mohanty JG, Jaffe JS, Schulman ES and Raible DG. A highly sensitive fluorescent micro-assay of H2O2 release from activated human leukocytes using a dihydroxyphenoxazine derivative. *Journal of immunological methods*. 1997;202:133-41.
176. Verkhratsky A and Fernyhough P. Mitochondrial malfunction and Ca2+ dyshomeostasis drive neuronal pathology in diabetes. *Cell calcium*. 2008;44:112-22.
177. Kass DA, Bronzwaer JG and Paulus WJ. What mechanisms underlie diastolic dysfunction in heart failure? *Circ Res*. 2004;94:1533-42.
178. Holloway GP, Snook LA, Harris RJ, Glatz JF, Luiken JJ and Bonen A. In obese Zucker rats, lipids accumulate in the heart despite normal mitochondrial content, morphology and long-chain fatty acid oxidation. *J Physiol*. 2011;589:169-80.
179. Williamson CL, Dabkowski ER, Baseler WA, Croston TL, Alway SE and Hollander JM. Enhanced apoptotic propensity in diabetic cardiac mitochondria: influence of subcellular spatial location. *American journal of physiology Heart and circulatory physiology*. 2010;298:H633-42.
180. Pechanova O, Varga ZV, Cebova M, Giricz Z, Pacher P and Ferdinandy P. Cardiac NO signalling in the metabolic syndrome. *Br J Pharmacol*. 2015;172:1415-33.

181. Cassuto J, Dou H, Czikora I, Szabo A, Patel VS, Kamath V, Belin de Chantemele E, Feher A, Romero MJ and Bagi Z. Peroxynitrite disrupts endothelial caveolae leading to eNOS uncoupling and diminished flow-mediated dilation in coronary arterioles of diabetic patients. *Diabetes*. 2014;63:1381-93.
182. Luczak ED and Anderson ME. CaMKII oxidative activation and the pathogenesis of cardiac disease. *J Mol Cell Cardiol*. 2014;73:112-6.
183. Maier LS and Bers DM. Role of Ca2+/calmodulin-dependent protein kinase (CaMK) in excitation-contraction coupling in the heart. *Cardiovasc Res*. 2007;73:631-40.
184. Zhang L, Shimoji M, Thomas B, Moore DJ, Yu SW, Marupudi NI, Torp R, Torgner IA, Ottersen OP, Dawson TM and Dawson VL. Mitochondrial localization of the Parkinson's disease related protein DJ-1: implications for pathogenesis. *Human molecular genetics*. 2005;14:2063-73.
185. Cali T, Ottolini D, Soriano ME and Brini M. A new split-GFP-based probe reveals DJ-1 translocation into the mitochondrial matrix to sustain ATP synthesis upon nutrient deprivation. *Human molecular genetics*. 2015;24:1045-60.
186. Sabe AA, Elmadhun NY, Dalal RS, Robich MP and Sellke FW. Resveratrol regulates autophagy signaling in chronically ischemic myocardium. *The Journal of thoracic and cardiovascular surgery*. 2014;147:792-8; Discussion 798-9.
187. Sabe AA, Elmadhun NY, Sadek AA, Chu LM, Bianchi C and Sellke FW. Differential effects of atorvastatin on autophagy in ischemic and nonischemic myocardium in Ossabaw swine with metabolic syndrome. *The Journal of thoracic and cardiovascular surgery*. 2014;148:3172-8.
188. Hsu HC, Chen CY, Lee BC and Chen MF. High-fat diet induces cardiomyocyte apoptosis via the inhibition of autophagy. *European journal of nutrition*. 2015.
189. Zhu XY, Daghini E, Rodriguez-Porcel M, Chade AR, Napoli C, Lerman A and Lerman LO. Redox-sensitive myocardial remodeling and dysfunction in swine diet-induced experimental hypercholesterolemia. *Atherosclerosis*. 2007;193:62-9.
190. Perales S, Alejandre MJ, Palomino-Morales R, Torres C, Iglesias J and Linares A. Effect of oxysterol-induced apoptosis of vascular smooth muscle cells on experimental hypercholesterolemia. *Journal of biomedicine & biotechnology*. 2009;2009:456208.

191. Chtourou Y, Slima AB, Makni M, Gdoura R and Fetoui H. Naringenin protects cardiac hypercholesterolemia-induced oxidative stress and subsequent necroptosis in rats. *Pharmacological reports : PR*. 2015;67:1090-7.
192. Hsueh W, Abel ED, Breslow JL, Maeda N, Davis RC, Fisher EA, Dansky H, McClain DA, McIndoe R, Wassef MK, Rabadan-Diehl C and Goldberg IJ. Recipes for creating animal models of diabetic cardiovascular disease. *Circ Res*. 2007;100:1415-27.
193. Russell JC and Proctor SD. Small animal models of cardiovascular disease: tools for the study of the roles of metabolic syndrome, dyslipidemia, and atherosclerosis. *Cardiovascular pathology : the official journal of the Society for Cardiovascular Pathology*. 2006;15:318-30.
194. Brooks BA, Franjic B, Ban CR, Swaraj K, Yue DK, Celermajer DS and Twigg SM. Diastolic dysfunction and abnormalities of the microcirculation in type 2 diabetes. *Diabetes, obesity & metabolism*. 2008;10:739-46.
195. Shivalkar B, Dhondt D, Goovaerts I, Van Gaal L, Bartunek J, Van Crombrugge P and Vrints C. Flow mediated dilatation and cardiac function in type 1 diabetes mellitus. *The American journal of cardiology*. 2006;97:77-82.
196. Lupachyk S, Watcho P, Obrosov AA, Stavniichuk R and Obrosova IG. Endoplasmic reticulum stress contributes to prediabetic peripheral neuropathy. *Experimental neurology*. 2013;247:342-8.
197. du Toit EF, Smith W, Muller C, Strijdom H, Stouthammer B, Woodiwiss AJ, Norton GR and Lochner A. Myocardial susceptibility to ischemic-reperfusion injury in a prediabetic model of dietary-induced obesity. *American journal of physiology Heart and circulatory physiology*. 2008;294:H2336-43.
198. Eguchi K, Boden-Albala B, Jin Z, Rundek T, Sacco RL, Homma S and Di Tullio MR. Association between diabetes mellitus and left ventricular hypertrophy in a multiethnic population. *The American journal of cardiology*. 2008;101:1787-91.
199. Barouch LA, Berkowitz DE, Harrison RW, O'Donnell CP and Hare JM. Disruption of leptin signaling contributes to cardiac hypertrophy independently of body weight in mice. *Circulation*. 2003;108:754-9.
200. Kim M, Oh JK, Sakata S, Liang I, Park W, Hajjar RJ and Lebeche D. Role of resistin in cardiac contractility and hypertrophy. *J Mol Cell Cardiol*. 2008;45:270-80.

201. Thandapilly SJ, Raj P, Louis XL, Perera D, Yamanagedara P, Zahradka P, Taylor CG and Netticadan T. Canola oil rich in oleic acid improves diastolic heart function in diet-induced obese rats. *The journal of physiological sciences : JPS*. 2017;67:425-430.
202. Rerkpattanapipat P, D'Agostino RB, Jr., Link KM, Shahar E, Lima JA, Bluemke DA, Sinha S, Herrington DM and Hundley WG. Location of arterial stiffening differs in those with impaired fasting glucose versus diabetes: implications for left ventricular hypertrophy from the Multi-Ethnic Study of Atherosclerosis. *Diabetes*. 2009;58:946-53.
203. Christoffersen C, Bollano E, Lindegaard ML, Bartels ED, Goetze JP, Andersen CB and Nielsen LB. Cardiac lipid accumulation associated with diastolic dysfunction in obese mice. *Endocrinology*. 2003;144:3483-90.
204. Kuwabara Y, Horie T, Baba O, Watanabe S, Nishiga M, Usami S, Izuhara M, Nakao T, Nishino T, Otsu K, Kita T, Kimura T and Ono K. MicroRNA-451 exacerbates lipotoxicity in cardiac myocytes and high-fat diet-induced cardiac hypertrophy in mice through suppression of the LKB1/AMPK pathway. *Circ Res*. 2015;116:279-88.
205. D'Souza A, Howarth FC, Yanni J, Dobryznski H, Boyett MR, Adeghate E, Bidasee KR and Singh J. Left ventricle structural remodelling in the prediabetic Goto-Kakizaki rat. *Experimental physiology*. 2011;96:875-88.
206. Yagi K, Kim S, Wanibuchi H, Yamashita T, Yamamura Y and Iwao H. Characteristics of diabetes, blood pressure, and cardiac and renal complications in Otsuka Long-Evans Tokushima Fatty rats. *Hypertension*. 1997;29:728-35.
207. Aragno M, Mastrocola R, Medana C, Catalano MG, Vercellinatto I, Danni O and Boccuzzi G. Oxidative stress-dependent impairment of cardiac-specific transcription factors in experimental diabetes. *Endocrinology*. 2006;147:5967-74.
208. Dyntar D, Sergeev P, Klisic J, Ambuhl P, Schaub MC and Donath MY. High glucose alters cardiomyocyte contacts and inhibits myofibrillar formation. *The Journal of clinical endocrinology and metabolism*. 2006;91:1961-7.
209. Boudia D, Domergue V, Mateo P, Fazal L, Prud'homme M, Prigent H, Delcayre C, Cohen-Solal A, Garnier A, Ventura-Clapier R and Samuel JL. Beneficial effects of exercise training in heart failure are lost in male diabetic rats. *Journal of applied physiology (Bethesda, Md : 1985)*. 2017:jap.00117.2017.

210. Frustaci A, Kajstura J, Chimenti C, Jakoniuk I, Leri A, Maseri A, Nadal-Ginard B and Anversa P. Myocardial cell death in human diabetes. *Circ Res*. 2000;87:1123-32.
211. Guo X, Chen KH, Guo Y, Liao H, Tang J and Xiao RP. Mitofusin 2 triggers vascular smooth muscle cell apoptosis via mitochondrial death pathway. *Circ Res*. 2007;101:1113-22.
212. Shen T, Zheng M, Cao C, Chen C, Tang J, Zhang W, Cheng H, Chen KH and Xiao RP. Mitofusin-2 is a major determinant of oxidative stress-mediated heart muscle cell apoptosis. *J Biol Chem*. 2007;282:23354-61.
213. Enos RT, Velazquez KT and Murphy EA. Insight into the impact of dietary saturated fat on tissue-specific cellular processes underlying obesity-related diseases. *The Journal of nutritional biochemistry*. 2014;25:600-12.
214. Di Lisa F, Giorgio M, Ferdinandy P and Schulz R. New aspects of p66Shc in ischemia reperfusion injury and cardiovascular diseases. *Br J Pharmacol*. 2016.
215. Kuroda J, Ago T, Matsushima S, Zhai P, Schneider MD and Sadoshima J. NADPH oxidase 4 (Nox4) is a major source of oxidative stress in the failing heart. *Proc Natl Acad Sci U S A*. 2010;107:15565-70.
216. Bianchi P, Kunduzova O, Masini E, Cambon C, Bani D, Raimondi L, Seguelas MH, Nistri S, Colucci W, Leducq N and Parini A. Oxidative stress by monoamine oxidase mediates receptor-independent cardiomyocyte apoptosis by serotonin and postischemic myocardial injury. *Circulation*. 2005;112:3297-305.
217. Lou PH, Lucchinetti E, Scott KY, Huang Y, Gandhi M, Hersberger M, Clanachan AS, Lemieux H and Zaugg M. Alterations in fatty acid metabolism and sirtuin signaling characterize early type-2 diabetic hearts of fructose-fed rats. *Physiological reports*. 2017;5.
218. Abdurrachim D, Ciapaite J, Wessels B, Nabben M, Luiken JJ, Nicolay K and Prompers JJ. Cardiac diastolic dysfunction in high-fat diet fed mice is associated with lipotoxicity without impairment of cardiac energetics in vivo. *Biochimica et biophysica acta*. 2014;1842:1525-37.
219. Hunter I, Soler A, Joseph G, Hutcheson B, Bradford C, Zhang FF, Potter B, Proctor S and Rocic P. Cardiovascular function in male and female JCR:LA-cp rats: effect of high-fat/high-sucrose diet. *American journal of physiology Heart and circulatory physiology*. 2017;312:H742-h751.

220. Bhamra GS, Hausenloy DJ, Davidson SM, Carr RD, Paiva M, Wynne AM, Mocanu MM and Yellon DM. Metformin protects the ischemic heart by the Akt-mediated inhibition of mitochondrial permeability transition pore opening. *Basic Res Cardiol*. 2008;103:274-84.
221. Huynh K, Kiriazis H, Du XJ, Love JE, Jandeleit-Dahm KA, Forbes JM, McMullen JR and Ritchie RH. Coenzyme Q10 attenuates diastolic dysfunction, cardiomyocyte hypertrophy and cardiac fibrosis in the db/db mouse model of type 2 diabetes. *Diabetologia*. 2012;55:1544-53.
222. Ladeiras-Lopes R, Fontes-Carvalho R, Bettencourt N, Sampaio F, Gama V and Leite-Moreira A. Novel therapeutic targets of metformin: metabolic syndrome and cardiovascular disease. *Expert opinion on therapeutic targets*. 2015;19:869-77.
223. Salles JE, Moises VA, Almeida DR, Chacra AR and Moises RS. Myocardial dysfunction in mitochondrial diabetes treated with Coenzyme Q10. *Diabetes research and clinical practice*. 2006;72:100-3.
224. Tanajak P, Pintana H, Siri-Angkul N, Khamseekaew J, Apaijai N, Chattipakorn SC and Chattipakorn N. Vildagliptin and caloric restriction for cardioprotection in pre-diabetic rats. *The Journal of endocrinology*. 2017;232:189-204.
225. Bayrami G, Karimi P, Agha-Hosseini F, Feyzizadeh S and Badalzadeh R. Effect of Ischemic Postconditioning on Myocardial Function and Infarct Size Following Reperfusion Injury in Diabetic Rats Pretreated With Vildagliptin. *Journal of cardiovascular pharmacology and therapeutics*. 2017:1074248417729881.
226. Sivasinprasasn S, Tanajak P, Pongkan W, Pratchayasakul W, Chattipakorn SC and Chattipakorn N. DPP-4 Inhibitor and Estrogen Share Similar Efficacy Against Cardiac Ischemic-Reperfusion Injury in Obese-Insulin Resistant and Estrogen-Deprived Female Rats. *Scientific reports*. 2017;7:44306.
227. Kusaka H, Koibuchi N, Hasegawa Y, Ogawa H and Kim-Mitsuyama S. Empagliflozin lessened cardiac injury and reduced visceral adipocyte hypertrophy in prediabetic rats with metabolic syndrome. *Cardiovascular diabetology*. 2016;15:157.
228. Sarkozy M, Zvara A, Gyemant N, Fekete V, Kocsis GF, Pipis J, Szucs G, Csonka C, Puskas LG, Ferdinandy P and Csont T. Metabolic syndrome influences cardiac gene expression pattern at the transcript level in male ZDF rats. *Cardiovascular diabetology*. 2013;12:16.

229. Ouwens DM, Boer C, Fodor M, de Galan P, Heine RJ, Maassen JA and Diamant M. Cardiac dysfunction induced by high-fat diet is associated with altered myocardial insulin signalling in rats. *Diabetologia*. 2005;48:1229-37.
230. Zhong Y, Ahmed S, Grupp IL and Matlib MA. Altered SR protein expression associated with contractile dysfunction in diabetic rat hearts. *American journal of physiology Heart and circulatory physiology*. 2001;281:H1137-47.
231. Luo M, Guan X, Luczak ED, Lang D, Kutschke W, Gao Z, Yang J, Glynn P, Sossalla S, Swaminathan PD, Weiss RM, Yang B, Rokita AG, Maier LS, Efimov IR, Hund TJ and Anderson ME. Diabetes increases mortality after myocardial infarction by oxidizing CaMKII. *J Clin Invest*. 2013;123:1262-74.
232. Sommese L, Valverde CA, Blanco P, Castro MC, Rueda OV, Kaetzel M, Dedman J, Anderson ME, Mattiazzi A and Palomeque J. Ryanodine receptor phosphorylation by CaMKII promotes spontaneous Ca(2+) release events in a rodent model of early stage diabetes: The arrhythmogenic substrate. *International journal of cardiology*. 2016;202:394-406.
233. Tuncay E, Zeydanli EN and Turan B. Cardioprotective effect of propranolol on diabetes-induced altered intracellular Ca2+ signaling in rat. *Journal of bioenergetics and biomembranes*. 2011;43:747-56.
234. Shao CH, Wehrens XH, Wyatt TA, Parbhu S, Rozanski GJ, Patel KP and Bidasee KR. Exercise training during diabetes attenuates cardiac ryanodine receptor dysregulation. *Journal of applied physiology (Bethesda, Md : 1985)*. 2009;106:1280-92.
235. Erickson JR, Pereira L, Wang L, Han G, Ferguson A, Dao K, Copeland RJ, Despa F, Hart GW, Ripplinger CM and Bers DM. Diabetic hyperglycaemia activates CaMKII and arrhythmias by O-linked glycosylation. *Nature*. 2013;502:372-6.
236. Zhong P, Quan D, Peng J, Xiong X, Liu Y, Kong B and Huang H. Role of CaMKII in free fatty acid/hyperlipidemia-induced cardiac remodeling both in vitro and in vivo. *J Mol Cell Cardiol*. 2017;109:1-16.
237. Okatan EN, Durak AT and Turan B. Electrophysiological basis of metabolic-syndrome-induced cardiac dysfunction. *Canadian journal of physiology and pharmacology*. 2016;94:1064-1073.
238. Canton M, Neverova I, Menabo R, Van Eyk J and Di Lisa F. Evidence of myofibrillar protein oxidation induced by postischemic reperfusion in isolated rat

hearts. *American journal of physiology Heart and circulatory physiology*. 2004;286:H870-7.

239. Canton M, Menazza S, Sheeran FL, Polverino de Laureto P, Di Lisa F and Pepe S. Oxidation of myofibrillar proteins in human heart failure. *Journal of the American College of Cardiology*. 2011;57:300-9.

240. Yu W, Zha W, Guo S, Cheng H, Wu J and Liu C. Flos Puerariae extract prevents myocardial apoptosis via attenuation oxidative stress in streptozotocin-induced diabetic mice. *PloS one*. 2014;9:e98044.

241. Hsu HC, Chen CY, Lee BC and Chen MF. High-fat diet induces cardiomyocyte apoptosis via the inhibition of autophagy. *European journal of nutrition*. 2016;55:2245-54.

242. Tanajak P, Sa-Nguanmoo P, Apaijai N, Wang X, Liang G, Li X, Jiang C, Chattipakorn SC and Chattipakorn N. Comparisons of cardioprotective efficacy between fibroblast growth factor 21 and dipeptidyl peptidase-4 inhibitor in prediabetic rats. *Cardiovascular therapeutics*. 2017;35.

243. Montaigne D, Marechal X, Coisne A, Debry N, Modine T, Fayad G, Potelle C, El Arid JM, Mouton S, Sebti Y, Duez H, Preau S, Remy-Jouet I, Zerimech F, Koussa M, Richard V, Neviere R, Edme JL, Lefebvre P and Staels B. Myocardial contractile dysfunction is associated with impaired mitochondrial function and dynamics in type 2 diabetic but not in obese patients. *Circulation*. 2014;130:554-64.

244. Fetterman JL, Holbrook M, Flint N, Feng B, Breton-Romero R, Linder EA, Berk BD, Duess MA, Farb MG, Gokce N, Shirihai OS, Hamburg NM and Vita JA. Restoration of autophagy in endothelial cells from patients with diabetes mellitus improves nitric oxide signaling. *Atherosclerosis*. 2016;247:207-17.

245. Pires KM, Buffolo M, Schaaf C, David Symons J, Cox J, Abel ED, Selzman CH and Boudina S. Activation of IGF-1 receptors and Akt signaling by systemic hyperinsulinemia contributes to cardiac hypertrophy but does not regulate cardiac autophagy in obese diabetic mice. *J Mol Cell Cardiol*. 2017;113:39-50.

246. Lejay A, Fang F, John R, Van JA, Barr M, Thaveau F, Chakfe N, Geny B and Scholey JW. Ischemia reperfusion injury, ischemic conditioning and diabetes mellitus. *J Mol Cell Cardiol*. 2016;91:11-22.

247. Baranyai T, Nagy CT, Koncsos G, Onodi Z, Karolyi-Szabo M, Makkos A, Varga ZV, Ferdinandy P and Giricz Z. Acute hyperglycemia abolishes cardioprotection by remote ischemic perconditioning. *Cardiovascular diabetology*. 2015;14:151.
248. Xie J, Cui K, Hao H, Zhang Y, Lin H, Chen Z, Huang X, Cao S, Liao W, Bin J, Kitakaze M and Liao Y. Acute hyperglycemia suppresses left ventricular diastolic function and inhibits autophagic flux in mice under prohypertrophic stimulation. *Cardiovascular diabetology*. 2016;15:136.
249. Ugurlucan M, Erer D, Karatepe O, Ziyade S, Haholu A, Gungor Ugurlucan F, Filizcan U, Tireli E, Dayioglu E and Alpagut U. Glutamine enhances the heat shock protein 70 expression as a cardioprotective mechanism in left heart tissues in the presence of diabetes mellitus. *Expert opinion on therapeutic targets*. 2010;14:1143-56.
250. Shamaei-Tousi A, Stephens JW, Bin R, Cooper JA, Steptoe A, Coates AR, Henderson B and Humphries SE. Association between plasma levels of heat shock protein 60 and cardiovascular disease in patients with diabetes mellitus. *European heart journal*. 2006;27:1565-70.
251. de Jong JW and Hulsmann WC. A comparative study of palmitoyl-CoA synthetase activity in rat-liver, heart and gut mitochondrial and microsomal preparations. *Biochimica et biophysica acta*. 1970;197:127-35.
252. Wilson EJ. Should nagarse be used during the isolation of brain mitochondria? *Neurochemical research*. 1987;12:831-4.
253. Picard M, Taivassalo T, Ritchie D, Wright KJ, Thomas MM, Romestaing C and Hepple RT. Mitochondrial structure and function are disrupted by standard isolation methods. *PloS one*. 2011;6:e18317.
254. Giorgio M, Migliaccio E, Orsini F, Paolucci D, Moroni M, Contursi C, Pelliccia G, Luzi L, Minucci S, Marcaccio M, Pinton P, Rizzuto R, Bernardi P, Paolucci F and Pelicci PG. Electron transfer between cytochrome c and p66Shc generates reactive oxygen species that trigger mitochondrial apoptosis. *Cell*. 2005;122:221-33.
255. Maita C, Maita H, Iguchi-Ariga SM and Ariga H. Monomer DJ-1 and its N-terminal sequence are necessary for mitochondrial localization of DJ-1 mutants. *PloS one*. 2013;8:e54087.
256. Dabkowski ER, Baseler WA, Williamson CL, Powell M, Razunguzwa TT, Frisbee JC and Hollander JM. Mitochondrial dysfunction in the type 2 diabetic heart is

associated with alterations in spatially distinct mitochondrial proteomes. *American journal of physiology Heart and circulatory physiology*. 2010;299:H529-40.
257. Sun J, Nguyen T, Aponte AM, Menazza S, Kohr MJ, Roth DM, Patel HH, Murphy E and Steenbergen C. Ischaemic preconditioning preferentially increases protein S-nitrosylation in subsarcolemmal mitochondria. *Cardiovasc Res*. 2015;106:227-36.
258. Hendgen-Cotta UB, Esfeld S, Jastrow H, Totzeck M, Altschmied J, Goy C, Haendeler J, Winterhager E and Rassaf T. Mouse cardiac mitochondria do not separate in subsarcolemmal and interfibrillar subpopulations. *Mitochondrion*. 2017.
259. Kavazis AN, Morton AB, Hall SE and Smuder AJ. Effects of doxorubicin on cardiac muscle subsarcolemmal and intermyofibrillar mitochondria. *Mitochondrion*. 2016.
260. Cipolat S, Martins de Brito O, Dal Zilio B and Scorrano L. OPA1 requires mitofusin 1 to promote mitochondrial fusion. *Proc Natl Acad Sci U S A*. 2004;101:15927-32.
261. Ishihara N, Eura Y and Mihara K. Mitofusin 1 and 2 play distinct roles in mitochondrial fusion reactions via GTPase activity. *Journal of cell science*. 2004;117:6535-46.
262. de Brito OM and Scorrano L. Mitofusin 2 tethers endoplasmic reticulum to mitochondria. *Nature*. 2008;456:605-10.
263. Chen Y, Csordas G, Jowdy C, Schneider TG, Csordas N, Wang W, Liu Y, Kohlhaas M, Meiser M, Bergem S, Nerbonne JM, Dorn GW, 2nd and Maack C. Mitofusin 2-containing mitochondrial-reticular microdomains direct rapid cardiomyocyte bioenergetic responses via interorganelle Ca(2+) crosstalk. *Circ Res*. 2012;111:863-75.
264. Chen KH, Guo X, Ma D, Guo Y, Li Q, Yang D, Li P, Qiu X, Wen S, Xiao RP and Tang J. Dysregulation of HSG triggers vascular proliferative disorders. *Nature cell biology*. 2004;6:872-83.
265. Zuchner S, Mersiyanova IV, Muglia M, Bissar-Tadmouri N, Rochelle J, Dadali EL, Zappia M, Nelis E, Patitucci A, Senderek J, Parman Y, Evgrafov O, Jonghe PD, Takahashi Y, Tsuji S, Pericak-Vance MA, Quattrone A, Battaloglu E, Polyakov AV, Timmerman V, Schroder JM and Vance JM. Mutations in the mitochondrial GTPase

mitofusin 2 cause Charcot-Marie-Tooth neuropathy type 2A. *Nature genetics*. 2004;36:449-51.

266. Hoppins S, Edlich F, Cleland MM, Banerjee S, McCaffery JM, Youle RJ and Nunnari J. The soluble form of Bax regulates mitochondrial fusion via MFN2 homotypic complexes. *Mol Cell*. 2011;41:150-60.

267. Roux PP, Shahbazian D, Vu H, Holz MK, Cohen MS, Taunton J, Sonenberg N and Blenis J. RAS/ERK signaling promotes site-specific ribosomal protein S6 phosphorylation via RSK and stimulates cap-dependent translation. *J Biol Chem*. 2007;282:14056-64.

268. Qi Y, Zhu Q, Zhang K, Thomas C, Wu Y, Kumar R, Baker KM, Xu Z, Chen S and Guo S. Activation of Foxo1 by insulin resistance promotes cardiac dysfunction and beta-myosin heavy chain gene expression. *Circulation Heart failure*. 2015;8:198-208.

269. Nishi H, Ono K, Horie T, Nagao K, Kinoshita M, Kuwabara Y, Watanabe S, Takaya T, Tamaki Y, Takanabe-Mori R, Wada H, Hasegawa K, Iwanaga Y, Kawamura T, Kita T and Kimura T. MicroRNA-27a regulates beta cardiac myosin heavy chain gene expression by targeting thyroid hormone receptor beta1 in neonatal rat ventricular myocytes. *Mol Cell Biol*. 2011;31:744-55.

270. Giorgianni F, Koirala D, Weber KT and Beranova-Giorgianni S. Proteome analysis of subsarcolemmal cardiomyocyte mitochondria: a comparison of different analytical platforms. *International journal of molecular sciences*. 2014;15:9285-301.

12 List of own publications

12.1 Own publications involved in the current thesis

1. Koncsos, G., Varga, Z.V., Baranyai, T., Boengler, K., Rohrbach, S., Li, L., Schluter, K.D., Schreckenberg, R., Radovits, T., Olah, A., Matyas, C., Lux, A., Al-Khrasani, M., Komlodi, T., Bukosza, N., Mathe, D., Deres, L., Bartekova, M., Rajtik, T., Adameova, A., Szigeti, K., Hamar, P., Helyes, Z., Tretter, L., Pacher, P., Merkely, B., Giricz, Z., Schulz, R., Ferdinandy, P. Diastolic dysfunction in prediabetic male rats: Role of mitochondrial oxidative stress. *American journal of physiology. Heart and circulatory physiology* 311(4), H927-h943, 2016 (IF: 3.324)

2. Giricz, Z., Koncsos, G., Rajtik, T., Varga, Z.V., Baranyai, T., Csonka, C., Szobi, A., Adameova, A., Gottlieb, R.A., Ferdinandy, P. Hypercholesterolemia downregulates autophagy in the rat heart. *Lipids in health and disease* 23; 16(1): 60, 2017. (IF: 2.137)

3. Koncsos G., Varga, Z.V., Baranyai, T., Ferdinandy, P., Schulz, R., Giricz, Z., Boengler, K. Nagarse treatment of cardiac subsarcolemmal and interfibrillar mitochondria leads to artefacts in mitochondrial protein quantification. *Journal of Pharmacological and Toxicological Methods* 31;91:50-58, 2018 (IF: 2.238)

12.2 Own publications not involved in the current thesis

4. Baranyai, T., Nagy, C.T., Koncsos, G., Onodi, Z., Karolyi-Szabo, M., Makkos, A., Varga, Z.V., Ferdinandy, P., Giricz, Z. Acute hyperglycemia abolishes cardioprotection by remote ischemic perconditioning. *Cardiovascular diabetology* 14: 151, 2015. (IF: 4.015)

5. Baranyai, T,, Giricz, Z., Varga, Z.V., Koncsos, G., Lukovic, D., Makkos, A., Sárközy, M., Pávó, N., Jakab, A., Czimbalmos, C., Vágó, H., Ruzsa, Z., Tóth, L., Garamvölgyi, R., Merkely, B., Schulz, R., Gyöngyösi, G., Ferdinandy, P. In vivo MRI and ex vivo histological assessment of the cardioprotection induced by ischemic preconditioning, postconditioning and remote conditioning in a closed-chest porcine model of reperfused acute myocardial infarction: importance of microvasculature. *Journal of translational medicine* 15: 67, 2017. (IF: 3.991)

6. Giricz, Z., Varga, Z.V., Koncsos, G., Nagy, C.T., Görbe, A., Mentzer, R.M. Jr., Gottlieb, R.A., Ferdinandy, P. Autophagosome formation is required for cardioprotection by chloramphenicol. *Life Sciences* 186:11-16, 2017 (IF: 2.936)

7. Varga, ZV., Pipicz, M., Baán, JA., Baranyai, T., Koncsos, G., Leszek, P., Kuśmierczyk, M., Sánchez-Cabo, F., García-Pavía, P., Brenner, GJ., Giricz, Z., Csont, T., Mendler, L., Lara-Pezzi, E., Pacher, P., Ferdinandy, P. Alternative Splicing of NOX4 in the Failing Human Heart. *Front Physiol.* 8:935, 2017 (IF: 4.134)

8. Nagy, A.M., Fekete, R., Horváth, G., Koncsos, G., Kriston, C., Sebestyén, A., Giricz, Z., Környei, Z., Madarász, E., Tretter, L. Versatility of microglial bioenergetics machinery under starving conditions. *Biochim Biophys Acta.* S0005-2728(17)30193-7. 2017 (IF: 4.932)

9. Nagy, C.T., Koncsos, G., Varga, Z.V., Baranyai, T., Tuza, S., Kassai, F., Ernyei, A.J., Gyertyán, I., Király, K., Oláh, A., Radovits, T., Merkely, B., Bukosza, N., Szénási, G., Hamar, P., Mathé, D., Szigeti, K., Pelyhe, C., Jelemenský, M., Onódi,

Z, Helyes, Z., Schulz, R., Giricz, Z., Ferdinandy, P. Selegiline reduces adiposity induced by high-fat, high-sucrose diet in male rats. *British Journal of Pharmacology*. In press. 2018 (IF: 6.810)

13 Acknowledgements

The presented studies were supported by the following grants: European Foundation for the Study of Diabetes (EFSD) New Horizons Collaborative Research Initiative from European Association for the Study of Diabetes (EASD), the National Research, Development and Innovation Office of Hungary (NKFIA; NVKP-16-1-2016-0017 National Heart Program), the Hungarian Scientific Research Fund (OTKA K 109737 and OTKA PD 109051) and Semmelweis University (EFOP-3.6.3-VEKOP-16-2017-00009). Furthermore, Pharmahungary Group (Szeged, Hungary) also financed the experiments.

I greatly acknowledge to Prof. Dr. Péter Ferdinandy for providing me the possibility to work in the Cardiometabolic Research Group at the Department of Pharmacology and Pharmacotherapy. I am also grateful for the excellent laboratory environment that gave me the opportunity to create this thesis.

I am indebted to my supervisor, Dr. Zoltán Giricz who pushed my carrier with his helpful suggestions, scientific attitude and guidance. I am thankful for his constant motivation, support and patience.

I would like to express my enormous gratitude to Dr. Zoltán V. Varga, He always inspired my way of thinking and helped me with his encouragements during my PhD years. I am especially thankful to Melinda Károlyi-Szabó and Jenőné Benkes for their technical assistance. I thank Tamás Baranyai, Csilla Nagy, Gábor Brenner, András Makkos, Zsófia Onódy and all fellow PhD-students and all members of the Department of Pharmacology and Pharmacotherapy for the friendly support and environment. I am also grateful to my undergraduate students, Balázs Czakó, Sebestyén Tuza and Máté Ézsiás for their contribution to my work. I am especially thankful to Tomáš Rajtík, who became a good friend via our collaborations (Comenius University in Bratislava, Slovakia); and Monika Barteková (Slovak Academy of Sciences, Bratislava, Slovakia), who helped me with her kindness, patience and scientific attitude. I am also grateful to Prof. Rainer Schulz and Kerstin Boengler (Justus-Liebig University, Giessen, Germany), Prof. Béla Merkely, Tamás Radovits and Attila Oláh (Heart and Vascular Center, Semmelweis University), Tímea Komlódi and Prof. László Tretter (Department of Medical Biochemistry, Semmelweis University), Adriana Adameová (Comenius

University in Bratislava, Slovakia) and all my collaborators, who participated in the studies of this thesis.

Last, but not least, I am greatly thankful for my family to support me with their patient, belief and kindness.